``

STRUCTURAL AND BIOCHEMICAL MECHANISMS OF THE ACTIVATION OF ARF1 AT THE GOLGI

A Dissertation
Presented to the Faculty of the Graduate School
of Cornell University
In Partial Fulfillment of the Requirements for the Degree of
Doctor of Philosophy

By
Arnold Muccini
August 2022

``

``

ABSTRACT

STRUCTURAL AND BIOCHEMICAL MECHANISMS OF THE ACTIVATION OF ARF1 AT THE GOLGI

Arnold Muccini, Ph.D.
Cornell University

Eukaryotic cells use vesicles to transport material between their cellular compartments. The Golgi complex is the central sorting organelle for most of vesicular trafficking events in the cell. To control these trafficking events, the cell utilizes small GTPases that act as on/off switches. At the Golgi, the GTPase Arf1 coordinates most of the outgoing vesicle formation. Arf1 is regulated by the standard GTPase cycle and is activated when a GEF exchanges GDP for GTP. Once GTP bound, Arf1 undergoes a conformational change that allows it to localize to the Golgi complex and recruit effector proteins.

At the Golgi, Arf1 is activated by three different GEFs, Gea1, Gea2, and Sec7. These proteins share a common catalytic GEF domain and regulatory domains of unclear function. While they activate the same substrate, Gea1/2 are functionally distinct from Sec7, which activates Arf1-dependent vesicle formation at later parts of the Golgi. Gea1 and Gea2 activate Arf1 at the early and medial Golgi respectively for COPI vesicle formation. While Gea1 and Gea2 are genetically redundant, they have distinct localization *in vivo*.

``

To understand the regulation of the Golgi Arf-GEFs, I used a structural approach to determine the function and mechanism of these regulatory domains. I present the first full-length structure of a large Arf-GEF, Gea2, and the structure of Gea2 bound to its substrate Arf1. Using these structures, I was able to structurally and biochemically characterize the activation of Arf1 by Gea2.

``

BIOGRAPHIC SKETCH

Arnold Muccini was born and raised outside of New York City on Long Island. He went to the local Catholic elementary school and graduate from Kellenberg Memorial High School in 2012.

Arnold received a Chemistry degree from Fordham university in 2016. While working on his degree he joined the lab of Dr. Saba where he studied the stereo-selectivity of the reduction of benzoin guided by the Falkin-Ahn model which led to a publication. After this work he joined the lab of Dr. Paul Smith in which he was first exposed to biochemistry and structural biology. In this work he tried to crystalize various viral and CRISPR proteins.

Arnold started graduate school in August 2016 and joined the lab of Dr. Chris Fromme to do his thesis work. While in the lab Arnold was able to publish the first structure of a large Arf GEF and used this structure to structural and biochemically characterize the activation of Arf1 at the Golgi.

``

DEDICATION

To the Blessed Virgin Mary, Mother of God

``

ACKNOWLEDGEMENTS

Firstly, I am very thankful for my amazing and wonderful advisor Chris for his support and mentorship throughout my 5+ years in his lab. He taught me invaluable skills that have launched me into my scientific career. I will be forever thankful for the wonderful graduate school experience I received under his mentorship.

I am thankful for my committee members Carolyn and Gunther who have also been with me since the beginning. Your guidance and encouragement have always been invaluable to me.

I am very fortunate to have had an extremely supportive and collaborate lab environment. Thanks to Carolyn Highland, Brian Richardson, Laura Thomas, Ryan Vignogna, Bryce Brownfield, Ryan Feathers, Saket Badge, Kaitlyn Manzer, Ari Broad, and Shamar Wallace for their constant day to day help and support in the lab. Good luck to Anna Allen who will be taking over this project. I would also like to thank those outside my lab that have helped me along the way such as Karim Omar, Ethan Sanford, Abigail Sulpizo, Alan Sulpizo, Riasat Zaman, Megan Rothstein and Jessica West.

I would also like to thank the various members of the Weill Institute family. The faculty have always been helpful and supportive during talks and seminars. Weill support staff David McDermit, Sarah Griffin, Nadia Nikulin, and Revelin Bonomo who have made life easier in the lab.

``

Also the support staff at the CCMR especially Mariena Silvestry Ramos and Katie Spoth who provided with training that made this work possible.

I thank all my friends both in graduate school and back home who helped get me through this journey.

Finally, I would like to thank my entire family but especially my parents who supported me throughout my entire education.

``

TABLE OF CONTENTS

Abstract iii

Biographic Sketch v

Dedication vi

Acknowledgements vii

Chapter 1. Introduction

Figure 1.1. Overview of the secretory pathway 2

Figure 1.2 Models for Golgi maturation 5

Figure 1.3 Overview of vesicle formation 9

Figure 1.4 Gea1/2 and Sec7 have distinct functions 17

Chapter 2. Prelimary Pursuits of a Structure of Gea2 18

Introduction 18

Results 20

Figure 2.1 Preliminary cryoEM structure of K.m. Gea 21

Figure 2.2 CryoEM data processing for K.m. Gea 22

Figure 2.3 Assessment of the orientation bias of Gea2-Arf1 26

Figure 2.4 Preliminary cryoEM structure of the Gea2-Arf1 complex 27

Figure 2.5 Data processing for Gea2-Arf1 complex 28

Discussion 29

Chapter 3. Structural basis for the activation of Arf1 at the Golgi Complex 31

Introduction 31

Results 34

Figure 3.1 Structure of Gea2 determined by cryoEM 36

Figure 3.2 Protein reagents used in this study 37

Figure 3.3 Gea2 cryoEM data processing 38

Figure 3.4 Gea2 cryoEM map and model validation 39

Figure 3.5 The closed/closed and open/open conformations of Gea2 41

Table 3.1 CryoEM data collection, processing and model validation statistics 42

Figure 3.6 Ordered linkers connect the GEF domain to the HUS and HDS1 domains 44
Figure 3.7 Gea2 dimerizes via the DCB-HUS domains 49
Figure 3.8 A conserved amphipathic α-helix mediates Gea2 membrane binding 50
Figure 3.9 CryoEM structure of a Gea2-Arf1 activation intermediate complex 55
Figure 3.10 Gea2-Arf1 activation intermediate complex cryoEM data processing 56
Figure 3.11 Structural comparisons 57
Figure 3.12 Steric constraints appear to enforce Gea2 conformational change 59
Figure 3.13 Model for activation of Arf1 by Gea2 on the Golgi membrane surface 63
Discussion 65
Chapter 4. Mechanism for the differential localization of Gea1 and Gea2 69
Introduction 69
Figure 4.1 Organization of SNAREs at the Golgi 71
Results 72
Figure 4.2 Gea1 and Gea2 have distinct localizations 74
Figure 4.3 DCB-HUS domain determines Gea location. 75
Figure 4.4 Localization of Gea1 and Gea2 does not change 79
Figure 4.5 Attempts at testing SNARE interactions with Gea1 and Gea2 80
Discussion 81
Chapter 5. Future Directions 84
Appendix I. Materials and Methods 87
Appendix II. Plasmids generated in this study 94
Appendix III. Strains generated in this study 97
References 99

``

CHAPTER 1

INTRODUCTION

Cellular compartments

One of the hallmarks that separates eukaryotic cells from bacterial cells is the use of various intracellular compartments. Unlike bacteria, eukaryotes use membranes to sequester cellular compartments. One of the first major organelles that comes to mind is the nucleus which is separated from the rest of the cell by the nuclear membrane. The nucleus contains the cell's genetic material and all the machinery for DNA replication, transcription, and mRNA processing. The proteome of the nucleus is maintained by the nuclear pore complex that regulates the import and export of biomolecules (Beck and Hurt, 2017).

Eukaryotic cells also contain organelles that are thought to be derived from independent organisms, the mitochondria and chloroplasts (Martin et al., 2015). Mitochondria use the electron transport chain to produce ATP that is used as an energy source for the cell's cellular processes (Kühlbrandt, 2015). Chloroplasts use photosystems for the fixation of carbon for future energy production. These organelles also contain their own small genome and express their own specialized ribosomes.

The most complex of membrane bound organelles is the endomembrane system which consists of the endoplasmic reticulum (ER),

``

lysosomes, endosomes, and the Golgi complex (Fig.1.1). The endomembrane system is responsible for the transport of protein cargo that undergo secretory or endocytic trafficking. The flow of the endomembrane system is bidirectional with anterograde and retrograde traffic.

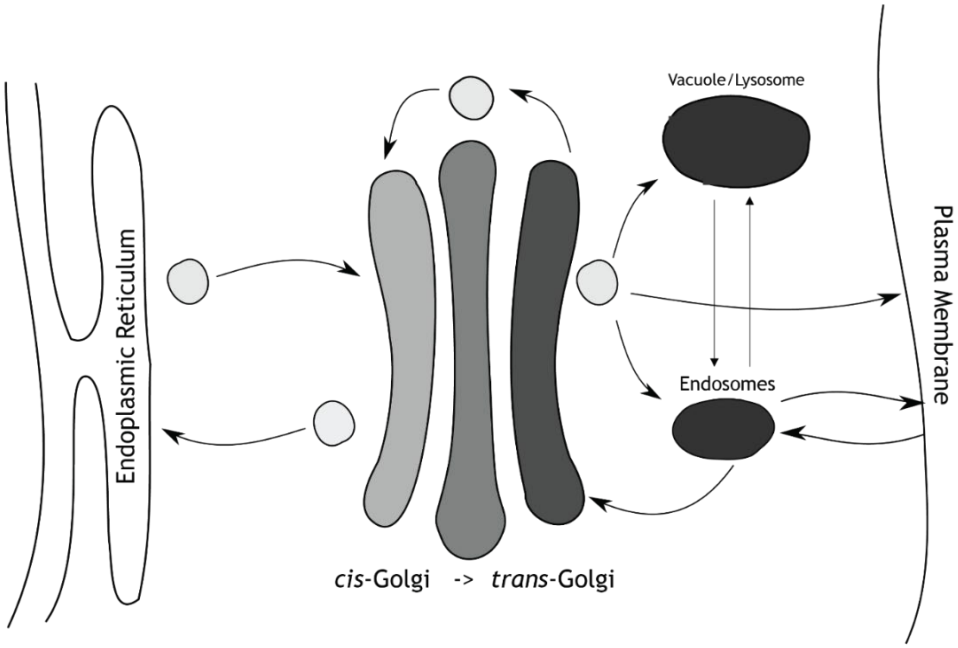

Figure 1.1. Overview of the secretory pathway

``

Overview of the Secretory Pathway

The secretory pathway was first identified in mammalian cells but was initially genetically characterized in the Sec screen using the simpler model organism *Saccharomyces cerevisiae* (S.c.). (Novick et al., 1980; Palade, 1975). Cargo destined for secretion is synthesized into the ER before being sorted into vesicles and transported to the Golgi. At the Golgi, cargo can undergo additional posttranslational modifications before eventually being packaged again into vesicles where they are transported to the PM.

Endocytosis involves uptake of extracellular material and recycling of cell surface receptors and other plasma membrane (PM) proteins. Endocytic cargo binds to cell surface receptors and is then sorted through the endosomal system in which the cargo finally arrives at the lysosome/vacuole where it can be degraded into free amino acids and carbohydrates.

Trafficking at the Golgi

The Golgi is a polarized organelle that has *cis*/early and *trans*/late compartments with *medial*/transitional compartments in between. Cargos arrive at the Golgi in COPII vesicles that originated from the ER. Retrograde intra-Golgi trafficking is mediated by COPI vesicles. Cargos are modified and trafficked through the Golgi by a maturation process where they eventually reach the most *trans* face of the Golgi known as the *trans*-Golgi network (TGN). At the TGN, cargos undergo final sorting and packaging into vesicles

``

and are sent off to their final destinations such as the PM or the lysosome (Glick, 2000; Glick and Luini, 2011).

Proteins at the Golgi can be characterized into two types, resident Golgi proteins and secretory cargos. The resident Golgi proteins are the enzymes essential for Golgi function and post translational modifications whereas the secretory cargos are just passerby and are destined for a different cellular compartment. With the discovery of COPI vesicles, it was hypothesized that the secretory cargos are transported through the various Golgi cisternae in these vesicles. This was problematic because COPI vesicles are too small to hold some known large cargo of some organisms (Gaynor and Emr, 1997; Glick, 2000; Mironov et al., 2001). Using live cell imaging in yeast, the transition between Golgi markers at the same compartment was observed (Losev et al., 2006; Matsuura-Tokita et al., 2006). This understanding of Golgi transport is called the Golgi maturation model in which cargos remain in the same Golgi compartments as the compartments change over time and resident Golgi proteins are continuously recycled to earlier compartments (Fig.1.2).

``

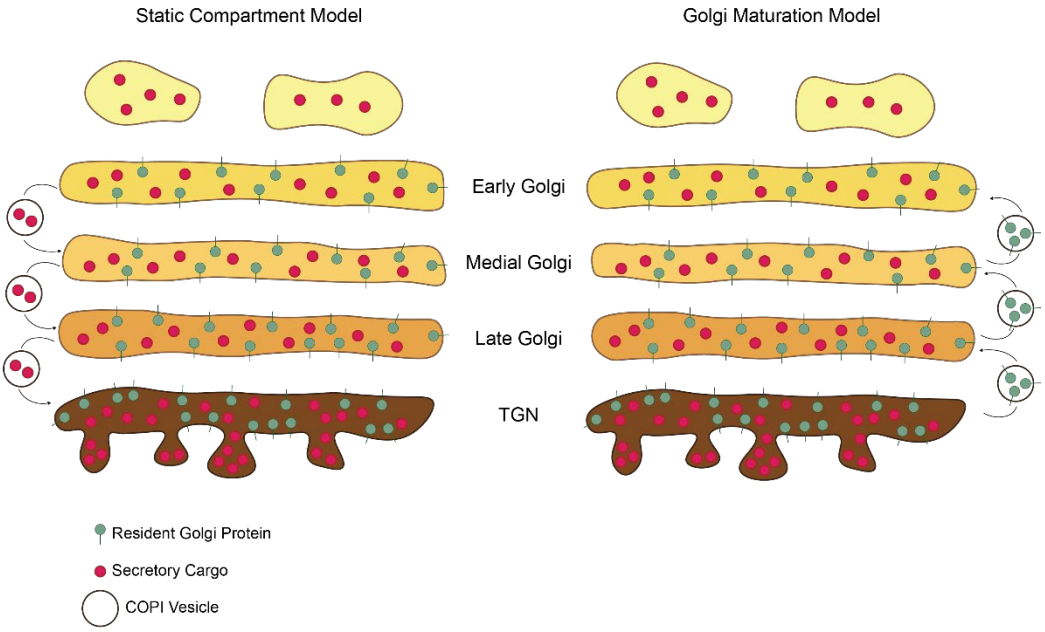

Figure 1.2. Models for Golgi trafficking

``

Vesicle Formation

Vesicles are the primary method by which cargos are transported through the endomembrane system by budding from a donor compartment and fusing with an acceptor compartment (Bonifacino and Glick, 2004). In the secretory pathway small GTPases are the master regulators of vesicle formation. The process begins with the activation of a GTPase by its guanine-nucleotide exchange factor (GEF) in which the GTPase is recruited to and binds to the donor compartment membrane (Fig.1.3-A). The activated GTPase then recruits the components required for vesicle formation (Fig1.3-B). Transmembrane cargos directly bind to the coat components while soluble cargos require an adaptor protein. As the coat assembles the vesicle starts to bud and eventually pinches off from the membrane (Fig.1.3C-D) (Cai et al., 2007; Santiago-Tirado and Bretscher, 2011; Trahey and Hay, 2010).

After budding, the GTPase is inactivated by a GTPase-activating protein (GAP), and the coat complex fully or partially dissociates from the vesicle (Fig.1.3-E). In some cases, other small GTPases will bind to the vesicle and recruit motor proteins that transport the vesicle (Lipatova et al., 2008). Once the vesicle reaches its destination, the vesicle will interact with a tethering complex (Cao, 1998; Pfeffer, 1999). To facilitate fusion, the vesicle contains a v-SNARE that interacts with and assembles with three t-SNAREs on the donor compartment (Cai et al., 2007). This provides the energy required to fuse the lipids together. The membrane from the vesicle fuses with

``

the donor membrane delivering the cargo to the donor compartment (Fig.1.3 F-H).

Vesicle Coats

Each type of vesicle is generally classified by the name of its coat. Vesicle coats are proteins or protein complexes that oligomerize. The coat proteins are recruited by small GTPases, such as Arf1 and Sar1, or by coat adaptors such as the AP protein complexes (Alberts et al., 2002; Bonifacino, 2014). The coat proteins assemble around the membrane, and their oligomerization can start to deform the membrane. The coat proteins can also recruit their cargos by physical interactions between signal sequences and cargo adaptor proteins (Vincent et al., 1998). Vesicles use coats to identify themselves from other vesicles so the correct machinery will be recruited to them to ensure they reach their proper destination. At some point the coat must be shed so that the vesicle can fuse with the acceptor compartment.

The first of these coats to be discovered was the clathrin complex, which coats the endocytic vesicles that are derived from the plasma membrane (Pearse, 1975). Clathrin forms a triskelion complex consisting of three clathrin heavy chains and three clathrin light chains that further oligomerize to form a cage (Kirchhausen, 2000). Clathrin requires adaptor protein complexes that bind to cargo and recruit the clathrin complex (Park and Guo, 2014). The AP-1 complex recruits clathrin at the TGN for trafficking

``

to endosomes and intra-Golgi recycling (Casler et al., 2019; De Matteis and Luini, 2008). The AP-2 adaptor localizes to the plasma membrane where it recognizes cargo signal sequences and then recruits clathrin for endocytosis. AP-2 is not recruited by an Arf GTPase but rather localizes to the PM by PIP_2 binding (Park and Guo, 2014).

Trafficking out of the ER requires COPII vesicles. The small GTPase Sar1 is activated by its GEF Sec12 and then recruits the inner COPII coat layer consisting of the Sec23-Sec24 complex (Barlowe et al. 1994; Nakańo and Muramatsu 1989). Then the outer coat layer consisting of Sec13-Sec31 finishes coat formation and budding of the vesicle. Sec23 also doubles as a GAP for Sar1 and interaction with Sec31 stimulates its GAP activity. With the inactivation of Sar1 the coat dissociates from the vesicle (Fromme et al., 2008; Jensen and Schekman, 2011).

Retrograde traffic at the Golgi is carried out by COPI coated vesicles. The coat consists of 7 proteins that associate into two sub complexes, the B and F subcomplexes (Arakel et al., 2018). Activated Arf1 recruits the F-subcomplex while the B complex can directly interact with cargo. The combination of B-complex-cargo interaction and Arf1-F-subcomplex drives the completion of the coat, and further polymerization of the coat on the complex. After vesicle formation, Arf1 is inactivated by GAPs that are associated with

``

the coat which drives the dissociation of the coat from the vesicle (Arakel et al., 2018; Jackson, 2014).

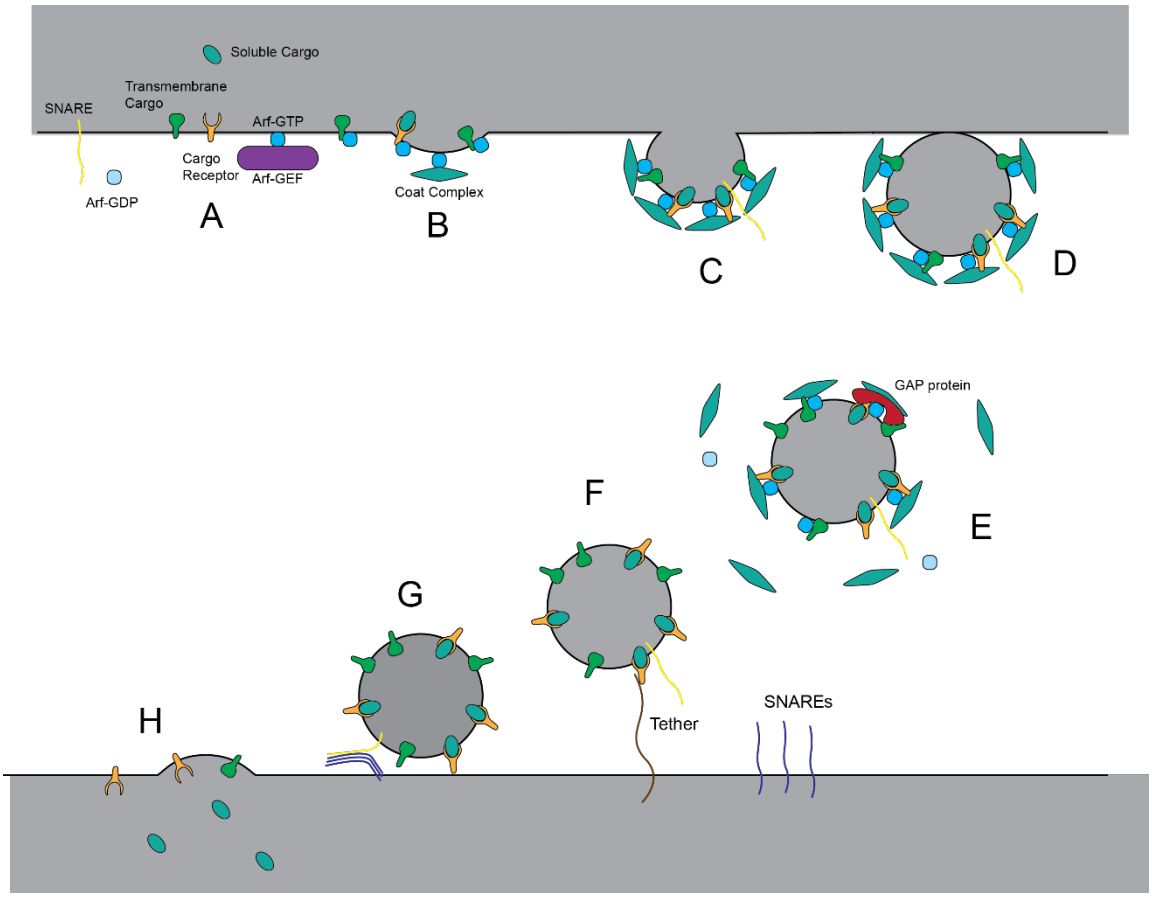

Figure 1.3 Overview of vesicle formation
(A) GEF activates Arf at the membrane. (B) Arf-GTP recruits coat complex and cargo/cargo adapters. (C) Membrane deformation. (D) Membrane budding. (E) GAP catalyzes GTP hydrolysis of Arf. (F) Uncoated vesicle binds to tether. (G) Docking and fusion of vesicle. (H) Cargo release into the donor compartment.

``

Signal sequences and sorting signals

The cell uses signal sequences and sorting signals to determine the fate of a particular cargo. These are usually amino acid motifs that interact with cargo adaptors, coat proteins, or scaffolding proteins. For example the AP adapter complexes bind directly to their cargo via various sorting signal motifs (Bonifacino and Lippincott-Schwartz, 2003).

The first step of the secretory pathway is co-translational translocation into the ER. When a protein is being translated there is a motif called the signal peptide that directly interacts with the signal recognition particle (SRP), halting translation (Akopian et al., 2013; Walter and Blobel, 1980). The stalled ribosome is then recruited to the ER where it can bind to the translocon component Sec61. Sec61 acts as a channel across the ER membrane through which the protein can be translocated. Soluble cargo is released into the ER lumen while transmembrane cargo are inserted into the membrane by Sec61 (Römisch, 1999; Trueman et al., 2012).

While proteins enter the secretory pathway to eventually be secreted at the PM, much of the machinery of the secretory pathway also needs to enter the pathway but remain resident in a particular compartment such as the ER or Golgi. Resident ER proteins sometimes find themselves at the Golgi because of bulk flow at ER exit sites. Cells evolved multiple strategies for retrograde transport. Soluble resident proteins contain an H/KDEL sequence

``

that binds with the H/KDEL receptor (Erd2 in yeast) which is then recycled back to the ER in COPI vesicles. Due the pH difference between the Golgi and the ER, the soluble cargo dissociates from Erd2 and can freely function again the ER lumen (Ellgaard and Helenius, 2003; Semenza et al., 1990). Several transmembrane proteins contain a C-terminal KKXX motif which interacts directly with the COPI vesicle machinery for recycling back to the ER (Gomez-Navarro and Miller, 2016; Jackson et al., 2012).

GTPase cycle

As described briefly above, small GTPases are the master regulators of trafficking in the endomembrane system. The complexity of the secretory pathway requires a method for cells to turn on and off certain processes. When activated, the GTPase recruits its effector proteins that are specialized to carry out a specific function. The activation and deactivation of GTPases is called the GTPase cycle (Gillingham and Munro, 2007).

When most small GTPases involved in trafficking are bound to GDP, they are “inactive” and cannot localize to a membrane or recruit effectors. GEFs are proteins that catalyze the exchange of GDP for GTP by destabilizing the nucleotide binding domain causing the GDP to dissociate. Since the cellular concentration of GTP is ~10x greater than that of GDP, GTP then binds to the GTPase causing a conformation change to the active state which

``

also causes it to dissociate from its GEF. Now the GTPase is bound to a membrane compartment and recruits various effector proteins.

A GTPase is deactivated when it is in the GDP bound state, however despite their name, GTPases have very low intrinsic GTPase activity. This is so the cell can control when to shut down a cellular process. GAPs are proteins that complete the active site which allows the GTPase to hydrolyze the GTP to GDP.

Types of GTPases

At the Golgi there are two types of GTPases, Rabs and Arfs. The Rab family contain a small globular domain followed by a variable linker that is prenylated (Alexandrov et al., 1994). When GDP-bound and inactive, Rabs bind to a GDI protein to protect the hydrophobic prenyl groups from the cytosol. Rabs are free to sample different organelle membranes and while GDP-bound will rebind the GDI. When a Rab is on a membrane and encounters its GEF, GTP exchange occurs and it can no longer rebind to the GDI. Therefore the localization of a Rab-GEF is what confers the localization of the Rab (Cherfils and Zeghouf, 2013; Kelly et al., 2012).

Various Rab GTPases localize to the Golgi to perform actions for vesicle formation and fusion events. Ypt1 (yeast homolog of Rab1) resides throughout most of the Golgi and is responsible for recruiting tethering factors

``

such as Uso1 (Barr, 2009). Ypt6 (yeast Rab6 paralog) functions at the *medial* Golgi and recruits effectors to facilitate fusion of incoming vesicles. At the TGN, the paralogs Ypt31/32 (yeast Rab11 paralogs) orchestrate the final stages of secretory vesicle formation (Barr, 2009).

Unlike the Rabs, the Arfs have a simpler mechanism regarding membrane binding. Arfs contain a N-terminal amphipathic helix with a myristoyl group. Arfs do not need a chaperone when GDP-bound because the amphipathic helix is shielded by the Arf protein itself. Upon activation, Arfs undergo a conformation change that exposes the amphipathic helix and myristoyl group for membrane binding (Gillingham and Munro, 2007).

In yeast there are two Arf GTPases, Arf1/2 and Arf3. Arf3 localizes to the plasma membrane and is involved with cell polarity. Arf1/2 operates at the Golgi and regulates outgoing vesicle formation. At the early and medial Golgi, active Arf1 recruits the COPI vesicle coat for formation of vesicles destined for the ER and early Golgi. Arf1 also recruits the components required for trafficking events at the TGN (D'Souza-Schorey and Chavrier, 2006; Gillingham and Munro, 2007).

There are additional members of the Arf family in yeast. Sar1 recruits the COPII vesicle coat for vesicles destined for the early Golgi. Other

``

examples are the Arf like proteins Arl3 and Arl1 which recruits the golgin Imh1 to the TGN (Chen et al. 2019)

Types of GEFs

The TRAPP family of GEFs activate some of the Rabs at the Golgi complex. In yeast, three TRAPP complexes were initially identified. TRAPPI, the TRAPP core, is a set of 7 subunits. TRAPPII and TRAPPIII include the TRAPP core but have unique accessory proteins that distinguish them (Thomas and Fromme, 2016; Thomas et al., 2018). More recently, our lab determined that TRAPPI does not exist in cells (Thomas et al., 2018). TRAPPII contains four additional subunits and activates Ypt31/32 at the TGN during vesicle formation. The other complex, TRAPPIII, contains a single additional subunit and activates Ypt1.

The TRAPP complexes are not the only proteins that act as GEFs for Rabs. At the medial Golgi, the Rab Ypt6 is activated by the Ric1-Rgp1 complex (Siniossoglou et al., 2000). On secretory vesicles, the coiled-coil protein Sec2 activates the Rab Sec4 (yeast Rab8 paralog) (Walch-Solimena et al., 1997).

Arf GEFs are characterized by the possession of a highly conserved Sec7/GEF domain. This domain has been thoroughly characterized structurally and biochemically (Goldberg, 1998; Renault et al., 2003). The

``

domain interacts with Arf-GDP and works to physically pry open the nucleotide binding pocket releasing the GDP.

Arf GEFs

While the ‘Sec7’ GEF domain is highly conserved, Arf GEFs need accessory domains so they can maintain localization and regulation. Several Sec7 domain-containing proteins, such as human Arno1 and yeast Yel1 and Syt1, also have a PH domain that recruits them to their target organelle. The BIG/GBF family of proteins also contain a Sec7 domain however they are much larger and contain domains of previously unknown function. Human GBF1 (Gea1/2 in yeast) and BIG1/2 (Sec7 in yeast) are the GEFs which are responsible for activating Arf1 at the Golgi for vesicle formation. These proteins all contain domains of unknown function flanking the GEF domain. These ‘homology upstream’ (HUS) and ‘homology downstream’ (HDS) of the ‘Sec7 domain’ are conserved across species however are not found in any other protein. The domains likely play a role in localization and regulation of these proteins (Casanova, 2007).

Sec7 was first identified in the famous Sec screen and mutants were identified that resulted in the formation of Berkeley bodies in yeast cells (Novick et al., 1980). The protein is relatively large and contains four HDS domains while GBF/Gea contains three. Sec7 has been shown to interact with four of the GTPases at the Golgi. Arl1 and Ypt1 interact with the regulatory

``

domains for recruitment to the TGN. The activity of Sec7 has been shown to be autoinhibited and the activity is stimulated interacting with Ypt31 and recruited in a positive feedback loop with interactions with Arf1 (McDonold and Fromme, 2014; Richardson et al., 2012, 2016).

There is not much structural information known for the large Arf GEFs. There are several crystal structures of isolated GEF domains with and without Arf1 bound. The first structure of the unique domains found in these proteins was the crystal structure of the DCB-HUS N-terminal region. The structure showed that these two domains form a single structure domain (Richardson et al., 2016).

Gea1 and Gea2 are genetically redundant but have distinct function from that of Sec7 (Fig.1.4). Sec7 activates Arf1 for the creation of vesicles at the TGN while Gea1/2 activates Arf1 for the creation of COPI vesicles. While appearing similar based on primary structure and domain organization, their recruitment and regulation mechanisms appear to be different. Gea is recruited by the GTPase Ypt1, but not by Arl1, Ypt1, or Ypt31/32 like Sec7. Gea1/2 are not recruited via positive feedback with Arf1 and is not autoinhibited. Gea1/2 prefer a neutral lipid environment while Sec7 prefers anionic lipid like that of the TGN. While being genetically redundant, Gea1 and Gea2 localize distinctly to the early and medial Golgi. (Gustafson, 2017; Gustafson and Fromme, 2017).

``

In this study I took a structural approach to understand how Gea1/2 function at the Golgi. I used cryoEM to determine the structure of Gea2, which is the first reported structure of a large-Arf GEF, and the structure of Gea2 bound to Arf1. With these structures, I was able to biochemically and structurally characterize Gea2 activation of Arf1 at the Golgi.

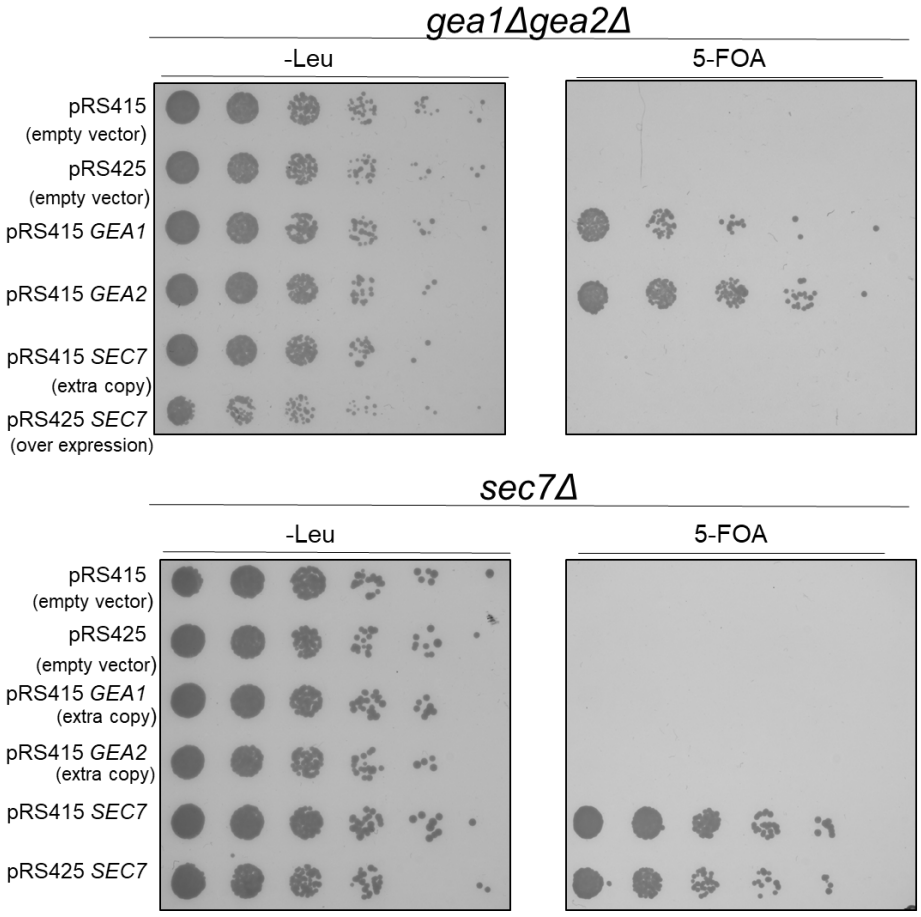

Figure 1.4. Gea1/2 and Sec7 have distinct functions
Yeast complementation assay

``

CHAPTER 2

PRELIMINARY PURSUITS OF A STRUCTURE OF GEA2

INTRODUCTION

For centuries biologists have developed strategies for visualizing biological processes and systems. The first technique used to determine the structure of biomolecules was X-ray crystallography. In this approach, a biomolecule of interest first needs to crystalize into a homogeneous crystal and then is exposed to X-rays (Duke and Johnson, 2010; Rupp, 2010). The scattering pattern is collected, and a high-resolution 3D model can be generated. These models can be accurate enough to resolve individual atoms and determine reaction mechanisms. As powerful as it is, crystallography depends on the creation of the protein crystal itself which can be very challenging and sometimes impossible. Also, the packing of a protein into a very high concentration packed crystal might cause non-physiological structural changes.

Electron microscopy is another technique that has been used to visualize biological molecules. Instead of using visible light, electron microscopes use electrons to illuminate the sample and therefore and are not limited in resolution by the wavelength of visible light. Negative staining is a technique in which biological samples can be prepared so they can be imaged using an electron microscope (Barreto-Vieira and Barth, 2015). A biomolecule is added to a grid and treated with a staining agent. The stain adheres to the

``

molecule blocking the beam from the detector. This technique has resolution limitations since one is imaging the shell of the stain and not the molecule itself. The sample is also dehydrated and can be damaged during the staining process.

A biomolecule's native environment is aqueous, which is a challenge for EM since imaging is performed in a vacuum. This is not an issue for negative stain imaging, but staining the sample has its drawbacks which have been stated above. A solution to this was the creation of the technique known as cryogenic electron microscopy (Dubochet et al., 1988). In this method the biomolecule of interest is frozen in vitreous ice, which not only allows the molecule to stay in an aqueous environment, but now the frozen sample can be imaged under vacuum in an electron microscope. This technique has been around for decades, but resolution has been limited because of limitations with data collection. This all changed with the "resolution revolution" in the 2010s with the introduction of the direct electron detector (Kühlbrandt, 2014).

Another advantage of having a sample frozen in ice is that, in theory, the molecule can sample orientations freely floating in the solution. When the sample is imaged, projection images are classified and then can be aligned and averaged into a 3D reconstruction to produce an electron density map (Rosenthal and Henderson, 2003). It is crucial that multiple views are

``

observed so that information from those angles can be added to the reconstruction.

Our lab has been trying to solve the structure of a large Arf GEF for some time. Previous efforts have failed or only produced subdomains of the protein (Gustafson, 2017; Richardson et al., 2016). These proteins contain unique domains and the knowledge of what these domains do is limited (Bui et al., 2009; Mouratou et al., 2005). Obtaining the full-length structure will be a vital tool in characterizing these domains. Given that crystallographic efforts have not been successful and its large size, Gea2 is a good candidate for cryoEM.

RESULTS

Gea2 from *Kluyveromyces marxianus*

Gea2 from *K. marxianus* (*K.m.*) was purified from *Pichia pastoris* and was used for cryoEM studies. Gea appears to exist as a long helical repeat molecule with a globular appendage, giving the molecule a “Y” shape (Fig. 2.1-E). Since this the first time we have seen a full length large Arf GEF, we wanted to identify the domains of the particle. There are available crystal structures of DCB-HUS from Sec7 and Gea2 GEF domain (Goldberg, 1998; Richardson et al., 2016). We were able to dock the DCB-HUS crystal structure into the smaller part of the helical repeats (Fig2.1-D) and to dock the GEF crystal structure into the globular appendage (Fig2.1-C) confirming the

``

identification of these domains. CryoEM processing has the caveat of not being able to determine the correct handedness of a reconstruction. We were able to confirm we had the correct hand using the crystal structures. Since we identified the DCB-HUS and GEF domain, the rest of the helical repeat structure must be the HDS1-3 domains. As with the DCB-HUS, at this resolution it appears that they form a single structural element and not “beads on a string.”

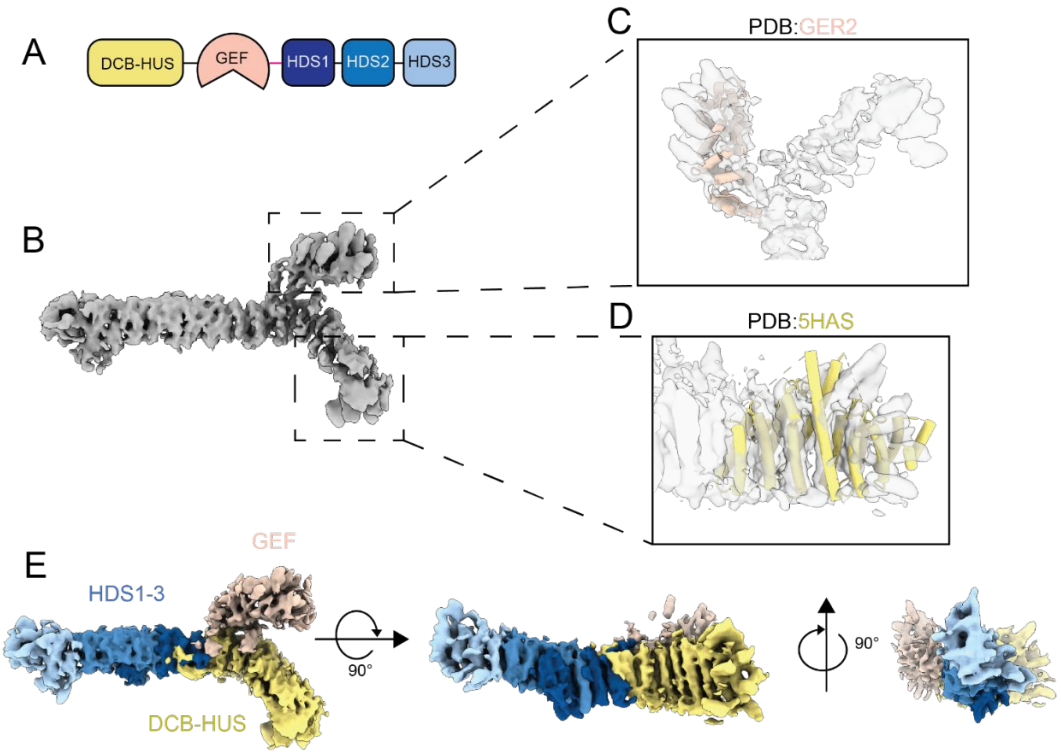

Figure 2.1. Preliminary cryoEM structure of K.m. Gea
(A) Schematic of the Domains of K.m. Gea. DCB: dimerization and cyclophilin binding; HUS: homology upstream of Sec7; GEF: guanine nucleotide exchange factor (aka “Sec7 domain”); HDS: homology downstream of Sec7. (B) Consensus refinement of K.m.Gea. (C) Crystal Structure of the Gea2 GEF domain docked into the cryoEM density. (D) Crystal structure of Sec7 DCB-HUS docked into the cryoEM density (E) CryoEM density of the composite map of K.m. Gea.

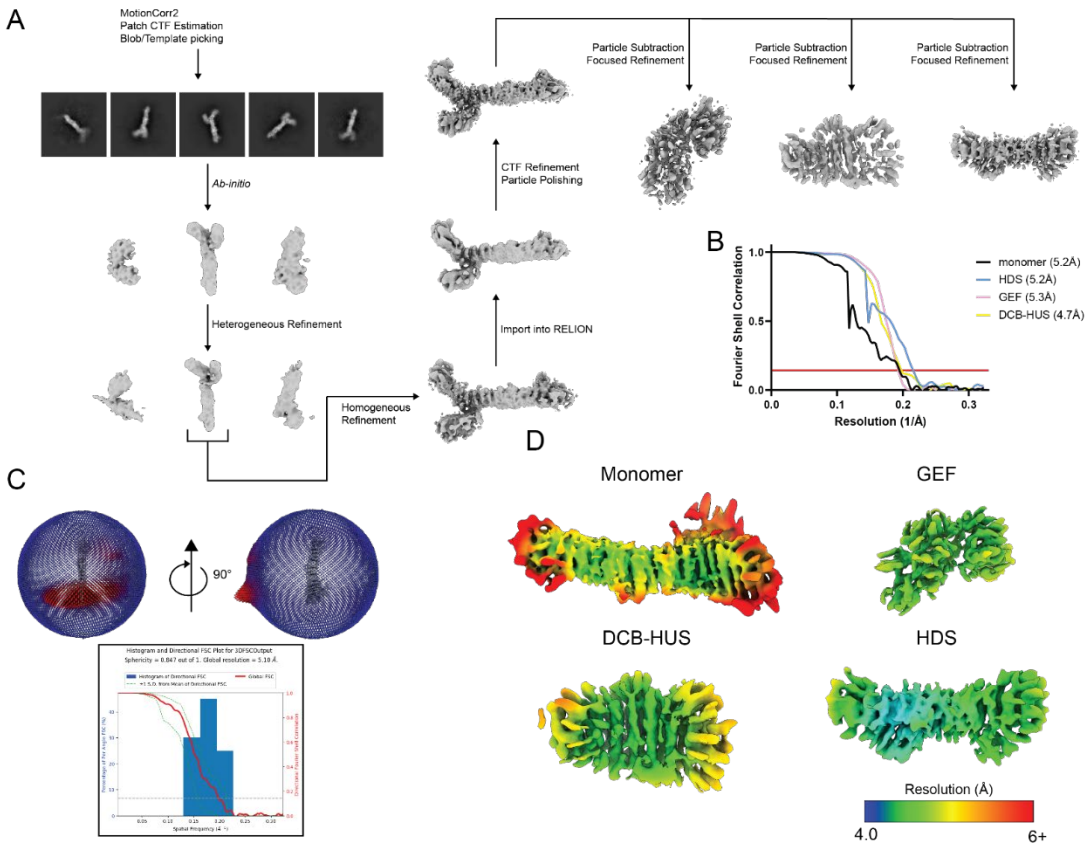

Figure 2.2. CryoEM data processing for K.m. Gea
(A) Flowchart for image processing of K.m. Gea. (B) FSC curves for various maps, red line indicates 0.143 cutoff. (C) Orientation distribution and sphericity plot of consensus refinement. (D) Consensus and focused maps colored by local resolution.

``

We were able to perform standard image processing in cryoSPARC and RELION to obtain consensus reconstruction (Fig. 2.2-A) (Punjani et al., 2017; Zivanov et al., 2018).

Despite having high resolution original images, we were unable to obtain a high-resolution reconstruction. As evident in the 2D classes, our particle was highly orientation biased. We also visualized the particle alignments of the refined reconstruction in Chimera and observed that almost of the particles where focused around the top-down view (Fig. 2.2-C). We quantified the level of anisotropy in our reconstruction by calculating the sphericity value which was 0.85 in our case which is far from the ideal of 0.95 (Aiyer et al., 2021). Orientation bias is impossible to overcome by processing techniques because the information is simply not in the micrographs.

While it appears to be evident that orientation bias is limiting the resolution of this dataset, we wanted to rule out the possibility that flexibility was causing issues with the refinements. To do this we employed computational techniques such as particle subtraction and focused refinements (Nakane et al. 2018). We took our consensus refinement and focused on the DCB-HUS, GEF-Arf1, and HDS1-3 regions individually (Fig. 2.2-A). Masks were made around these regions and used for particle subtraction. Since these domains are smaller, we had to use focused

``

refinements with local searches only. While we did see modest improvement with local refinements, the resolution was still limited (Fig2.2-B,D).

Gea2-Arf1

We then decided to pursue a structure of Gea2 bound to Arf1 in hopes that with adding Arf1 would change how the particles interact with the air-water interface. We purified *S.c.* Gea2 from *Pichia pastoris* and made a complex with ΔNArf1 and attempted to determine the structure by cryoEM. Movies were collected and standard data processing was performed (Fig. 2.5-A,B). Like *K.m.* Gea, we observed both monomer and dimer particles (90:10 ratio) and we split these into separate particle sets for standard cryoEM processing. The monomer appears to be very similar to our *K.m.* Gea2 (Figure 2.4-B). In these datasets we can see extra density in the GEF domain which corresponds to Arf1.

Unfortunately, as with the *K.m.* Gea, S.c. Gea2 also showed a preferred orientation. To overcome this we collected data at 30 degrees and 37 degrees tilt angles (Zi Tan et al. 2017). We added the tilt datasets to the flat data and performed similar orientation bias analysis (Fig. 2.3). It is usual to see a "donut" in the orientations corresponding to the tilt added. In our data we see something similar however the donut appears to be incomplete. We believe this is because with an elongated particle, the refinement is having a hard time

``

making assignments and puts them at either end of the rod. Even with this imperfect alignment, we observed that with the addition of tilt, the sphericity improved from 0.81 to 0.89 and 0.92 with the addition of 30° and 37° tilt respectively (Fig. 2.3 B,D,F). While it appeared we were reducing the effects of preferred orientation, the reconstruction still would not reach high resolution. In attempt to push the data even farther, we again employed particle subtraction and focused refinements (Fig. 2.5-A). While we observed modest improvement in resolution (Fig. 2.5-D), there was no side chain density, and it was not possible to build into any regions.

Previous work has shown that Gea2 is a homodimer (Ramaen et al., 2007; Richardson et al., 2016) but only ~10% of our particles appear to be dimers. We set to classify and refine those particles in hope that perhaps that the dimer might interact with the air-water interface differently. We were able to process these particles separately and obtain an initial low-resolution reconstruction of the dimer (Fig. 2.4-C, 2.5-B). The dimer's domains adopt a similar organization, and the two protomers dimerize via the DCB-HUS domain consistent with previous reports (Ramaen et al., 2007). Our data was limited not only by orientation bias but also a limited number of particles. For these reasons we were unable to obtain a high resolution structure of the Gea2-Arf1 dimer using this dataset.

``

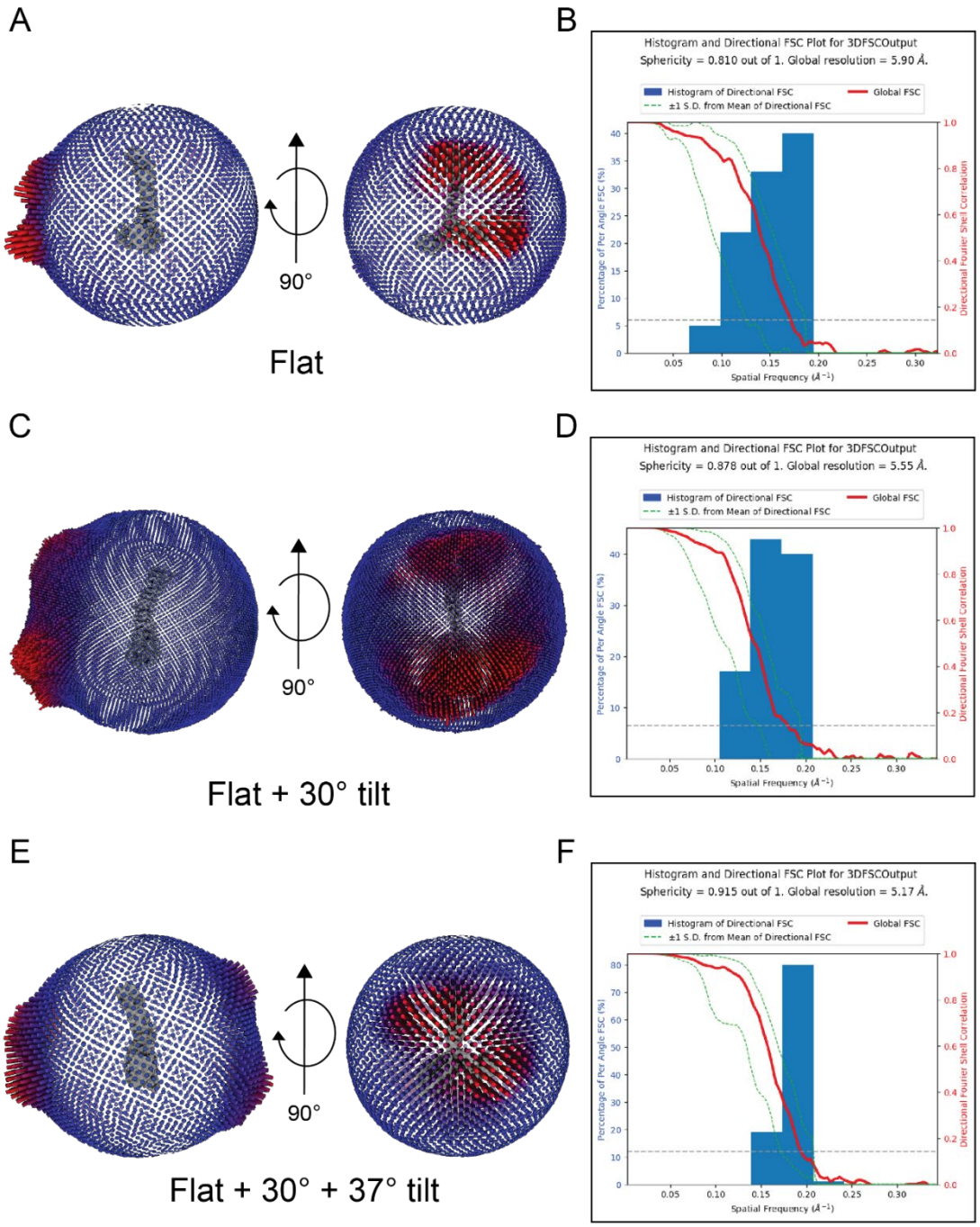

Figure 2.3. Assessment of the orientation bias of Gea2-Arf1
(A)Particle orientation distribution for flat data. (B). Output of ThreeDFSC analysis for flat data. (C)Particle orientation distribution for flat plus 30° data. (D). Output of ThreeDFSC analysis for flat plus 30° data. (E) Particle orientation distribution for flat plus 30°and 37° data. (F). Output of ThreeDFSC analysis for flat plus 30°and 37° data.

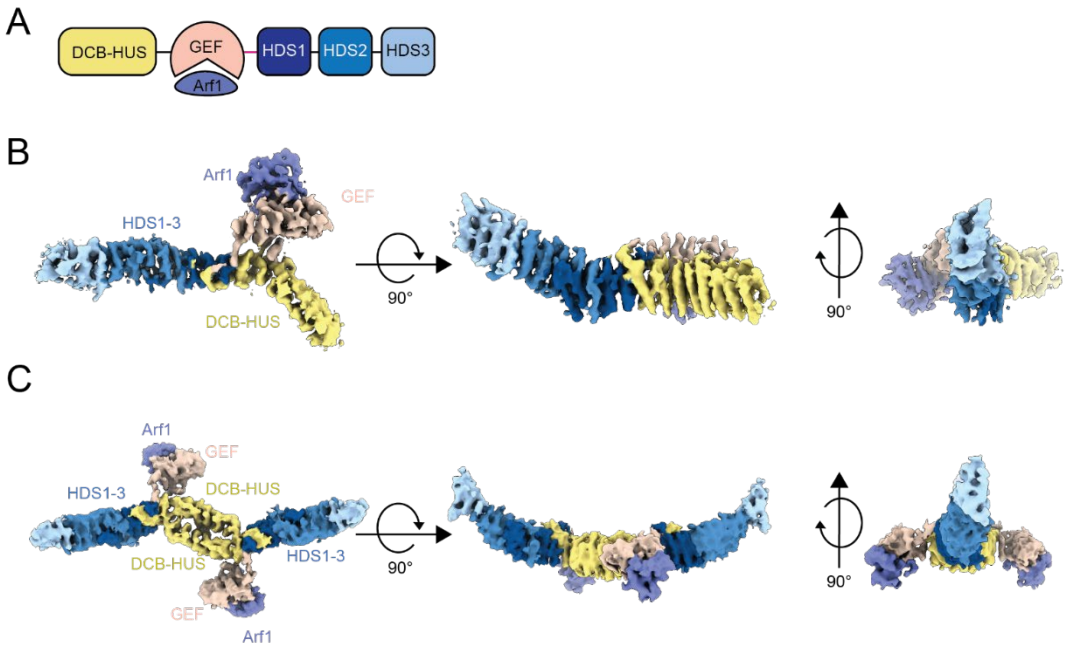

Figure 2.4. Prelimary CryoEM structure of the Gea2-Arf1 complex
(A) Schematic of Gea2-Arf1 domains. (B) Composite cryoEM structure of Gea2-Arf1 monomer complex. (C) Consensus reconstruction of Gea2-Arf1 complex dimer.

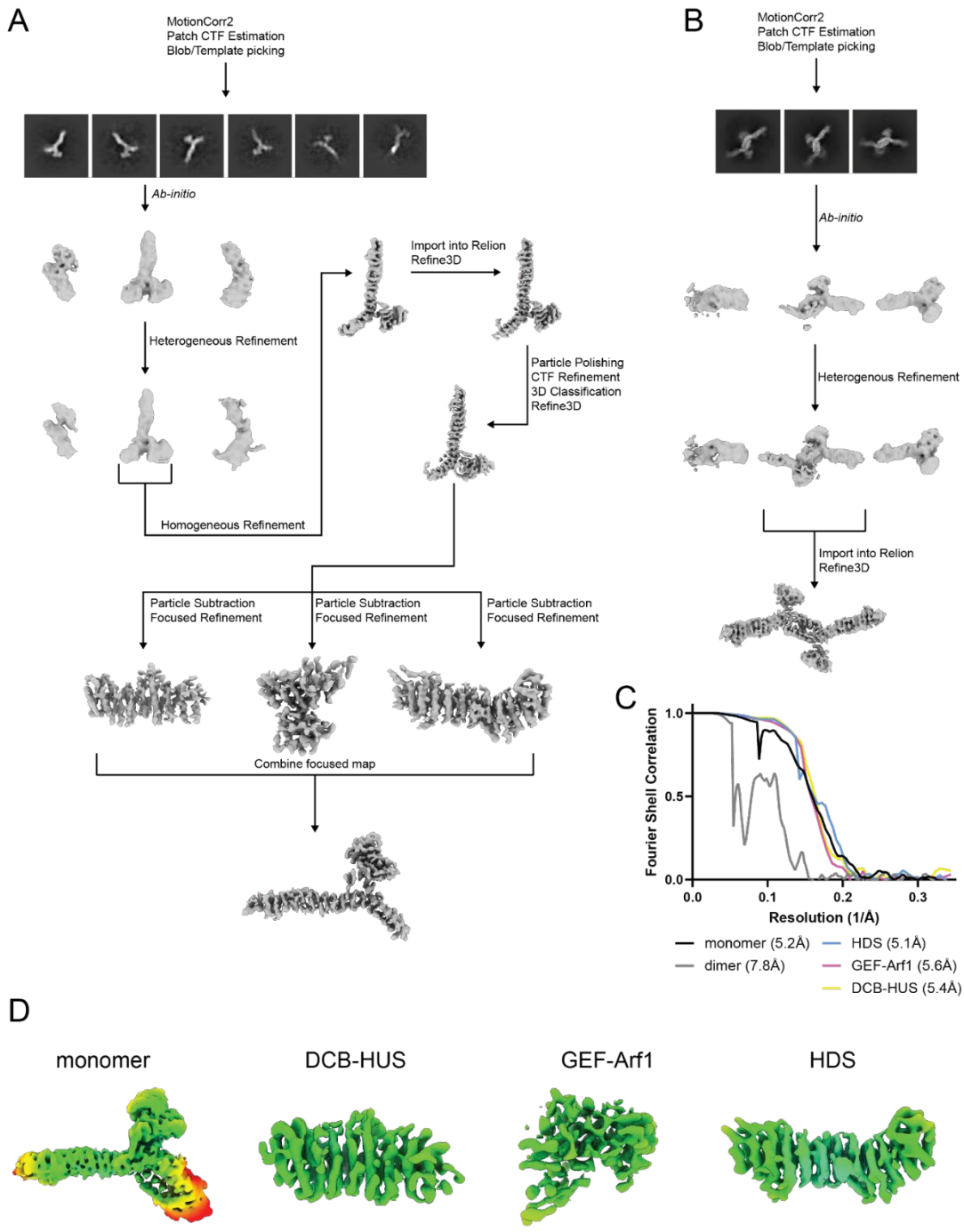

Figure 2.5. Data processing for Gea2-Arf1 complex

(A) CryoEM image processing flowthrough for Gea2-Arf1 monomer. (B) CryoEM image processing flowthrough for Gea2-Arf1 dimer. (C) FSC Curves for maps. Red line denotes 0.143 cut off. (D) CryoEM maps colored by local resolution

``

DISCUSSION

Even though we were unable to determine a high-resolution reconstruction with these datasets, there is still some information gained from the low-resolution reconstructions. We were able to dock known crystal structures into multiple domains to identify the DCB-HUS and GEF domains, and the position of bound substrate Arf1, in our structure. Similar to the DCB-HUS domain, the HDS1-3 domains appear to form a single structural unit consisting of helical repeats.

Orientation bias was a major problem with processing our data. We tried adding tilt data to overcome this issue. Although adding the tilt provided new orientations and increased sphericity, the resolution of our reconstruction did not significantly increase. Collecting data with a tilt introduces more issues in the collection process. During data collection, the energy from the electron beam causes motion that moves the particles, and we correct for that in the processing. Since we are collecting projection images, when the stage is flat the motion in the Z direction not observed. But when stage is tilted, there is now another dimension for motion to be observed and affect the data. The higher the tilt angle, the more motion that is added to your sample. So, while we were adding missing views in our reconstruction, the additional motion could be affecting the quality of these particles. Another issue with tilted micrographs is that there is a wide range of defocus across particles in the same micrograph. We did our best efforts to correct for this by using per-

``

particle defocus refinements and performing particle polishing. We were still unable to produce a high-resolution structure.

We assume that Gea2 binding the air-water interface is what causes the orientation bias. This could also cause Gea2 to partially denature at this interface. Evidence for this possibility is that in our high-resolution data obtained using detergent, Gea2 is a dimer that does not appear to interact with the air-water interface. This suggests that in the absence of detergent, Gea2 dimers could dissociate at the air-water interface

``

CHAPTER 3

STRUCTURAL BASIS FOR ACTIVATION OF ARF1 AT THE GOLGI COMPLEX

*The work presented in this chapter has been posted to bioRxiv and is has been accepted in principle at Cell Reports. *

INTRODUCTION

The endomembrane system provides essential compartmentalization for all eukaryotic cells. Most transmembrane and lumenal proteins are synthesized at the ER and then travel through the secretory pathway to reach their target organelle. At the center of the secretory pathway is the Golgi complex, which modifies secretory proteins and serves as a trafficking hub. Arf1 and its close paralogs are essential regulators of cargo sorting and vesicle formation at the Golgi complex that function by recruiting a large number of prominent effectors including COPI/coatomer, clathrin cargo adaptors, lipid signaling enzymes, vesicle tethers, and regulators of other GTPases (Adarska et al., 2021; Cherfils, 2014; Donaldson and Jackson, 2011; Gillingham and Munro, 2007). Arf1 is a GTPase, cycling between an inactive GDP-bound state and an active GTP-bound state (Kahn and Gilman, 1986). Arf1 possesses an N-terminal myristoylated amphipathic helix that anchors it to the Golgi membrane (Haun et al., 1993; Kahn et al., 1988). When GDP-bound, this membrane-binding feature is masked and Arf1 is cytosolic. When Arf1 is activated to its GTP-bound state, a change in conformation exposes the myristoylated amphipathic helix, resulting in stable membrane-association

``

(Amor et al., 1994;Antonny et al., 1997; Franco et al., 1995; Goldberg, 1998). The active conformation of Arf1 is therefore required to recruit its numerous effectors to the Golgi membrane surface.

Arf1 activation in cells requires nucleotide exchange by specific guanine-nucleotide exchange factors (GEFs). Arf1 is activated at the Golgi complex by at least two distinct but related Arf-GEFs, GBF1 and BIG1/2 (Claude et al., 1999; Togawa et al., 1999). The budding yeast homolog of BIG1/2 is Sec7, which localizes to late Golgi compartments and activates Arf1 to control trafficking to endosomes and the plasma membrane (Franzusoff et al., 1991; Novick et al., 1981). The budding yeast homologs of GBF1, named Gea1/2, localize to early and medial Golgi compartments where Arf1 activation orchestrates the formation of COPI vesicles destined for the endoplasmic reticulum and earlier Golgi compartments (Gustafson and Fromme, 2017; Peyroche et al., 1996; Spang et al., 2001).

The Golgi Arf-GEFs share a homologous GEF domain, referred to as a “Sec7” domain, with members of other Arf-GEF families (Casanova, 2007). The structural and biochemical basis for nucleotide exchange by Sec7 GEF domains is well-established, and involves remodeling of the Arf1 nucleotide-binding site by interaction with the GEF (Goldberg, 1998; Renault et al., 2003). The ARNO/cytohesin/Grp1 and BRAG/IQSec7 Arf-GEFs possess structurally characterized plekstrin homology (PH) domains that direct membrane binding

``

and regulation of GEF activity (Aizel et al., 2013; Cronin et al., 2004; Das et al., 2019; DiNitto et al., 2007; Malaby et al., 2018). In contrast, the Golgi-localized “large” Arf-GEFs do not contain PH domains and instead contain multiple regulatory domains that are conserved across species but are not found in other proteins (Bui et al., 2009; Mouratou et al., 2005). Previous studies have dissected the biochemical and cell biological roles of these regulatory domains, and identified which domains are required for Golgi membrane binding and activation of Arf1 (Bouvet et al., 2013; Christis and Munro, 2012; Gustafson and Fromme, 2017; Meissner et al., 2018; Pocognoni et al., 2018; Richardson and Fromme, 2012; Richardson et al., 2012). Structures are available for the N-terminal ‘DCB-HUS’ domains in isolation (Galindo et al., 2016; Richardson et al., 2016; Wang et al., 2016), but the lack of structural information for the full-length proteins has prevented an understanding of how the regulatory domains function together with the GEF domain during Arf1 activation.

Here we present cryoEM structures of full-length Gea2 and a Gea2-Arf1 activation intermediate. These structures reveal the organization of the regulatory domains within the Gea2 dimer. We identify two new conserved structural elements in Gea2, one is an amphipathic helix within the HDS2 domain that is required for membrane binding, and the other is an ordered linker between the GEF and HDS1 domains. Unexpectedly, the GEF domain of Gea2 adopts two conformational states. Structural analysis indicates that

``

the GEF-HDS1 linker plays a role in conformational switching: the “closed” state of the GEF domain is compatible with initial binding to Arf1-GDP but incompatible with subsequent binding to nucleotide-free Arf1 due to a steric clash between nucleotide-free Arf1 and the linker. The structural data therefore suggest that the Arf1 nucleotide exchange reaction involves conformational change of its GEF from the closed state to the “open” state. Based on the orientation of Gea2 on the membrane, this GEF conformational change appears to directly couple Arf1 activation to membrane insertion.

RESULTS

Architecture of the Gea2 homodimer

Gea2 and its paralogs possess an N-terminal DCB-HUS regulatory domain and C-terminal HDS1, HDS2, and HDS3 regulatory domains (Mouratou et al., 2005) (Fig. 3.1A). We produced full-length *S. cerevisiae* Gea2 by overexpression in *Pichia pastoris* (Fig. 3.2A) and determined its structure using cryoEM (Figs 3.3,3.4). 3D classification of the particles revealed three distinct conformations of Gea2 homodimers that differed only in the positioning of the GEF domain, with each monomer adopting either an “open” or “closed” position relative to the regulatory domains (Fig. 3.3). Based on the relative numbers of particle images that sorted into each of these three classes (~30% “closed/closed”, ~30% “open/open”, and ~40% “closed/open”), the conformation adopted by each monomer within the dimer appears to be independent of that of its binding partner. We took advantage of the 2-fold

``

symmetry of the Gea2 homodimer by using symmetry expansion and focused refinements during data processing (see Methods) to obtain higher resolution maps for the closed and open monomers and for the three different dimeric states (Figs. 3.1B and 3.5). These maps were then used to build and refine atomic models (Figs. 3.1C and 3.5, Table 3.1). We begin our description of the structure using the “closed/open” dimer as it exhibits both the open and closed states of the GEF domain.

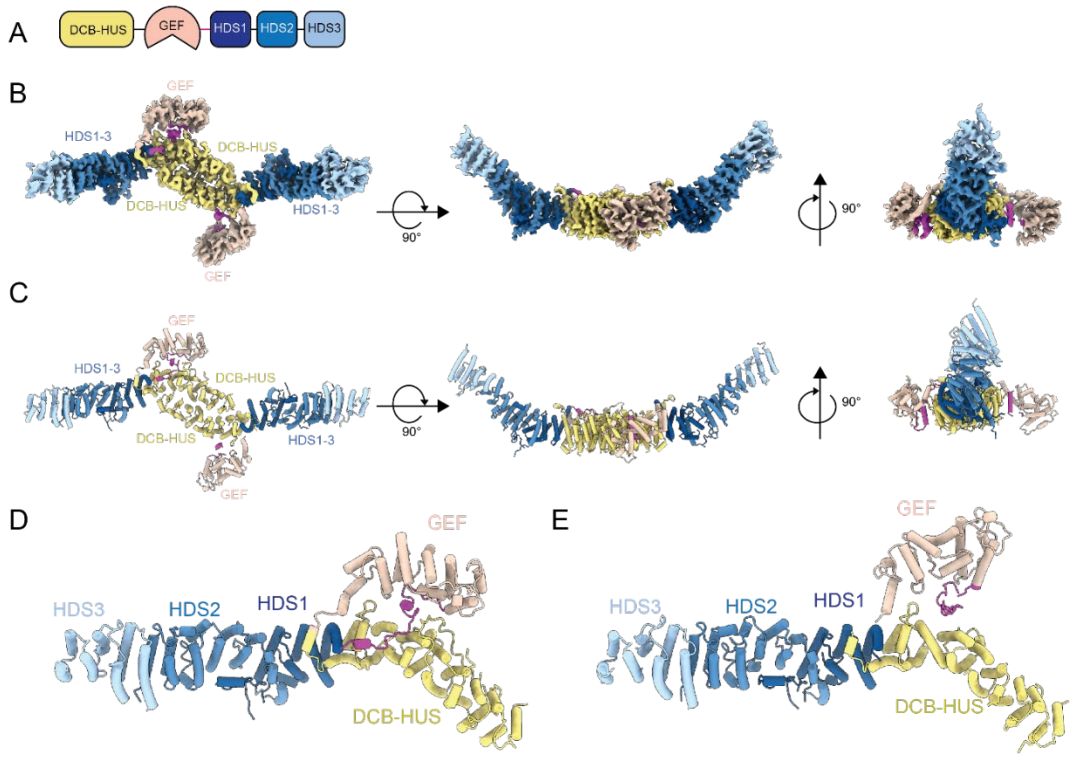

Figure 3.1. Structure of Gea2 determined by cryoEM
A) Schematic of Gea2 primary structure indicating conserved domains. DCB: dimerization and cyclophilin binding; HUS: homology upstream of Sec7; GEF: guanine nucleotide exchange factor (aka “Sec7 domain”); HDS: homology downstream of Sec7. B) CryoEM density of the Gea2 dimer in its closed/open conformation. One monomer adopts an open conformation of the GEF domain, the other monomer adopts a closed conformation. The GEF-HDS1 linker is colored magenta. C) Atomic model of the Gea2 dimer, shown in cartoon depiction. D) Close-up view of the closed monomer. E) Close-up view of the open monomer.

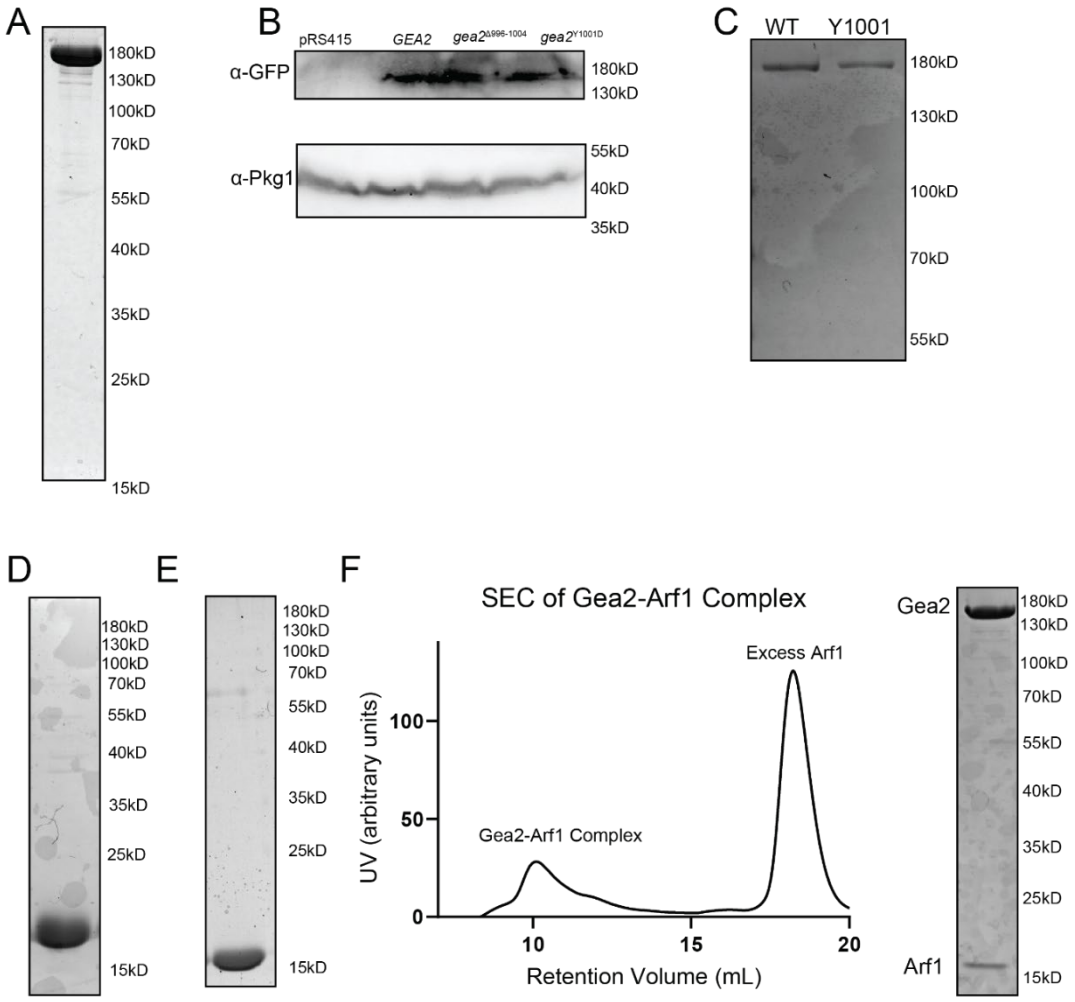

Figure 3.2. Protein reagents used in this study.
A) SDS-PAGE analysis of *S. cerevisiae* Gea2 purified from *P. pastoris.* B) Immunoblot showing expression of Gea2-GFP constructs used in yeast localization experiments. C) SDS-PAGE analysis of wild-type and Y1001D mutant *S. cerevisiae* Gea2 proteins purified from *P. pastoris.* D) SDS-PAGE analysis of Myristoylated, full-length *S. cerevisiae* Arf1 purified from *E. coli*. E) SDS-PAGE analysis of ΔN17-mutant *S. cerevisiae* Arf1 purified from *E. coli*. F) Gel filtration chromatography trace and SDS-PAGE analysis of the Gea2-Arf1 activation intermediate complex

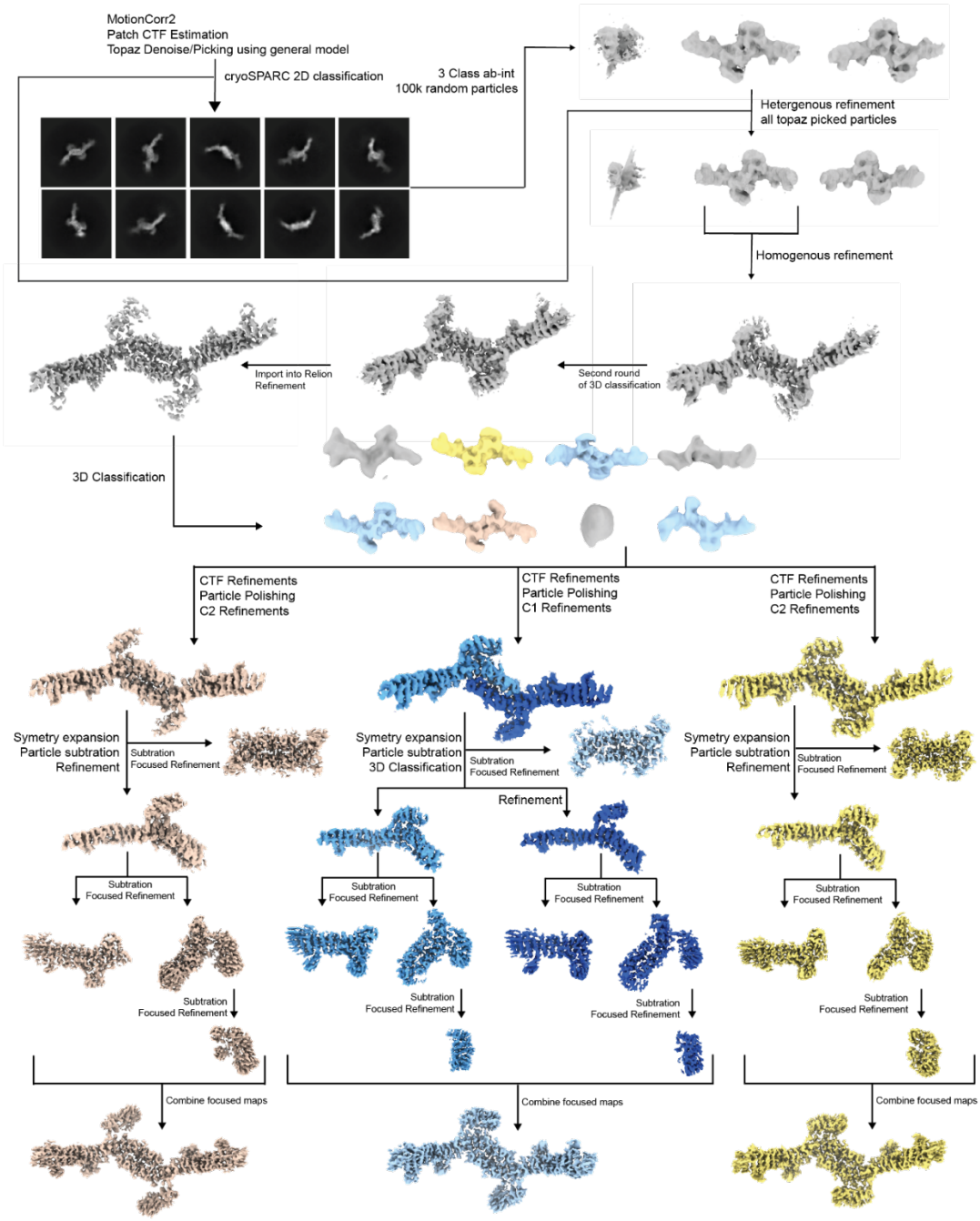

Figure 3.3. Gea2 cryoEM data processing
Flowchart illustrating the data processing strategy for the Gea2 cryoEM data (see Methods).

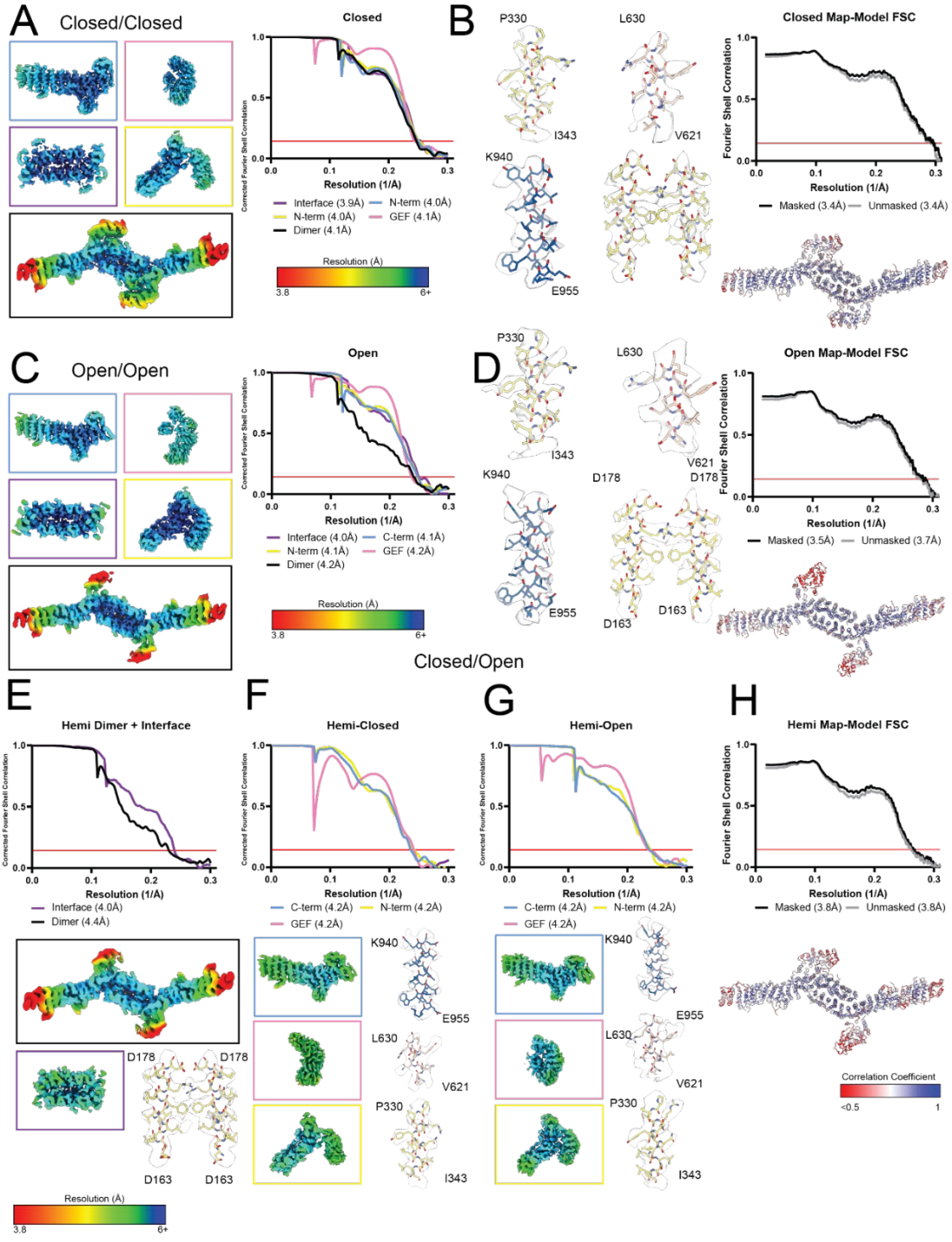
A
Closed/Closed
Closed
Corrected Fourier Shell Correlation
Resolution (1/Å)
Interface (3.9Å)
N-term (4.0Å)
N-term (4.0Å)
GEF (4.1Å)
Dimer (4.1Å)
Resolution (Å)
3.8
6+
B
P330
I343
K940
E955
L630
V621
Closed Map-Model FSC
Fourier Shell Correlation
Masked (3.4Å)
Unmasked (3.4Å)
C
Open/Open
Open
Interface (4.0Å)
C-term (4.1Å)
N-term (4.1Å)
GEF (4.2Å)
Dimer (4.2Å)
D
D178
D163
Open Map-Model FSC
Masked (3.5Å)
Unmasked (3.7Å)
Closed/Open
E
Hemi Dimer + Interface
Interface (4.0Å)
Dimer (4.4Å)
F
Hemi-Closed
C-term (4.2Å)
N-term (4.2Å)
GEF (4.2Å)
G
Hemi-Open
H
Hemi Map-Model FSC
Masked (3.8Å)
Unmasked (3.8Å)
Correlation Coefficient
<0.5
1

``

Figure 3.4. Gea2 cryoEM map and model validation
A) Fourier shell correlation plots and example cryoEM density for focused refinements are shown for the cryoEM map and model of the Gea2 closed/closed conformation. B) Same but for the open/open conformation. C) Same but for the closed/open conformation. Note that the open conformation of the GEF domain exhibits more flexibility compared to the closed conformation.

``

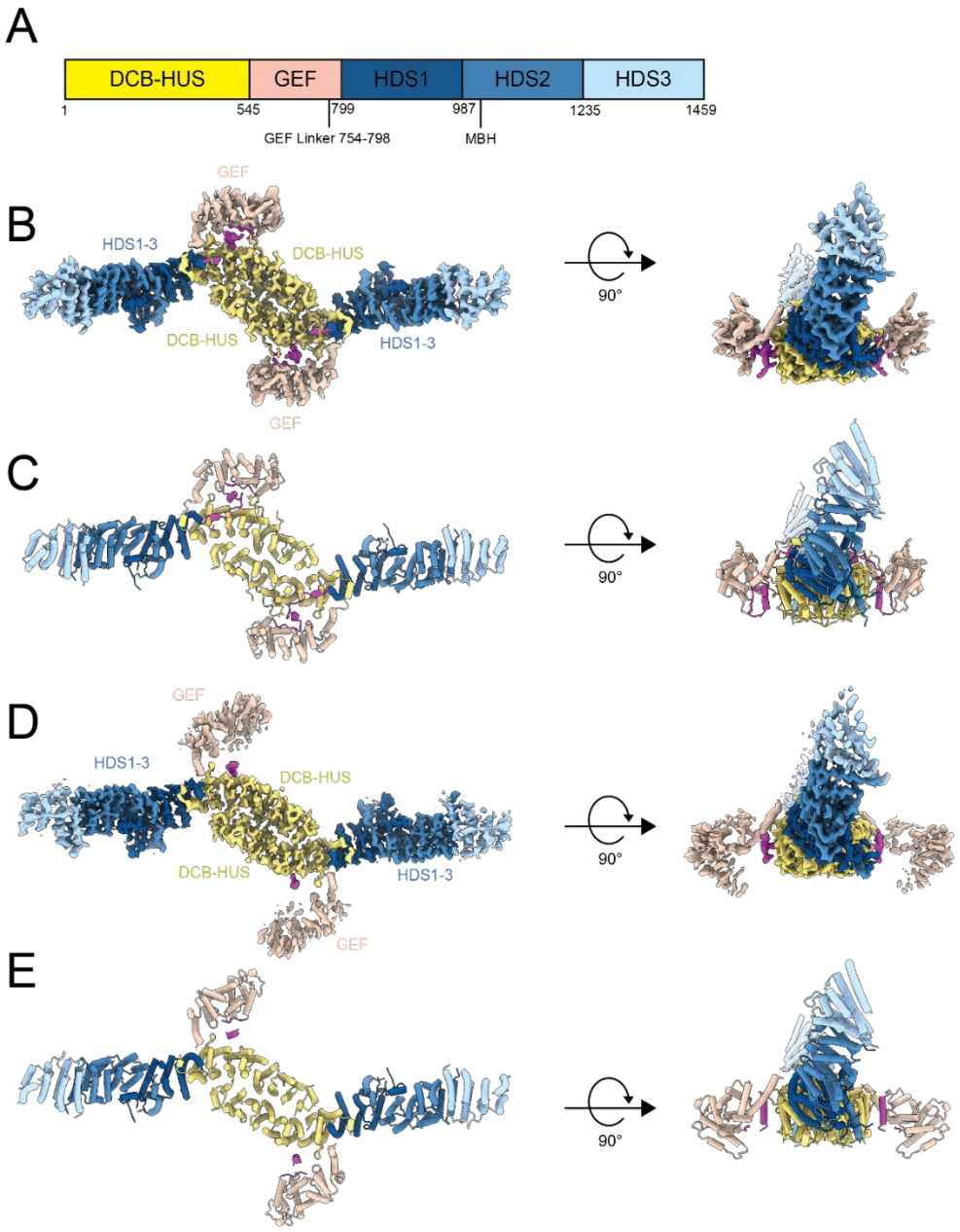

Figure 3.5. The closed/closed and open/open conformations of Gea2
A) CryoEM density of the Gea2 dimer in its closed/closed conformation. Coloring as in Fig. 1, the GEF-HDS1 linker is colored magenta. B) Atomic model of the Gea2 closed/closed dimer, shown in cartoon depiction. C) CryoEM density of the Gea2 dimer in its open/open conformation. Coloring as in Fig. 1, the GEF-HDS1 linker is colored magenta. D) Atomic model of the Gea2 open/open dimer, shown in cartoon depiction

``

	Gea2 closed/open (composite map)	Gea2 closed/open (consensus map)	Gea2 closed/closed (composite map)	Gea2 closed/closed (consensus map)	Gea2 open/open (composite map)	Gea2 open/open (consensus map)	Gea2-Arf1 complex (composite map)	Gea2-Arf1 complex (consensus map)
Nominal magnification	**63000**							
Voltage (kV)	**200**							
Total dose (e-/Å^2)	**50**							
Defocus range (μm)	**-1.0 to -2.0**							
Pixel Size (Å)	**1.29**						**1.30**	
Symmetry imposed	**N/A**	**C1**	**N/A**	**C2**	**N/A**	**C2**	**N/A**	**C2**
Particle images		**101014**		**83665**		**74385**		**391360**
Map resolution, 0.143-FSC (Å)		**4.7**		**5.1**		**5.1**		**4.23**
Map sharpening B factor	**N/A**	**-76**	**N/A**	**-83**	**N/A**	**-73**	**N/A**	**-167**
# atoms	**38358**	**N/A**	**39735**	**N/A**	**36590**	**N/A**	**42915**	**N/A**
# protein residues	**2360**		**2448**		**2242**		**2647**	
B factor, protein	**186.1**		**145.70**		**124.29**		**124.83**	
R.m.s deviation, bond length (Å)	**0.006**		**0.006**		**0.006**		**0.006**	
R.m.s. deviation, bond angles	**1.039**		**0.969**		**0.976**		**0.944**	
MolProbity score	**1.68**		**1.62**		**1.49**		**1.57**	
Clashscore	**5.26**		**4.96**		**3.69**		**5.13**	
Poor rotamers (%)	**0.68**		**0.48**		**0.38**		**0.04**	
Ramachandran plot								

``

Favored (%)	94.03		94.85		95.28		95.68	
Allowed (%)	5.89		5.11		4.54		4.28	
Disallowed (%)	0.09		0.04		0.18		0.04	

Table 3.1 CryoEM data collection, processing and model validation statistics

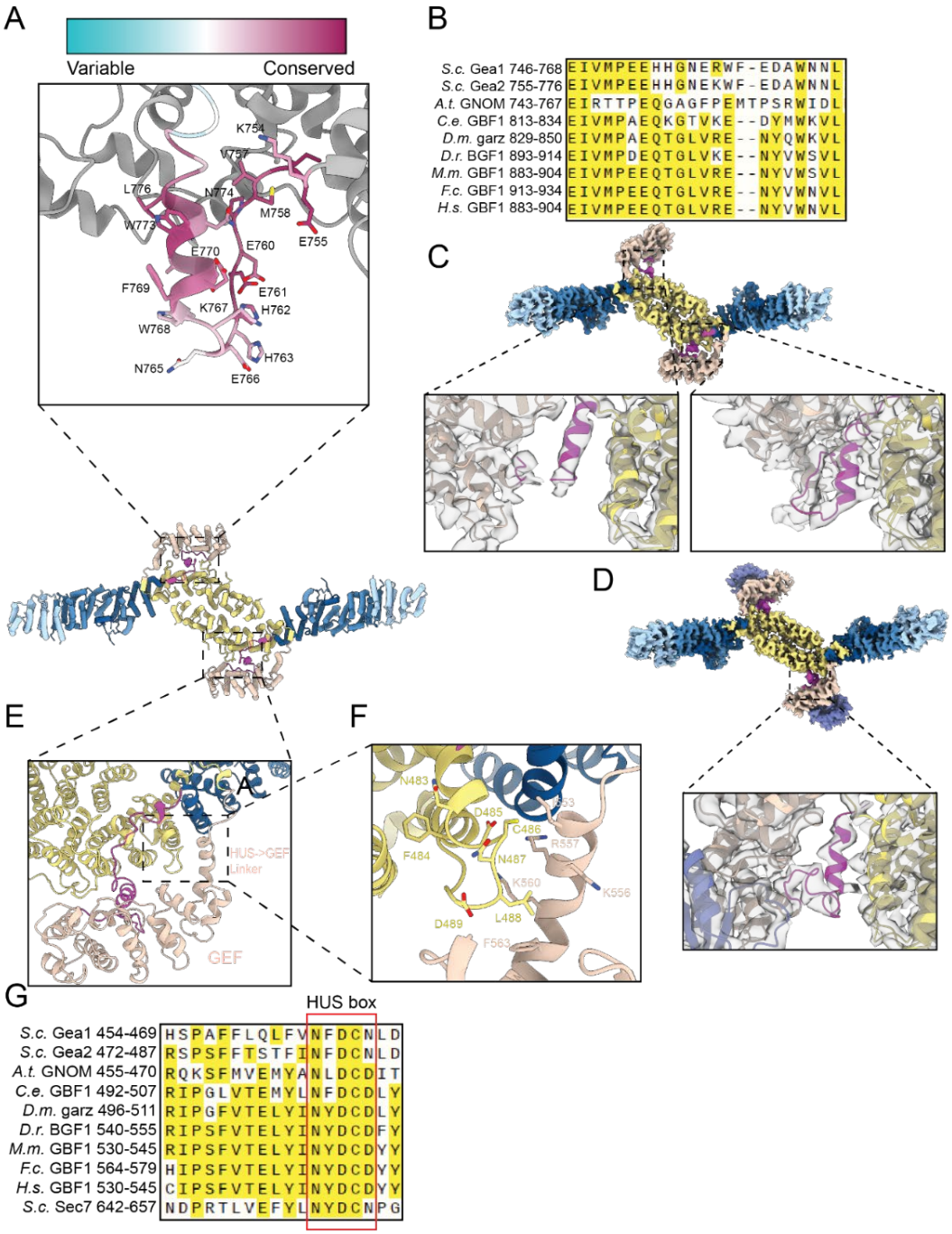
A
Variable
Conserved
K754
V757
L776
N774
M758
W773
E755
E760
E770
F769
E761
K767
H762
W768
H763
N765
E766
B
S.c. Gea1 746-768 EIVMPEEHHGNERWF-EDAWNNL
S.c. Gea2 755-776 EIVMPEEHHGNEKWF-EDAWNNL
A.t. GNOM 743-767 EIRTTPEQGAGFPEMTPSRWIDL
C.e. GBF1 813-834 EIVMPAEQKGTVKE--DYMWKVL
D.m. garz 829-850 EIVMPAEQTGLVRE--NYQWKVL
D.r. BGF1 893-914 EIVMPDEQTGLVKE--NYVWSVL
M.m. GBF1 883-904 EIVMPEEQTGLVRE--NYVWSVL
F.c. GBF1 913-934 EIVMPEEQTGLVRE--NYVWNVL
H.s. GBF1 883-904 EIVMPEEQTGLVRE--NYVWNVL
C
D
E
A
HUS->GEF
Linker
GEF
F
N483
D485
C486
F484
N487
K560
K556
D489
L488
F563
G
HUS box
S.c. Gea1 454-469 HSPAFFLQLFVNFDCNLD
S.c. Gea2 472-487 RSPSFFTSTFINFDCNLD
A.t. GNOM 455-470 RQKSFMVEMYANLDCDIT
C.e. GBF1 492-507 RIPGLVTEMYLNFDCDLY
D.m. garz 496-511 RIPGFVTELYINYDCDLY
D.r. BGF1 540-555 RIPSFVTELYINYDCDFY
M.m. GBF1 530-545 RIPSFVTELYINYDCDYY
F.c. GBF1 564-579 HIPSFVTELYINYDCDYY
H.s. GBF1 530-545 CIPSFVTELYINYDCDYY
S.c. Sec7 642-657 NDPRTLVEFYLNYDCNPG

``

Figure 3.6. Ordered linkers connect the GEF domain to the HUS and HDS1 domains

A) Close-up view of the GEF-HDS1 linker in the closed monomer colored by conservation as indicated. B) Sequence alignment of the GEF-HDS1 linker from Gea2 homologs in several model organisms and humans. Yellow highlights indicate identical residues at a given position. C) Views of the GEF-HDS1 linker cryoEM density in the open (left) and closed (right) monomers. D) View of the GEF-HDS1 linker cryoEM density in the Gea2-Arf1 complex. E,F) Close-up views of the HUS-GEF linker and 'HUS-box' region in the closed monomer. G) Sequence alignment of the HUS-GEF linker from Gea2 homologs in several models organisms and humans. Yellow highlights indicate identical residues at a given position.

``

The HDS1, 2, and 3 domains form an extended helical repeat structure that is contiguous with the DCB-HUS domain, such that the HDS3 domains of each monomer lie at the distal ends of the homodimer (Fig. 3.1B,C). The GEF domain lies adjacent to the HUS domain and is connected to the HUS and HDS1 domains through ordered linker regions (Fig. 3.6). The “HUS box”, which is a conserved region near the C-terminal end of the HUS domain (Mouratou et al., 2005), interacts directly with the HUS-GEF linker, which is simply an extension of the first α-helix of the GEF domain (Fig. 3.6E-G). Temperature sensitive mutations have been identified in the region surrounding the HUS box (Park et al., 2005), lending support to the importance of this interaction. The linker that connects the GEF domain to the HDS1 domain (GEF-HDS1 linker) comprises ~45 conserved ordered residues and is discussed in detail further below (Fig. 3.6A-C).

Dimerization occurs through extensive hydrophobic, polar, and electrostatic interactions between the DCB-HUS domains of each monomer (Fig. 3.7A-F), consistent with the established role of this domain for dimerization of Gea2/GBF1 homologs (Bhatt et al., 2016; Grebe et al., 2000; Ramaen et al., 2007). The fold of the Gea2 DCB-HUS domain is quite similar to that of the distinct Arf-GEF Sec7 (Richardson et al., 2016), although this domain does not appear to mediate dimerization of Sec7. Previous studies identified substitution mutations in the DCB subdomain of GBF1 that disrupted its dimerization, in residues corresponding to K124 and D163 in Gea2 (Bhatt et al., 2016; Ramaen et al., 2007). Examination of the dimerization interface

``

indicates that K124 is involved in favorable interactions between monomers (Fig. 3.7E). Therefore the observed dimerization interface is supported by these published functional results and likely conserved across Gea2/GBF1 paralogs in different species.

Gea2 binds to the Golgi via a conserved amphipathic helix

Several Arf-GEFs possess pleckstrin homology (PH) domains that bind to membranes via specific interactions with phosphoinositide lipids (Casanova, 2007). The Golgi Arf-GEFs do not possess a PH domain and though the HDS1-3 domains are known to be important for Golgi localization of Gea1/2 and GBF1 (Bouvet et al., 2013; Gustafson and Fromme, 2017; Meissner et al., 2018; Pocognoni et al., 2018), their membrane binding mechanism is unknown.

Analysis of the Gea2 cryoEM structures revealed the presence of an unstructured but conserved sequence in the linker between the HDS1 and HDS2 domains (Fig. 3.8A-C). This sequence is predicted to form an amphipathic helix by both secondary and tertiary sequence prediction methods (Fig. 3.8D). We reasoned that its conservation, position, and flexible connection to the rest of the protein made this sequence a strong candidate for a membrane-inserting amphipathic helix (Drin and Antonny, 2010). We note that this helix is distinct from amphipathic helices in the HDS1-2 domains previously proposed by other groups to be important for membrane-binding.

``

Our structural data indicate that the amphipathic helices previously studied by others are instead part of the core helical repeat structure of these domains. As the hydrophobic faces of these helices are buried within the hydrophobic protein interior, they are unavailable for membrane interaction.

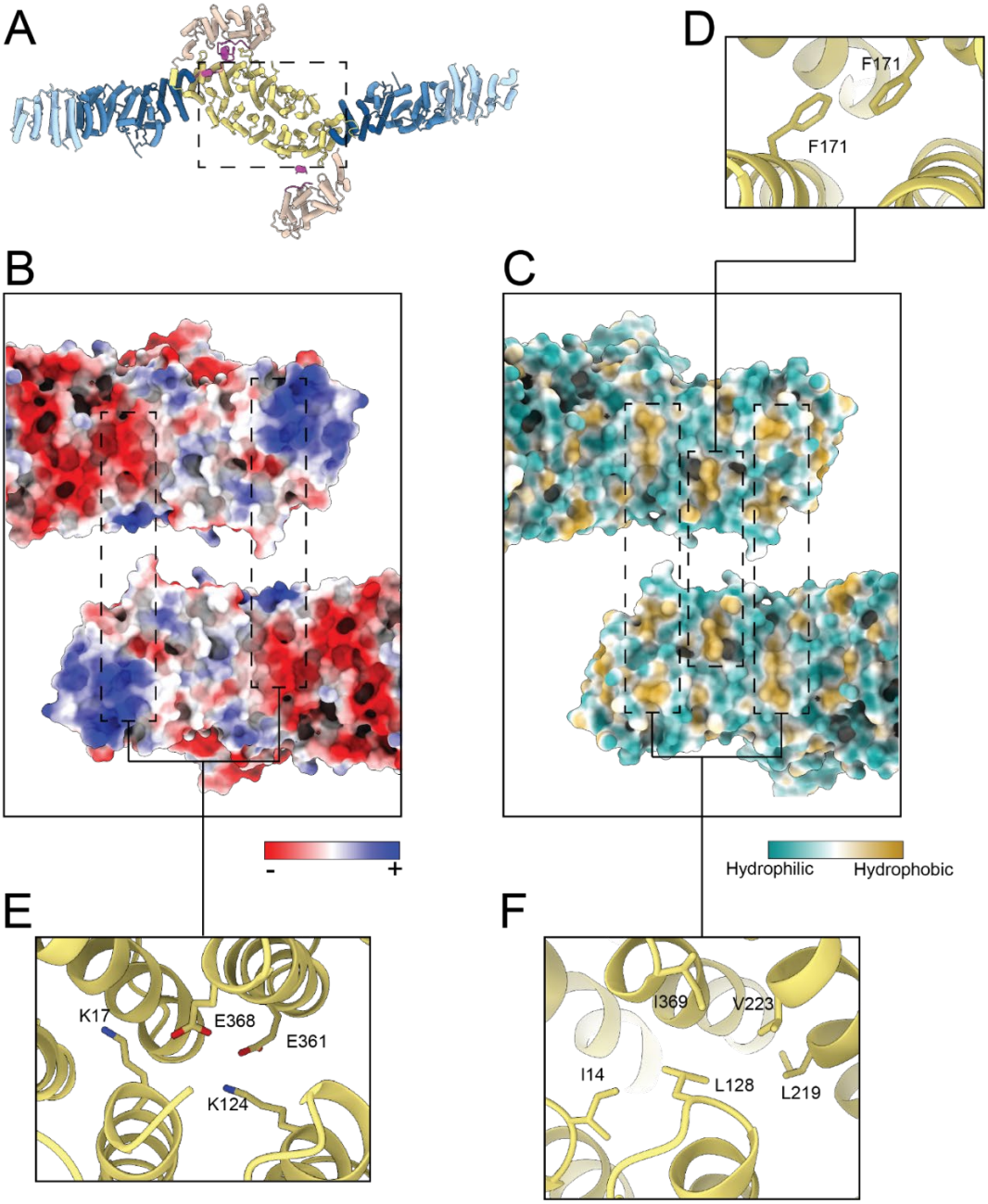

Figure 3.7. Gea2 dimerizes via the DCB-HUS domains
A) Gea2 dimer with a dashed box indicating the region depicted in (B) and (C). B) View of the dimerization interface peeled apart and colored by calculated charge potential. C) View of the dimerization interface peeled apart and colored by hydrophobicity. D-F) Close-up views highlighting residues involved in the dimerization interface.

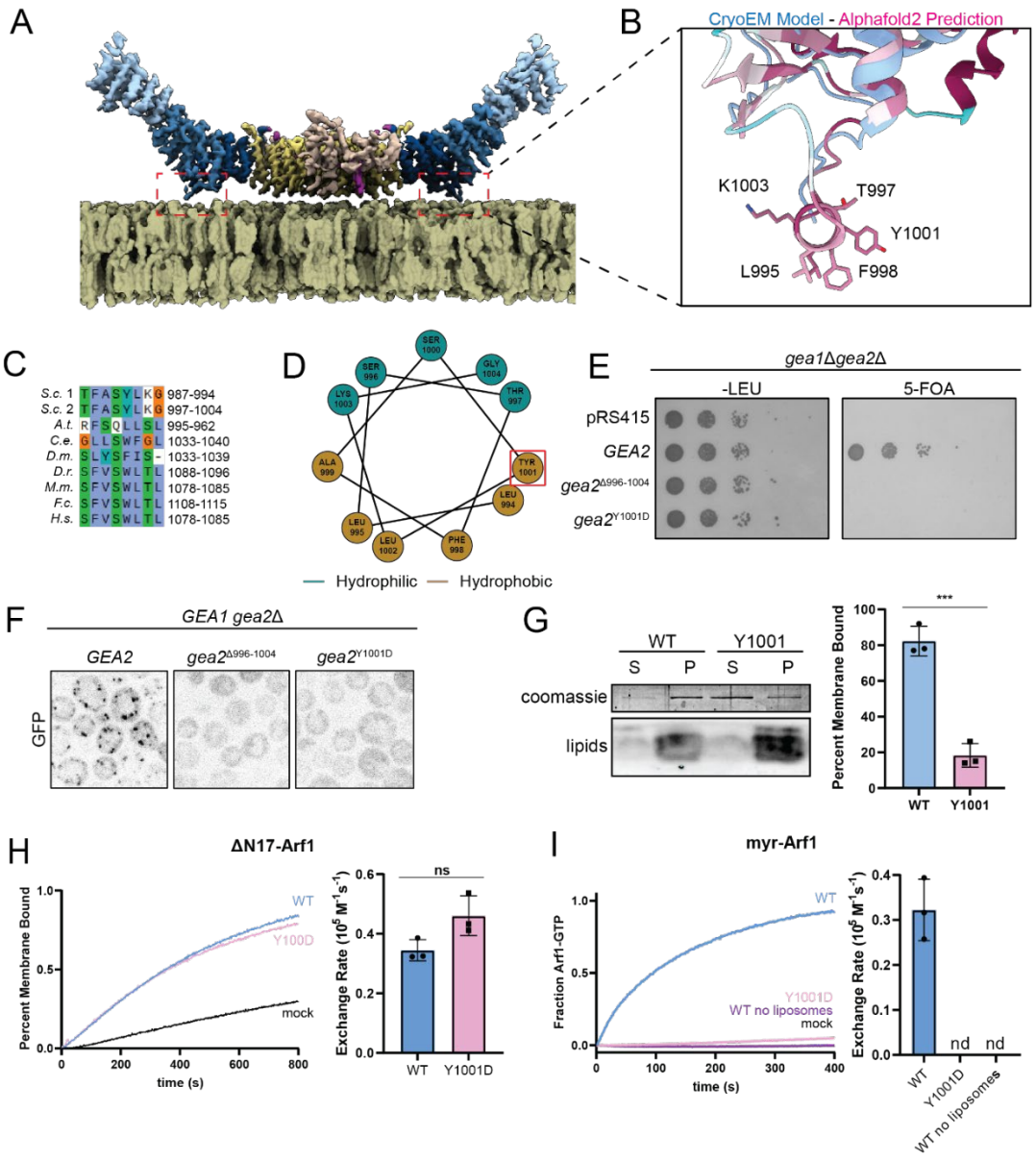
A
B
CryoEM Model - Alphafold2 Prediction
K1003
T997
Y1001
L995
F998
C
S.c. 1 TFASYLKG 987-994
S.c. 2 TFASYLKG 997-1004
A.t. RFSQLLSL 995-962
C.e. GLLSWFGL 1033-1040
D.m. SLYSFIS- 1033-1039
D.r. SFVSWLTL 1088-1096
M.m. SFVSWLTL 1078-1085
F.c. SFVSWLTL 1108-1115
H.s. SFVSWLTL 1078-1085
D
Hydrophilic
Hydrophobic
E
gea1Δgea2Δ
-LEU
5-FOA
pRS415
GEA2
gea2Δ996-1004
gea2Y1001D
F
GEA1 gea2Δ
GEA2
gea2Δ996-1004
gea2Y1001D
GFP
G
WT
Y1001
S
P
S
P
coomassie
lipids
Percent Membrane Bound
***
WT
Y1001
H
ΔN17-Arf1
Percent Membrane Bound
time (s)
WT
Y100D
mock
Exchange Rate (10^5 M^-1 s^-1)
ns
WT
Y1001D
I
myr-Arf1
Fraction Arf1-GTP
time (s)
WT
Y1001D
WT no liposomes
mock
Exchange Rate (10^5 M^-1 s^-1)
nd
nd
WT
Y1001D
WT no liposomes

``

Figure 3.8. A conserved amphipathic α-helix mediates Gea2 membrane binding

A) Gea2 depicted on a modeled membrane surface. B) Close-up view of the amphipathic helix predicted by both secondary and tertiary structure prediction methods, but absent from the experimentally determined cryoEM density. The structural model determined by cryoEM is superimposed onto the AlphaFold prediction (Jumper et al., 2021). The AlphaFold prediction is colored by conservation with dark red representing the most conserved residues and cyan representing the least conserved residues. C) Sequence alignment highlighting conservation of the helix, colors highlight conserved residues based on their biochemical properties. D) Helical wheel indicating the amphipathic nature of the helix. Red box indicates Tyr residue mutated for functional experiments. E) *GEA2* complementation test (plasmid shuffling). F) Localization analysis of Gea2 and amphipathic helix mutants. G) *In vitro* membrane-binding assay (liposome pelleting) using purified proteins and synthetic liposomes. S, supernatant; P, pellet. H) In vitro GEF activity assay using purified proteins, the myristoylated-Arf1 substrate, and synthetic liposomes. nd = not detectable. I) In vitro GEF activity assay using purified proteins and the ΔN17-Arf1 substrate without liposomes.

``

To test the role and importance of this newly identified amphipathic alpha helix, we produced two different mutants of Gea2, one in which this helix was removed (ΔAH) and another in which a conserved Tyr residue was substituted with Asp (Y1001D). We found that both of these mutants lost their ability to support cell growth, despite being expressed at endogenous levels (Figs. 3.8E, 3.2B). We observed that these mutant proteins lost their localization to the Golgi complex, localizing instead to the cytoplasm (Fig. 3.8F). These results indicate that this conserved amphipathic helix is required for Golgi membrane association *in vivo*.

To determine whether this amphipathic helix is involved in direct interaction between Gea2 and the membrane surface, we purified the Gea2 Y1001D mutant protein (Fig. 3.2C) and tested its ability to interact with liposome membranes in vitro. Using a lipid mix that wild-type Gea2 associates with robustly, we found that the Y1001D mutant protein exhibited a dramatic reduction in membrane-binding capability *in vitro* (Fig.3.8G). This indicates that the amphipathic helix is directly involved in Gea2 membrane binding. To determine whether the amphipathic helix is required for membrane-proximal Arf1 activation, we employed an established *in vitro* GEF assay (Gustafson and Fromme, 2017). We found that purified Gea2 Y1001D was well behaved biochemically but unable to activate full-length myristolated-Arf1 on phosphatidylcholine liposomes (Figs. 3.8H, 3.2D). A similar lack of activation was seen when liposome membranes were omitted from reactions including

``

wild-type Gea2 (Fig. 3.8H). Importantly, Gea2 Y1001D retained robust GEF activity towards ΔN17-Arf1 in the absence of liposome membranes (Fig. 3.8I, 3.1E). ΔN17-Arf1 is a truncated form of Arf1 that lacks its N-terminal amphipathic helix and therefore does not need to insert into membranes in order to be activated (Kahn et al., 1992; Paris et al., 1997). These results indicate that the Gea2 amphipathic helix is specifically required for activating Arf1 on the membrane surface.

Taken together our results indicate that Gea2 uses the conserved amphipathic helix in the HDS1-HDS2 linker to bind to the Golgi membrane surface in order to activate Arf1. The dimeric nature of the complex enables us to model the orientation of Gea2 on the membrane with high confidence (Fig. 3.8A). These findings also highlight how Arf1 activation and insertion of its myristoylated N-terminal helix into a membrane are intimately coupled.

Gea2 adopts an open conformation when bound to nucleotide-free Arf1

To further investigate the role of the regulatory domains in modulating the action of the GEF domain, we trapped the Gea2-Arf1 nucleotide-free activation intermediate (Fig. 3.2F) and determined its structure by cryoEM (Figs. 3.9A-C and 3.10, Table 3.1). The conformation of nucleotide-free Arf1 in our full-length Gea2-Arf1 complex structure was nearly identical to that of nucleotide-free Arf1 when bound to the isolated Gea2 GEF domain

``

determined previously by X-ray crystallography (Fig. 3.11A) (Goldberg, 1998). Strikingly, a closed conformation of the GEF domain was not observed in the Gea2-Arf1 complex cryoEM data; instead the position of the Arf1-bound GEF domain was most similar to that of the open conformation observed in the absence of Arf1 (Figs. 3.9D, 3.10, and 3.11B). We note that structural predictions of Gea2, its yeast paralog Gea1, and its human homolog GBF1 each adopt the closed conformation (Fig. 3.11C). The structural results suggest that binding to nucleotide-free Arf1 enforces an open conformation of the Gea2 GEF domain. Arf1 bound to the closed conformation of Gea2, we superimposed our structure of nucleotide-free Arf1 bound to the GEF domain onto the GEF domain of the closed complex (Fig. 3.9D). This modeled complex resulted in a steric clash between the ‘switch I’ region of Arf1 and the GEF-HDS1 linker of Gea2 (Fig. 3.9G). This indicates that the Gea2 closed conformation is incompatible with binding to the nucleotide-free state of Arf1. This steric clash with the closed conformation also explains why the nucleotide-free Gea2-Arf1 activation intermediate adopts an open conformation.

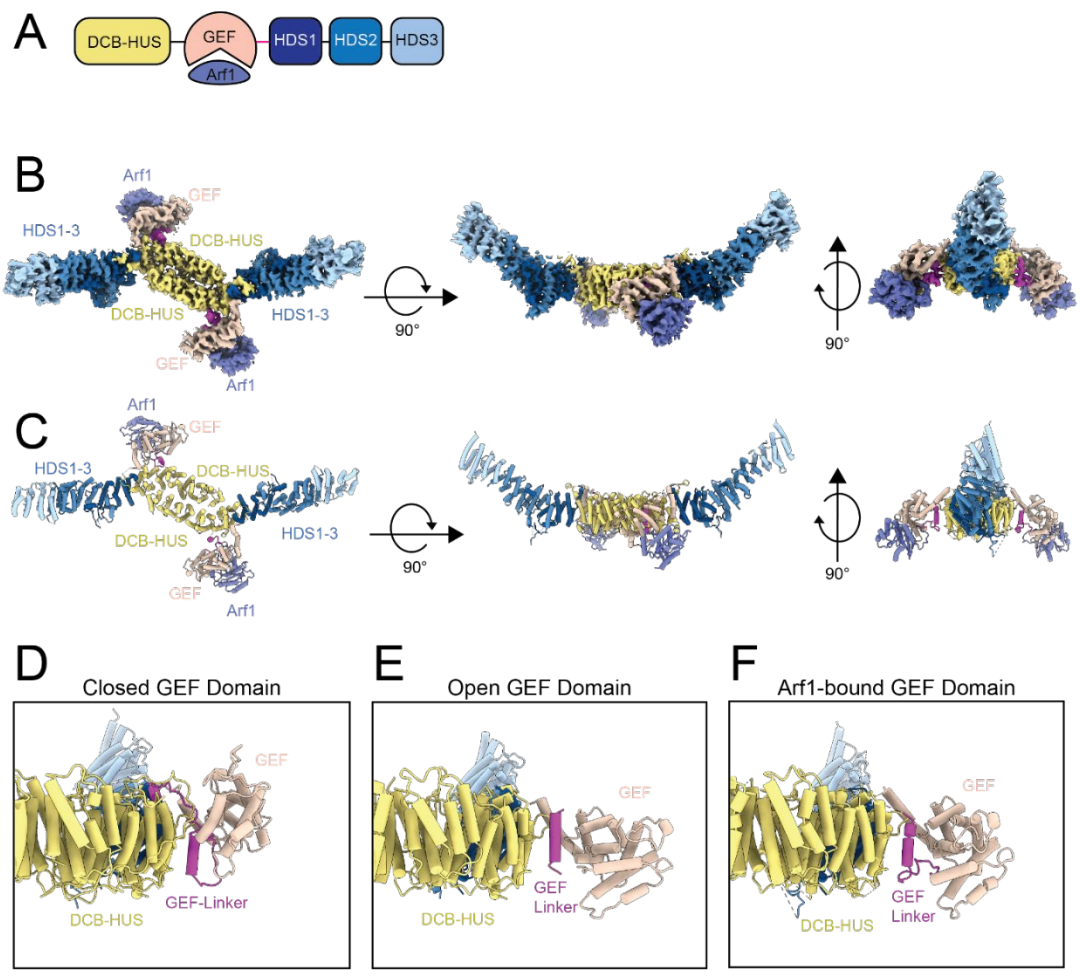

Figure 3.9. CryoEM structure of a Gea2-Arf1 activation intermediate complex

A) Schematic of the Gea2-Arf1 activation intermediate complex used for cryoEM. B) CryoEM density of the Gea2-Arf1 complex, colored and labeled as in Figure 1, with Arf1 colored purple. C) Atomic model of the Gea2-Arf1 complex. D) Views of the Gea2 GEF domain and GEF-HDS1 linker for each of the three conformations adopted by Gea2 in the Gea2 only (closed and open) and Arf1-bound conformations.

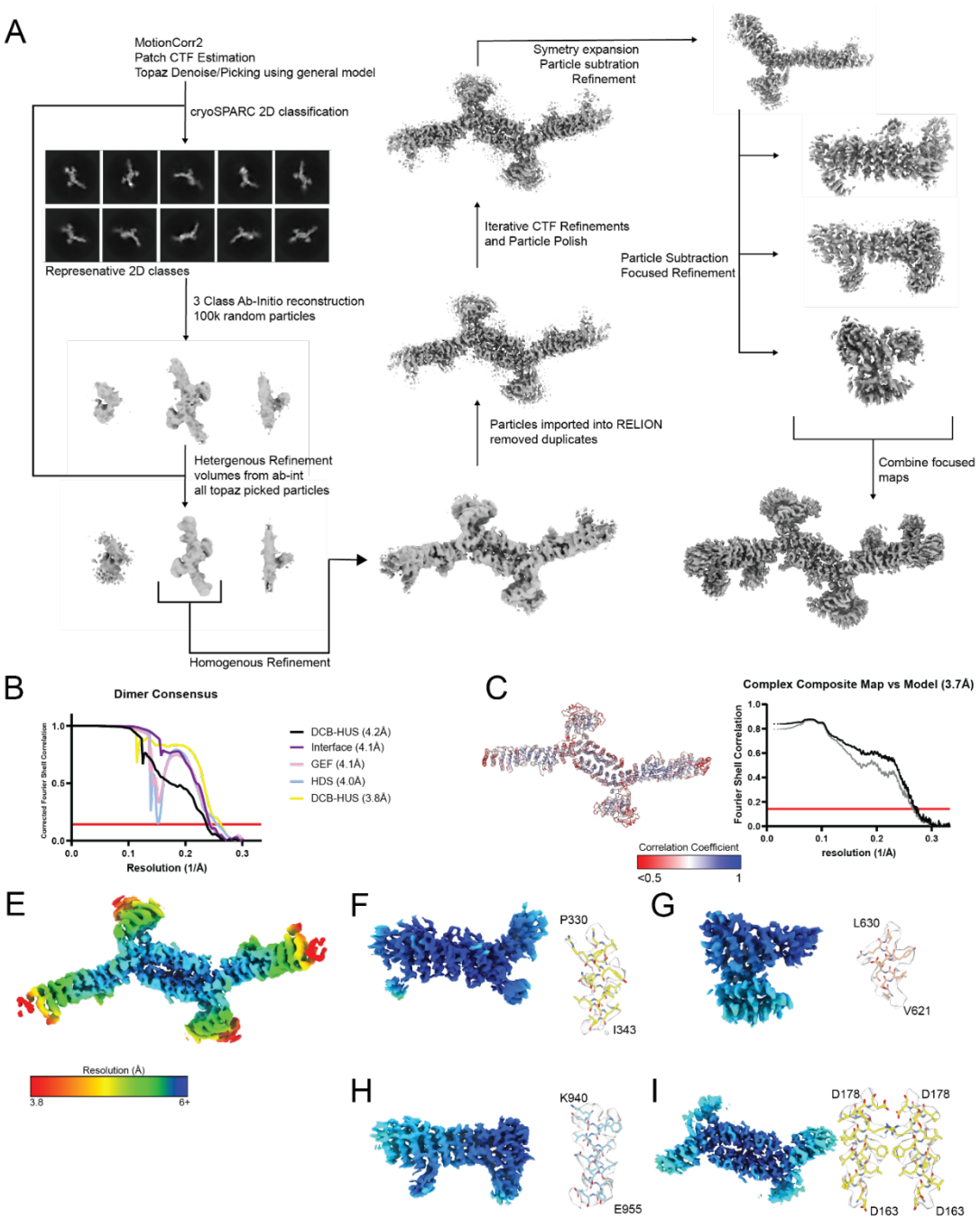

Figure 3.10. Gea2-Arf1 activation intermediate complex cryoEM data processing
A) Flowchart illustrating the data processing workflow for the Gea2-Arf1 complex cryoEM data (see Methods). B) Fourier shell correlation plots and example cryoEM density for focused refinements are shown for the cryoEM map and model of the Gea2-Arf1 complex.

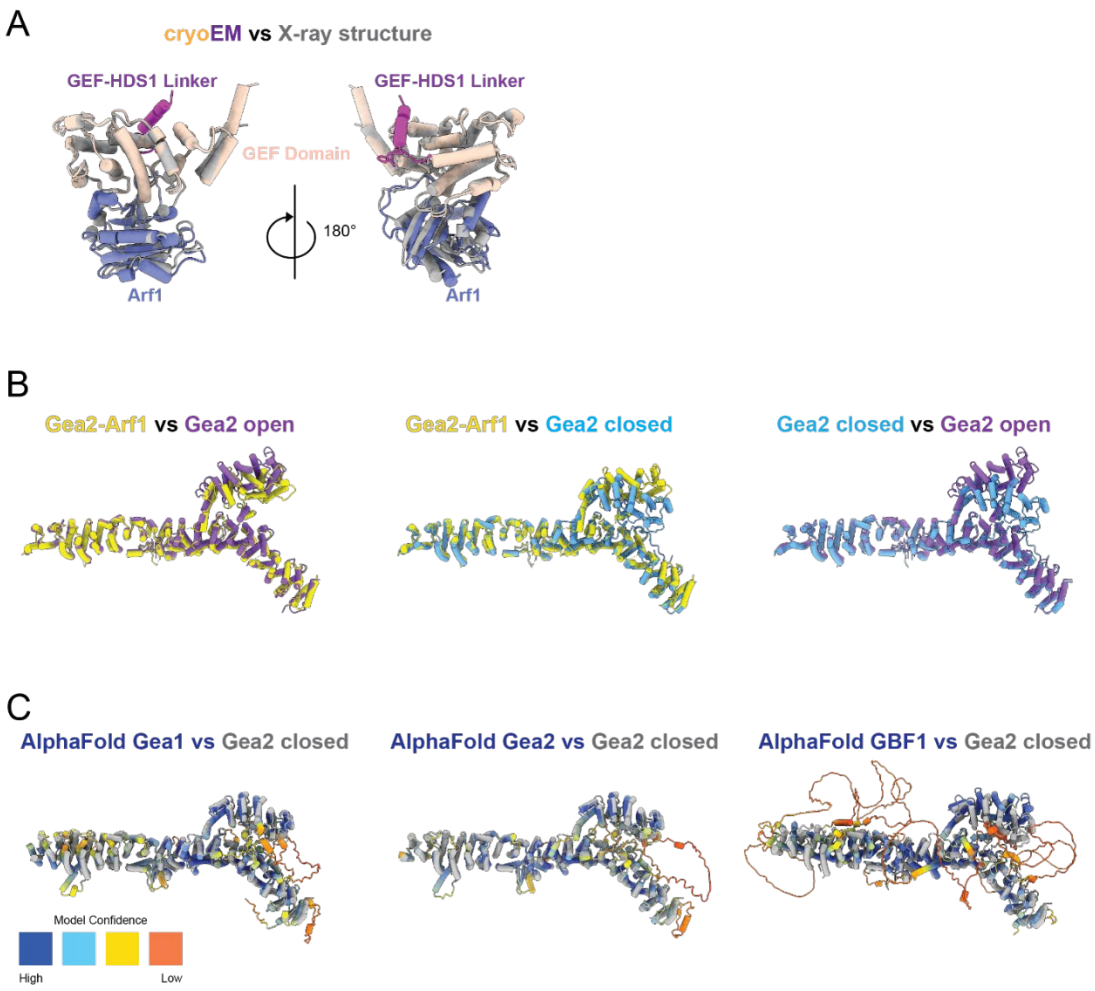

Figure 3.11. Structural comparisons
A) CryoEM structure of the Gea2 GEF domain bound to nucleotide-free Arf1 superimposed on the crystal structure of the Gea2 GEF domain bound to nucleotide-free Arf1 (Goldberg, 1998). B) Pairwise superpositions of the Gea2 open, closed, and Arf1-bound monomers. C) Superpositions of the Gea2 closed monomer onto AlphaFold models, colored by prediction confidence, of *S. cerevisiae* Gea1, *S. cerevisiae* Gea2, and human GBF1 (Jumper et al., 2021).

``

Evidence for GEF conformational switching during Arf1 nucleotide exchange

These findings raised the question of whether the closed conformation served any role in the nucleotide exchange reaction. We therefore superimposed the published structure of Arf1-GDP bound to the GEF domain from ARNO (Renault et al., 2003) onto the closed conformation of Gea2 (Fig. 3.12C). In contrast to the nucleotide-free state, Arf1-GDP appears able to bind to Gea2 in the closed conformation without clashes (Fig.3.12F), because the configuration of the Arf1 ‘switch I’ region is different in the GDP-bound and nucleotide-free states. This suggests that the closed conformation of Gea2 is compatible with binding to Arf1-GDP.

We were initially puzzled by our observation that the ‘open’ position of the GEF domain in the nucleotide-free Gea2-Arf1 complex appears unsuitable for the initial association event between Gea2 and Arf1-GDP, assuming Gea2 is already membrane-bound. The orientation of the GEF domain active site facing towards the membrane suggested its close proximity to the membrane would preclude it from productively encountering its substrate Arf1-GDP via diffusion, either from the cytosol or along the membrane surface. In contrast, the closed conformation, in which the GEF domain active site is oriented orthogonal to the membrane surface, appears much more suitable for productive encounters with the Arf1-GDP substrate than does the open conformation (Fig. 3.9I).

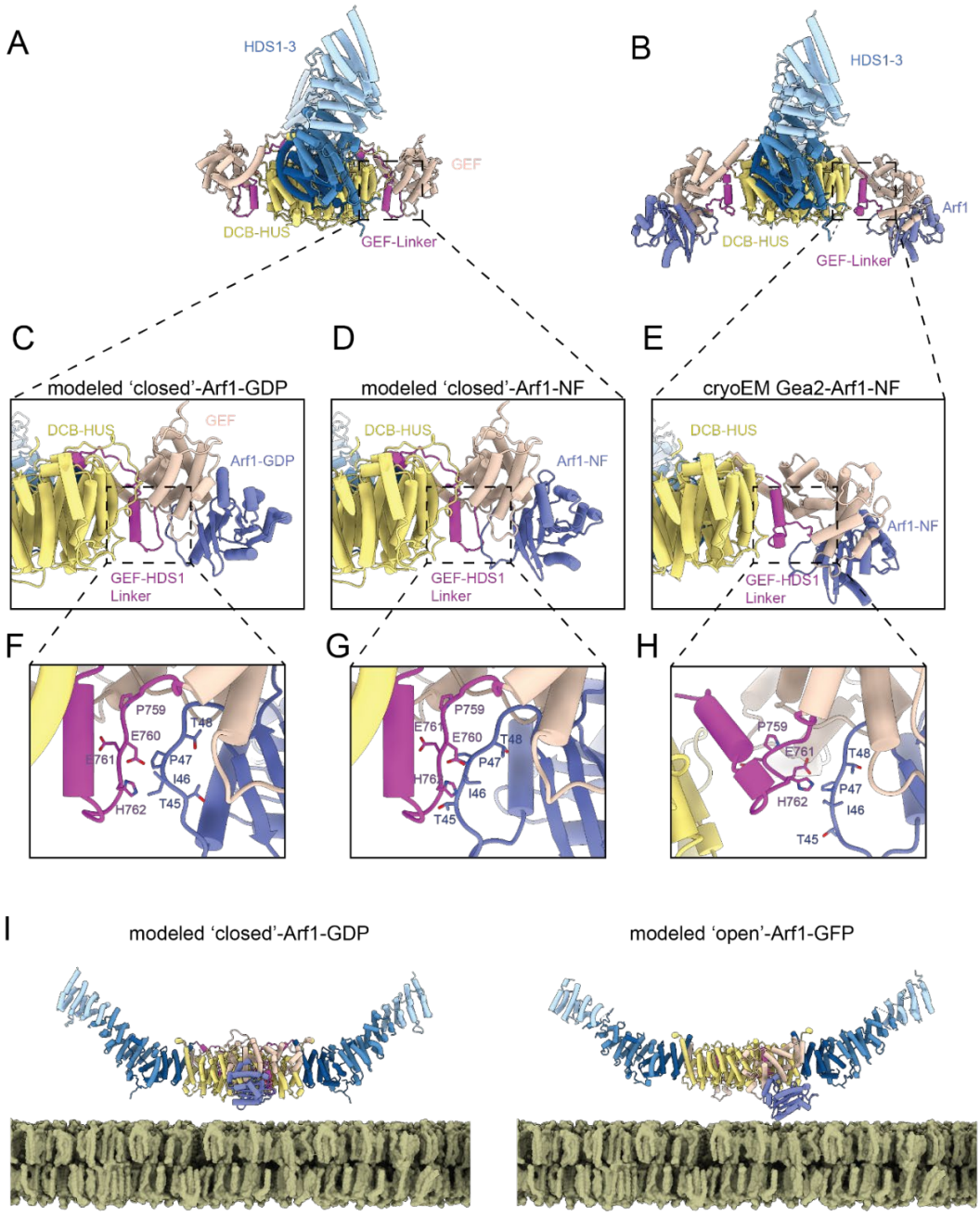
A
HDS1-3
GEF
DCB-HUS
GEF-Linker
B
HDS1-3
Arf1
DCB-HUS
GEF-Linker
C
modeled 'closed'-Arf1-GDP
DCB-HUS
GEF
Arf1-GDP
GEF-HDS1
Linker
D
modeled 'closed'-Arf1-NF
DCB-HUS
Arf1-NF
GEF-HDS1
Linker
E
cryoEM Gea2-Arf1-NF
DCB-HUS
Arf1-NF
GEF-HDS1
Linker
F
P759
E760
E761
T48
P47
I46
H762
T45
G
P759
E761
E760
T48
P47
H762
I46
T45
H
P759
E761
T48
P47
H762
I46
T45
I
modeled 'closed'-Arf1-GDP
modeled 'open'-Arf1-GFP

``

Figure 3.12. Steric constraints appear to enforce Gea2 conformational change

A) Structure of the closed/closed Gea2 dimer shown for context. B) Structure of the Gea2-Arf1 complex shown for context. C) Close-up view of the modeled Gea2 closed-Arf1-GDP complex. D) Close-up view of the modeled Gea2 closed-Arf1-NF (nucleotide-free) complex. E) Close-up view of the Gea2-Arf1-NF cryoEM structure. F-H) Magnified views of (C-E). Note the steric clash between Arf1 and the GEF-HDS1 linker in (D) and (G). I) Comparison of the modeled closed/closed Gea2-Arf1-GDP complex with the modeled open/open Gea2-Arf1-GDP complex. Note how in the closed conformation, the GEF domain appears more readily able to encounter freely-diffusing Arf1-GDP, compared to the open conformation.

``

Taken together, our structural analysis suggests that initial binding to Arf1-GDP likely occurs with the Gea2 GEF domain in the closed conformation (Fig. 3.9C, F). Subsequent release of GDP, triggered by interaction with the GEF domain, causes Arf1 to adopt its nucleotide-free structure. As this conformation of Arf1 is incompatible with the Gea2 closed state (Fig. 3.12D, G), the GEF domain likely switches to the open state concurrent with nucleotide release, adopting the nucleotide-free conformation we observed by cryoEM (Fig. 3.12E, H). Given the apparent independence of each GEF domain in the dimer, it is also possible that only one GEF domain is able to adopt the open conformation at a time when Gea2 is bound to the membrane.

A model for activation-coupled membrane insertion of Arf1

When bound to Gea2 in its nucleotide-free state, Arf1 is positioned such that its N-terminus is oriented towards the membrane surface, and we predict it to be in close proximity to the lipid headgroups (Fig. 3.12I). Although not present in the construct we used to determine the structure of the complex, the N-terminus of Arf1 folds into a membrane-inserting amphipathic helix upon GTP binding (Antonny et al., 1997; Liu et al., 2010). The conformation of Gea2 when bound to the nucleotide-free intermediate therefore appears to prime Arf1 for membrane insertion: GTP binding to the nucleotide-free intermediate induces formation of the N-terminal Arf1 amphipathic helix in a position optimal for its insertion into the cytoplasmic leaflet of the Golgi membrane.

``

Our structural results and analyses lead us to a complete model for nucleotide exchange-coupled membrane insertion of Arf1 by Gea2 (Fig. 3.13A-E). Arf1-GDP initially encounters membrane-bound Gea2 in its closed conformation (Fig. 3.13B,C). Nucleotide release then leads to an open conformation to avoid steric clash with the GEF-HDS1 linker. The resulting open conformation positions the N-terminus of Arf1 optimally for membrane insertion (Fig.3.13D). Finally, GTP binding triggers membrane insertion of Arf1 via folding of its myristoylated amphipathic helix and release from Gea2 (Fig.3.13E).

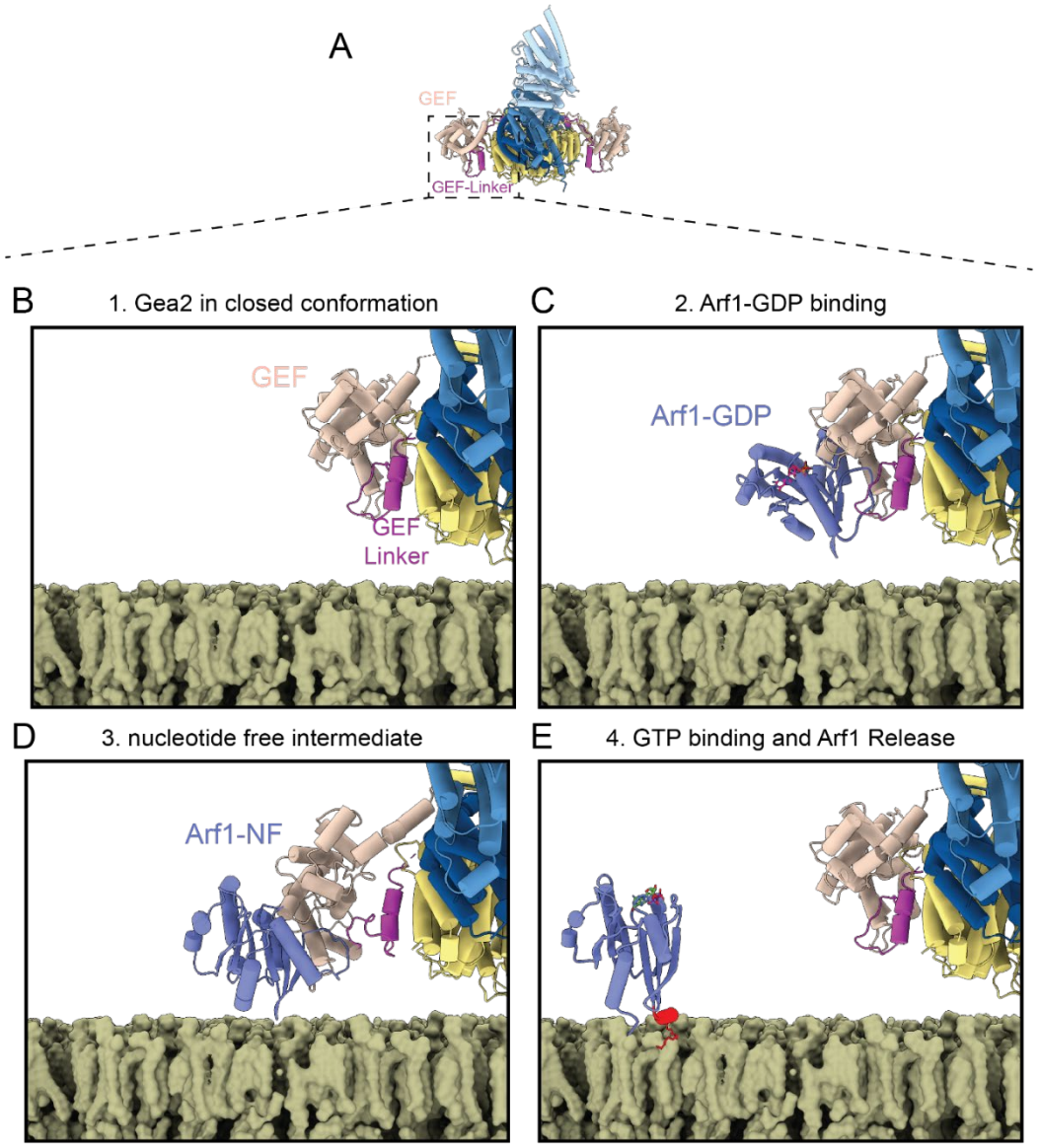
A
GEF
GEF-Linker
B
1. Gea2 in closed conformation
GEF
GEF
Linker
C
2. Arf1-GDP binding
Arf1-GDP
D
3. nucleotide free intermediate
Arf1-NF
E
4. GTP binding and Arf1 Release

``

Figure 3.13. Model for activation of Arf1 by Gea2 on the Golgi membrane surface

A) Gea2 in the closed/closed conformation shown for context. B) In Step 1, at least one of the Gea2 monomers adopt the closed conformation while bound to the membrane surface (the cryoEM structure of one side of the closed/closed conformation shown on a modeled membrane). C) In Step 2, Arf1-GDP binds to the GEF domain (the modeled closed-Arf1-GDP complex is shown). D) In Step 3, GDP dissociates from Arf1 (Arf1-NF = nucleotide free), and the resulting conformation change in Arf1 causes the GEF domain to switch from the closed state to an open state in order to avoid steric clash with Arf1 (the Gea2-Arf1 cryoEM structure is shown). E) In step 4, GTP binding causes another conformation change in Arf1, resulting in folding of its amphipathic helix (colored red) at the membrane surface and dissociation from Gea2 (the NMR structure of Arf1-GTP and cryoEM structure of the closed/closed conformation of Gea2 are shown). The structures of Arf1-GDP and Arf1-GTP were derived from RCSB entries 1R8S (Renault et al., 2003) and 2KSQ (Liu et al., 2010).

``

DISCUSSION

Arf1 is known for its role as a regulator of the function and regulation of the Golgi complex and recycling endosomes, but it's activity has also been implicated in endocytosis, TORC1 kinase signaling, lipid droplet homeostasis, and lysosomal and mitochondrial function (Ackema et al., 2014; Dechant et al., 2014; Kumari and Mayor, 2008; Su et al., 2020; Wilfling et al., 2014). A hallmark of Ras-related "small" GTPases like Arf1 is the structural transitions they undergo during nucleotide exchange and hydrolysis. Arf1 is the founding member of the Arf GTPase family, which includes over 20 proteins in humans which collectively regulate virtually all membrane trafficking pathways (Gillingham and Munro, 2007). Most Arf family GTPases are anchored to the membranes of organelles and vesicles by their N-terminal amphipathic helices. Unlike other Ras-related GTPases, these membrane-anchoring motifs are masked by direct interaction with the GDP-bound nucleotide-binding domain (Amor et al., 1994). In contrast, Rab and Rho family GTPases employ chaperone proteins (guanine-nucleotide displacement inhibitors) to mask their membrane-anchoring motifs in the GDP-bound state (Isomura et al., 1991; Soldati et al., 1994). GTP-binding exposes the Arf amphipathic helix, inducing stable membrane binding (Antonny et al., 1997). Although membrane insertion of GTP-bound Arf proteins is favorable, there is likely a kinetic 'activation energy' barrier that slows the membrane-insertion step, as it requires lipids to rearrange in order to accommodate the amphipathic helix. Our structural

``

findings point to a mechanism for how Gea2 may reduce this kinetic barrier by positioning Arf1 optimally for membrane insertion.

To our knowledge, conformational change of a GEF during the nucleotide exchange reaction has not been reported. Several GEFs are known to be autoinhibited and/or allosterically activated, and the structural basis for autoinhibition and activation has been documented for several GEFs, including the Ras-GEF SOS (Gureasko et al., 2008; Sondermann et al., 2004), the Rab-GEF Rabex5 (Delprato and Lambright, 2007; Lauer et al., 2019; Zhang et al., 2014), the Arf-GEF Cytohesin/Grp1 (Das et al., 2019; DiNitto et al., 2007; Malaby et al., 2013), and the Rho-GEF Vav (Yu et al., 2010). In the context of autoinhibition and allosteric activation, GEF conformational change is usually coupled to phosphorylation or binding to a regulatory protein or lipid, and is a prerequisite for the nucleotide exchange reaction. In contrast, Gea2 appears to capitalize on the conformational changes its substrate GTPase undergoes during nucleotide exchange to drive its own conformational change during the activation reaction.

A mutation has been identified in geaA, the *Aspergillus nidulans* homolog of Gea2, corresponding to a Y1001C substitution in *S. cerevisiae* Gea2, that partially suppressed the loss of the *A. nidulans* homolog of Sec7, hypB (Arst et al., 2014). Remarkably, this Y-to-C substitution mutation shifted the localization of geaA from early-Golgi compartments towards later Golgi

``

compartments normally occupied by hypB. Our findings provide a mechanistic interpretation of this observation, as we have identified Y1001 as a critical residue for Gea2 membrane interaction through our use of the Y1001D mutant. An interesting possibility is that the Y-to-C substitution, by modulating but not eliminating the hydrophobicity of the amphipathic helix, alters which membranes are most favored for stable binding due to their compositions or biophysical properties. We note that in contrast to the results reported for *A. nidulans* geaA, we found that the equivalent Y-to-C substitution did not enable Gea2 to suppress loss of Sec7 in *S. cerevisiae* (Gustafson, 2017). This highlights the proposed roles of regulatory protein-protein interactions in directing the localization of the Golgi Arf-GEFs to specific compartments (Christis and Munro, 2012; Gustafson and Fromme, 2017; Lowery et al., 2013; McDonold and Fromme, 2014; Monetta et al., 2007; Richardson et al., 2012). There are likely to be both similarities among and differences between the structural mechanisms underlying Arf1 activation by Gea2 and Sec7. Previous work on Sec7 highlighted the influence of the DCB-HUS domain on the activity of the GEF domain for activation of Arf1 on the membrane surface (Halaby and Fromme, 2018; Richardson et al., 2016). However, Sec7 likely adopts a very different overall architecture because Sec7 dimerizes via its HDS4 domain (Richardson et al., 2016). Sec7 is also regulated by distinct positive-feedback, autoinhibition, and cross-talk mechanisms (McDonold and Fromme, 2014; Richardson et al., 2012) and prefers more anionic membranes compared to Gea1/2 (Gustafson and Fromme, 2017).

``

Although we have now identified how Gea2 interacts with membranes, it remains unresolved how it achieves its specific localization. Both Gea1 and Gea2, as well as GBF1, interact with Rab1/Ypt1, which likely recruit these Arf-GEFs to the Golgi, yet Gea1 and Gea2 localize to distinct Golgi compartments (Gustafson and Fromme, 2017; Monetta et al., 2007). Future studies are required to characterize the Gea/GBF1-Rab1 interaction and determine how Gea1 and Gea2 achieve their specific localization.

``

CHAPTER 4

MECHANISM FOR THE DIFFERENTIAL LOCALIZATION OF GEA1 AND GEA2

INTRODUCTION

Gea1 and Gea2 are likely both recruited to the Golgi membrane by similar mechanisms. We assume that both are recruited by the small GTPase Ypt1 and can bind the Golgi with the same amphipathic helix. However, it has been reported before that Gea1 and Gea2 do not localize to the same Golgi compartments. Moreover, during Golgi maturation, Gea1 and Gea2 never colocalize. In efforts to find protein recruiters, SILAC mass spec was performed. The SNARE protein Gos1 was the top hit for interacting partner for Gea2 (Gustafson, 2017; Gustafson and Fromme, 2017).

SNARE bundles are an essential aspect of vesicle formation. The fusion of these bundles provides the driving force for membrane fusion. In general a SNARE bundle consists of 4 SNARE domain spanning across 3 or 4 proteins. In addition to the SNARE domain, they also can be anchored in the membrane with a transmembrane domain and a regulatory H_{ABC} domain. There are two types of SNARE domains: Q and R type snares. R and Q SNAREs contain an essential arginine and glutamine respectively. Once these residues interact, the SNARE bundles zipper together providing driving force for vesicle fusion.

``

In general, during formation, vesicles are loaded with a single type of SNARE protein which can be called the ‘v’ (vesicle) SNARE. On the destination membrane, three other SNAREs, called ‘t’ (target) SNAREs, are waiting for vesicle delivery. During vesicle tethering all the SNAREs engage together providing the force to fuse the vesicle membrane to the target membrane since this is unfavorable. A completed SNARE bundle does not necessarily have to be four independent proteins as a SNARE protein can contain two SNARE domains. SNAREs are recycled by NSF/SNAP protein complexes which use ATP to disassemble the bundle to use in another round of fusion.

At the Golgi complex there are at least three different four-protein SNARE complexes. The “Bos1” SNARE Complex operates at the early Golgi and consists of the Q-SNAREs Sed5, Bos1, Sec22 and the R SNARE Bet1 (Fig.4.1). Vesicles leaving the ER contain Bet1 as the v-SNARE and will interact with its partners at the early Golgi or in other COPII vesicles. For later medial traffic, the “Gos1” bundle consists of Sed5, Gos1, Stf1 with the R SNARE being Ykt6. Bos1 concentration decreases later in the Golgi while Gos1 increases. This matches the differential organization of Gea1 and Gea2 at the Golgi. Based on the data from previous mass spectrometry results, we hypothesized that Bos1 might be a recruiter for Gea1 and Gos1 might be a recruiter for Gea2 (Gustafson, 2017).

``

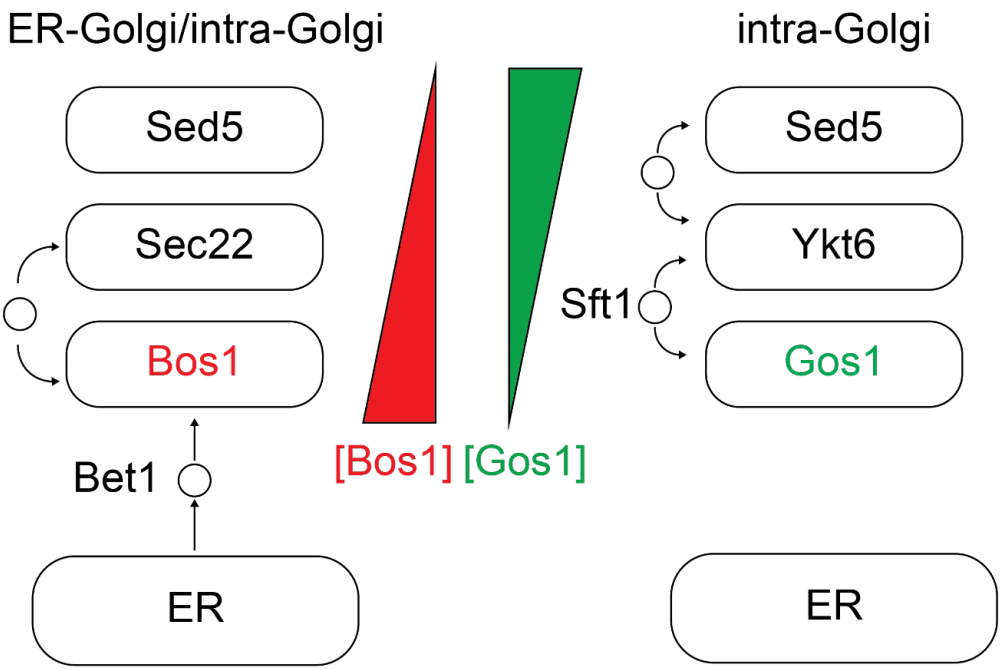

Figure 4.1. Organization of SNAREs at the Golgi
Distribution of two of the Golgi SNARE bundles. Bos1 concentration is higher at the early Golgi and Gos1 is higher in the medial Golgi.

``

RESULTS

Gea1 and Gea2 are temporally distinct

Gea1 and Gea2 have been shown to function at different compartments of the Golgi complex but appear to have the same function of activating Arf1 for COPI vesicle formation. Gea1 and Gea2 never colocalize with each other while colocalizing with other Golgi markers such as Vrg4 (Gustafson, 2017; Gustafson and Fromme, 2017). Therefore, the question arises whether Gea1 and Gea2 are just temporally distinct or represent two different “types” of Golgi compartments.

To test whether Gea1 and Gea2 are temporally separate we did timelapse imaging with the Golgi marker Vrg4. We found that Gea1 peaks before Vrg4 and Gea2 peaks after Vrg4 (Fig.4.2). Therefore it appears that Gea1 localizes to the earlier stages of the *cis*-Golgi and leaves before Gea2 arrives. These data explain why we see both Gea1 and Gea2 colocalizing with Vrg4 but not with each other. Therefore Gea1 and Gea2 localize to the same maturing Golgi compartments and there does not appear to be two distinct pools of Golgi compartments.

The N-terminus determine the localization of Gea1 and Gea2

To study the causes of the differential localization of Gea1 and Gea2, we wanted to determine which part of these proteins could be responsible for their specific localization. We made chimeric constructs between Gea1 and

``

Gea2 by swapping the DCB-HUS domains. When imaged in cells, we observed that each Gea chimera colocalized with the endogenous Gea paralog containing the same N-terminal domains. This implies that the signal for Gea1/2 localization is in the DCB-HUS region (Fig.4.3 A,B).

The DCB-HUS domain is highly conserved, especially between Gea1 and Gea2. It is therefore likely that the signal would be in variable residues and not conserved between the two paralogs. To assess this possibility, we took a simple sequence alignment between Gea1 and Gea2 and colored by conservation on the AlphaFold2 model in order to visualize disordered residues. As can be seen, helical repeats of the DCB-HUS domain are the most conserved regions while the loop regions (which aren't seen in our structure) are not conserved, especially the loop between residues 200-350 (Fig.4.3 D,E). Since this is a long unstructured loop, it possibly could be a place for an interacting partner. It is also of note that in general loops tend not to be conserved.

It is possible that each chimera binds to one of the endogenous Gea proteins, resulting in the observed localization. To control for this, it would be best to repeat the experiment in a shuffling strain lacking both Gea1 and Gea2, so the chimera is the only Gea protein expressed. Interestingly, each of the Gea chimeras are individually sufficient for cell growth.

``

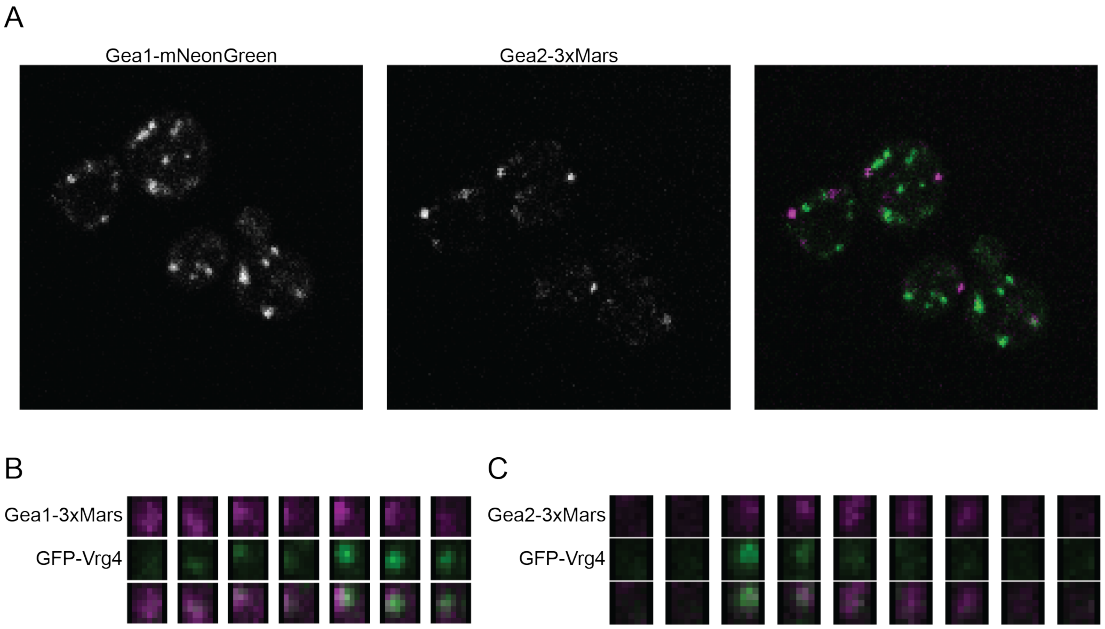

Figure 4.2. Gea1 and Gea2 have distinct localizations
(A) Gea1 and Gea2 localizations. (B) Time lapse imaging of Gea1 compared to Vrg4. (C) Time lapse imaging of Gea2 compared to Vrg4.

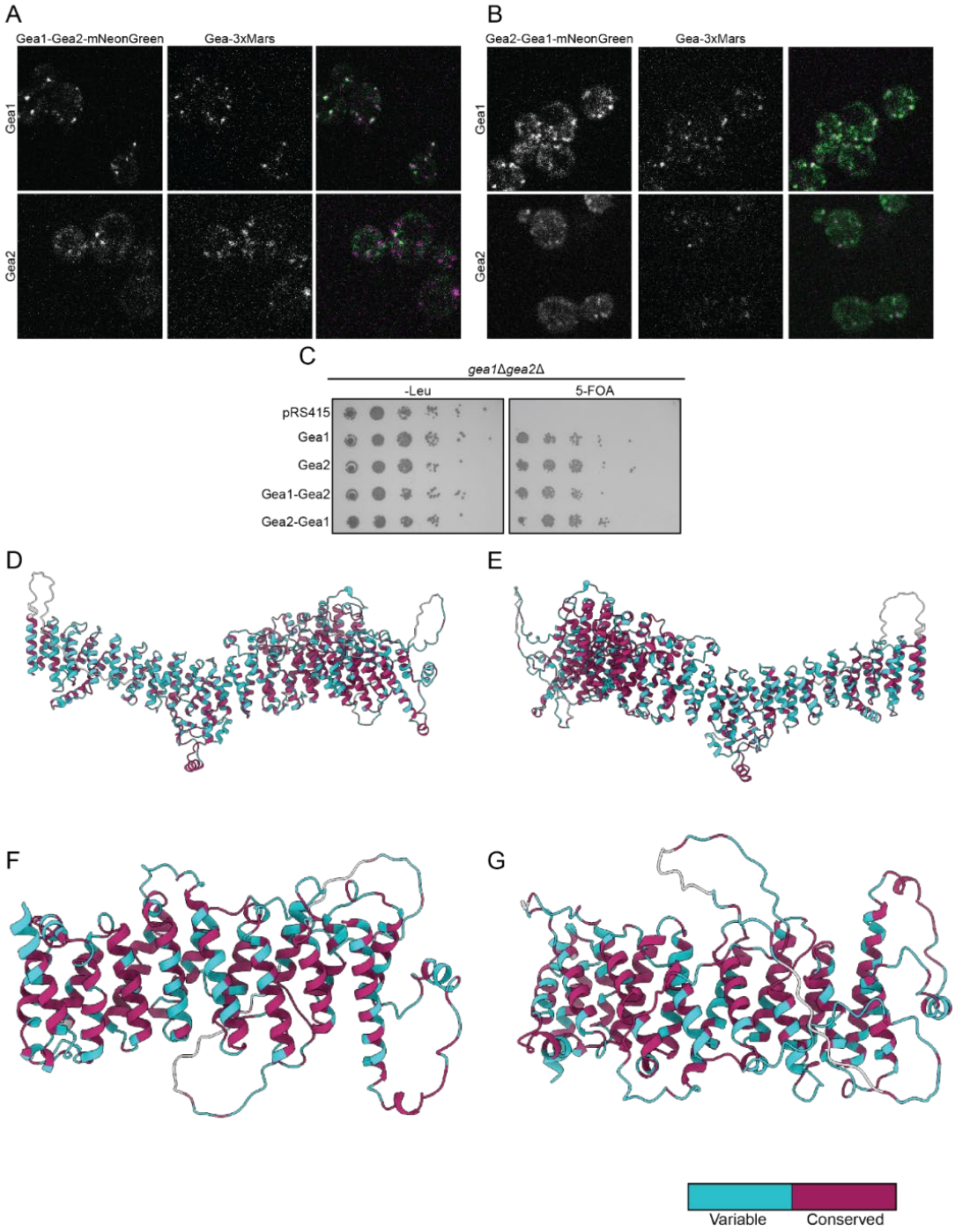

Figure 4.3. DCB-HUS domain determines Gea location
(A) Gea1-Gea2 chimera compared to endogenous Gea1 and Gea2. (B) Gea2-Gea1 chimera compared to endogenous Gea1 and Gea2. (C) Complenation assay of Gea chimeras. (D,E). conservation analysis of Gea1 and Gea2. (F,G) closed up conservation anayalus of DCB-HUS of Gea1 and Gea2.

``

Gea1 and Gea2 do not re-localize in the absence of their paralog

Since Gea1 and Gea2 are genetically redundant but have different localizations, we wanted to test they will re-localize in the absence of their paralog. To do this we wanted to compare Gea localization to a marker when the other paralog is deleted. This presented a potential challenge to use because we were concerned of trafficking defects due to possible recycling defects. For this reason, instead of using glycosyltransferases like Vrg4 and Mnn9, we used the Rab GTPase Ypt1. Rab GTPases are delivered to the Golgi by GDIs and then activated by their GEFs and could possibly be less sensitive to trafficking defects (Cherfils and Zeghouf, 2013).

We compared Gea1/2 localization to Ypt1 when its paralog is deleted to look for differences (Fig.4.4). For both Gea1 and Gea2, we saw no significant difference in colocalization with Ypt1 in WT and deletion strains (Fig.4.4B,D). Therefore, it appears that change in localization might not be required for the genetic complementation that is observed.

Efforts for studying SNARE recruitment of Gea1 and Gea2

To find possible protein recruiters for Gea1 and Gea2 a SILAC mass spectrometry experiment was previously performed, and one of the top hits for Gea2 was the SNARE Gos1 (Gustafson, 2017). These *in vivo* results were validated with a co-IP experiment which showed that Gos1 can interact with Gea2 (Gustafson, 2017). Furthermore, Gea1 and Gea2 colocalize with Bos1

``

and Gos1 respectively when overexpressed in cells. Purified Gos1 was able to pull down Gea2 *in vitro* on membranes (Gustafson, 2017).

In these previous *in vivo* colocalization experiments, the SNARE was being overexpressed on a plasmid which is not ideal. One of the hallmarks of yeast is the ability to tag the endogenous locus of a gene of interest and visualize it at endogenous levels. However, since SNAREs are anchored the Golgi via a C-terminal transmembrane domain, they need to be tagged at their N-terminus. We employed a variety of strategies but ultimately choose two-step gene replacement. In this technique, an extra tagged copy of the gene is integrated into the genome, and then the endogenous copy is removed via homologous recombination. Unfortunately, we were only able to generate strains that had two copies of the genes. When we imaged GFP-Gos1 with Gea1 and Gea2 we observed the same results as before (Fig.4.5A).

Since it appears that the SNAREs might interact with the Gea proteins *in vivo*, we wanted to test whether the interaction was direct *in vitro*. Preliminary data showed that Gos1 alone can recruit Gea2 to membranes *in vitro*, however when expressed alone in *E. coli*, Gos1 forms a non physiological trimer (Gustafson and Fromme, 2017). Also, t-SNAREs such as Gos1 are not known to exist as isolated monomers in vivo. To address these issues, we decided to produce the entire SNARE bundle. Since in our hands expressing individual SNARE seem to create non-physiological complexes, we

``

aimed to express all the SNAREs together in the same *E. coli* strain. We used a polycistronic method in which all four SNAREs were cloned into a vector in which they were expressed as one long transcript with a ribosome binding site before each ORF. We were successfully able to create these constructs and purified the Bos1 and Gos1 from bacteria (Fig.4.5 B,C)

To test if these SNARE bundles could recruit Gea to membranes we performed a liposome pelleting assay. The purified SNARE bundle contains a 6xHis-tag that allows it to bind to Ni^{2+}-conjugated lipids that are incorporated into our synthetic liposomes. Once the SNARE bundle was preloaded onto liposomes, they were incubated with Gea1 or Gea2, then the reactions were subjected to centrifugation to pellet the liposomes and visualized by SDS-PAGE. Unfortunately, in our experiments, Gea1/2 bound to the liposomes very well without the SNAREs, and therefore it was impossible to accurately test for a role of the SNAREs in recruiting Gea1/2 (Fig.4.5 D,E).

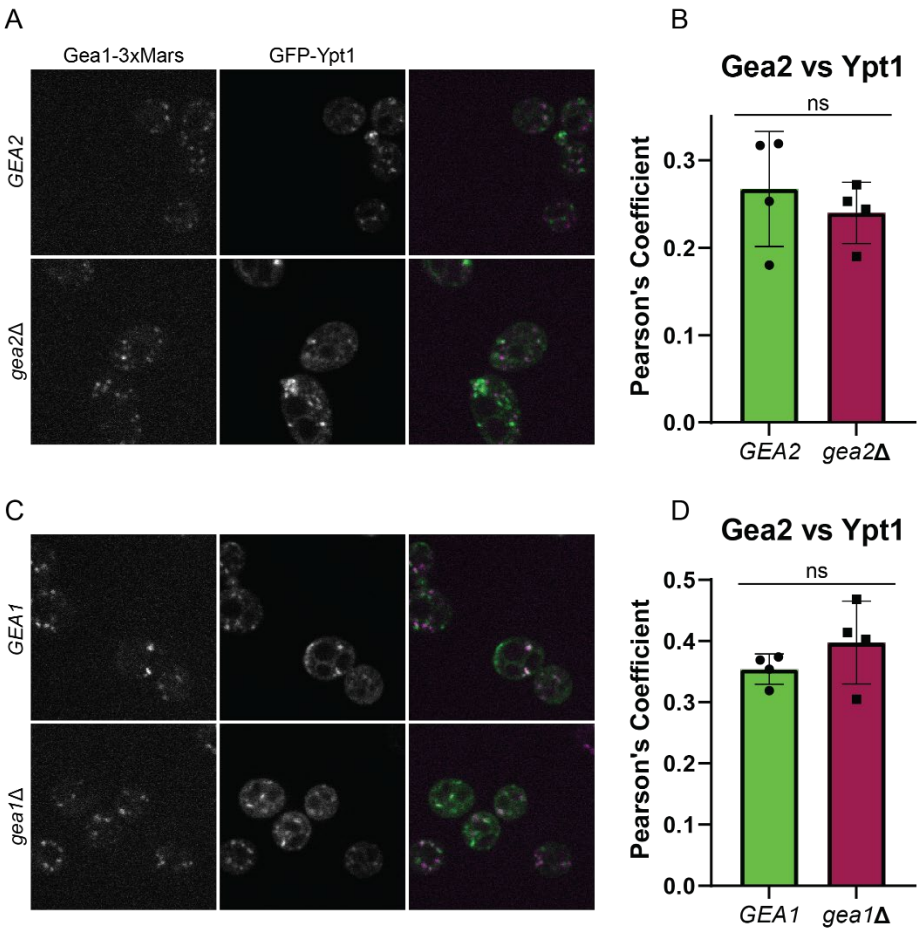

Figure 4.4. Localization of Gea1 and Gea2 does not change
(A) Gea2 localization compared to Ypt1 in WT and gea2Δ cells. (B) Quantification of Gea2 vs Ypt1. (C) Gea1 localization compared to Ypt1 in WT and gea1Δ cells. (D) Quantification of Gea1 vs Ypt1.

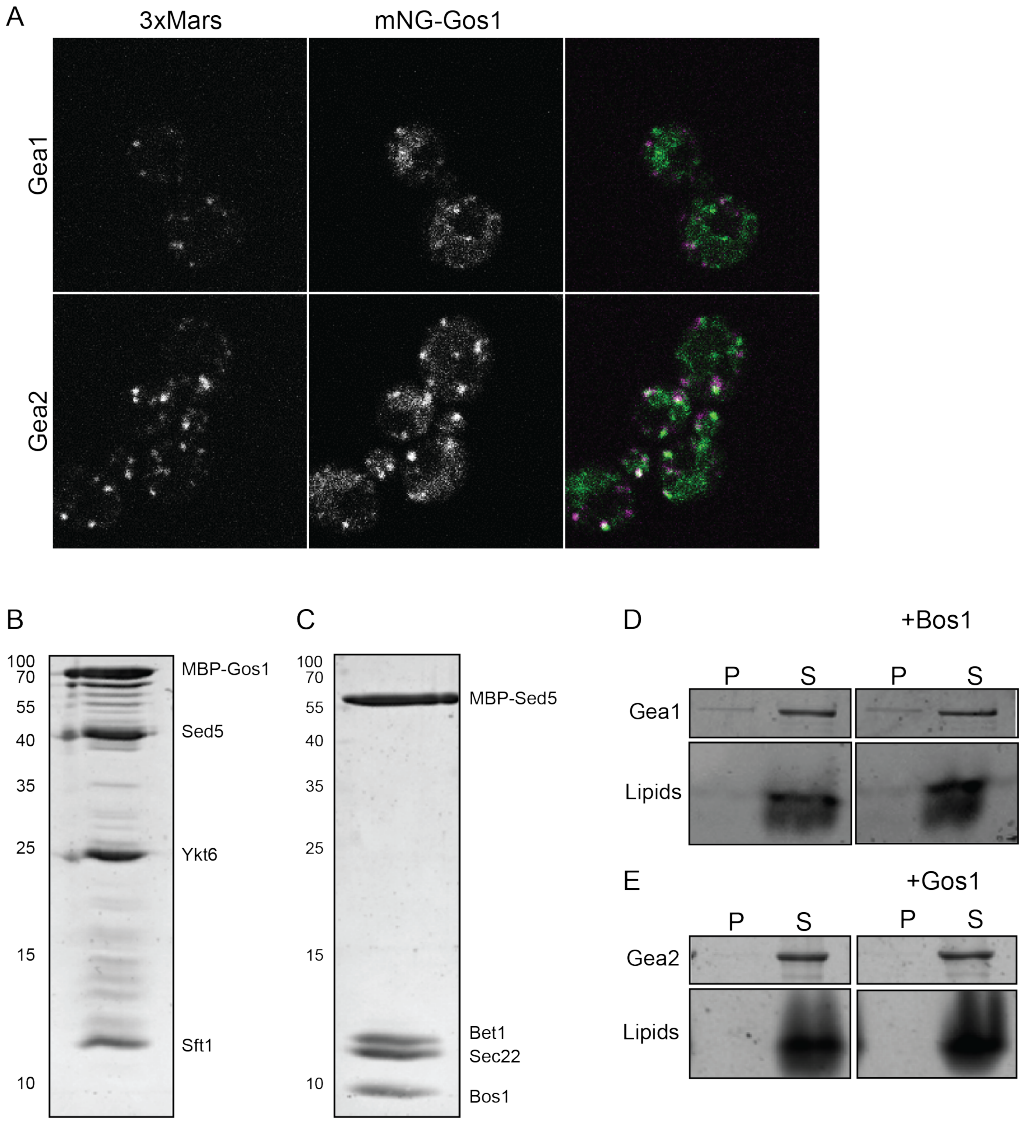

Figure 4.5. Attempts at testing SNARE interactions with Gea1 and Gea2
(A) Localization of Gea1 and Gea2 compared to Gos1. (B) Purified Gos1-Sed5-Ykt6-Sft1 SNARE bundle. (C) Purified Bos1-Sed5-Bet1-Sec22 SNARE bundle. (D) Liposome binding assay with the Bos1 SNARE bundle anchored onto liposomes. (E) Liposome binding assay with Gos1 SNARE bundle anchored onto liposomes.

``

DISCUSSION

Gea1 and Gea2 arose during the whole genome duplication in *S.ce.* and have evolved independently as separate loci. In *S.ce.* it appears that Gea1/2 have gained the ability to differentially localize while still being genetically redundant. It is puzzling that the cells have different roles for Gea1 and Gea2 that are not both necessary. Also it is interesting that Gea1 and Gea2 do not need to change their localization to compensate for each other. In a *gea1*Δ strain, we may not see a phenotype because cargo can be recycled later in the Golgi when Gea2 arrives. Since Gea1 does not re-localize to the medial Golgi in a *gea2*Δ strain, cargo that needs to be recycled at the medial Golgi by Gea2 must be recycled in another way. The whole genome duplication happened after the split from metazoans and therefore the presence of two Gea genes is specific to *S.ce*.

Arf1 activation is controlled by activation by its GEFs at a certain place and time at the Golgi. All cells have a minimum of two points of control for Arf1 activation by having a GBF/Gea GEF for COPI vesicle formation and BIG/Sec7 GEF for late Golgi trafficking events formation. This same reasoning could apply to Gea1 and Gea2 being an additional step of regulation for vesicle formation. Since Gea1 leaves the Golgi before Gea2 this might be a mechanism for the Golgi to have waves of Arf1 activation at the early and then medial Golgi. What is frustrating is that what, if any, mechanisms *S.ce.* has

``

developed, they are non-essential as cells do not appear to care which Gea protein they are expressing.

While the mechanism by which Gea1 and Gea2 are differentially located to the Golgi may not represent a conserved mechanism, it may be a useful tool. It is possible that Gea1 is sending COPI vesicles and its cargo to the ER and Gea2 handles intra-Golgi recycling. How COPI vesicles target to distinct destinations is an open question in the field. Therefore Gea1 and Gea2 can be used to target these individual pathways and probe the system.

If accepting that the DCB-HUS determines Gea localization this poses a slight problem. The DCB-HUS is fairly conserved between Gea1 and Gea2 and its hard to find variable regions other than linkers which tend to be variable in general. There are at least two explanations, one being that that DCB-HUS is not what determines differential localization. Since now we know that Gea dimerizes via DCB-HUS, it is likely that the chimeras are heterodimerizing with the endogenous proteins. Also it appears that the C-terminus is more variable then the DCB-HUS. Another option is that the differential localization not caused by protein interaction but something else. For example Gea1 and Gea2 might favor different lipid environments. It is known that the Golgi grows more anionic as the Golgi matures and its possible that Gea1 prefers more neutral lipids.

``

FUTURE DIRECTIONS

There are various caveats to these experiments. For example it is possible that in the domain swapping experiments, the chimeras are forming heterodimers with the endogenous Gea. A solution this problem would be to image chimeras in cells where they are the only copy, and we already know the chimeras can support cell growth fine. Then the chimeras can be compared to known Golgi markers such as Vrg4 and Sec7.

The Gea SNARE experiments are also promising but issues need to be addressed. For example the microscopy localization experiments were performed in cells with an extra copy of the SNARE, so more efforts can be made to generate strains with single copies. In the *in vitro* experiments, Gea was binding intrinsically to synthetic liposomes. Different lipid composition should be used to optimize these experiments.

``

CHAPTER 5

FUTURE DIRECTIONS

In my work I successfully produced multiple structures of a large Arf-GEF for the first time, providing a valuable tool for the field. While my structures provide a lot of information and have answered some questions, there are also many new interesting questions that have been raised.

The next goal would be to obtain a structure of the first step of Arf1 activation by determining the structure of Gea2 bound to Arf1-GDP. A simple point mutation can be made in the GEF domain which disrupts GEF activity and causes Arf1-GDP to bind to Gea2 without nucleotide exchange. Once the Gea2-Arf1-GDP complex is made, we can perform cryoEM to determine the structure. It would be interesting to see the conformation of the GEF domain when it is bound to Arf1-GDP instead of nucleotide free Arf1. Also, it would be interesting to see the interactions between Arf1-GDP and the GEF linker to see if they are consistent with our modeled structural prediction of this initial step.

Our structure was obtained in solution which may not represent how it exists on the membrane. With our data we were able to determine that the membrane binding helix (MBH) between HDS1-2 is required for membrane binding. However, in our complex structure it appears unlikely for both MBHs to be contacting the membrane if Arf1 occupies both GEF domains. Therefore,

``

it would be advantageous for us to determine a structure of Gea2 on membranes. There are two options for this, either on liposomes or on lipid nanodiscs. Independent of the method, Arf1 activation can be captured in its various activation states using GEF mutants and most importantly myristoylated Arf1.

Another question to characterize is the Gea1/2-Ypt1 interaction. We know that the MBH is sufficient for membrane binding, but what targets Gea to the Golgi membrane specifically *in vivo*? Previous work has shown that Ypt1 can recruit Gea1 and Gea2 to membranes and we assume this is the Golgi membrane targeting interaction. However there are still some questions as whether the Gea1/2-Ypt1 interaction is a stable or transient interaction. Also it is unknown if the MBH is sufficient for Golgi binding or does Ypt1 also need to be bound. We can take a structural approach to answer these questions by determining the structure of Ypt1 and Gea1/2 on lipids.

Gea1/2 dimerizes via the DCB-HUS domains and its dimerization may be essential. Unfortunately, in this study we were unable to disrupt the dimer to probe the necessity of dimerization. Therefore, careful study of the dimerization interface must be undertaken to develop a proper dimer mutant. A possible necessity for dimerization is to ensure proper orientation on the Golgi membrane. As a monomer, Gea1/2 will sit on the membrane with a single MBH in the membrane. Therefore Gea1/2 could be swinging back and

``

forth on the membrane instead of being bound with its proper orientation. This could cause the GEF domain to be in the wrong place as compared to the membrane. Therefore dimerization might be essential for the GEF domain to be in the proper position for Arf1 activation.

``

APPENDIX I

MATERIALS AND METHODS

Protein purifications and Gea2-Arf1 complex formation

Full-length *S. cerevisiae* Gea2 was cloned with an N-terminal cleavable 6xHis-tag into the pPICZ vector (Table S1), then purified using *Pichia pastoris*. An overnight culture of “BMGY” media was used to inoculate a 200mL BMGY starter culture. After 8 hours of shaking at 30°C, 120 mL of this starter culture was used to inoculate 6 liters of “autoinduction media” (Lee et al., 2017) and then shaken overnight at 30°C. After overnight growth, additional methanol was added (equivalent to additional 0.5% final concentration) and the cultures were shaken for an additional 24 hours at 30°C. Cells were harvested by centrifugation (2000 g, 10 min), resuspended in lysis buffer (50 mM Tris pH 8.0, 500 mM NaCl, 10% glycerol, 20 mM imidazole 10 mM βME), and lysed under liquid nitrogen using a SPEX 6875D freezer mill. Lysed cells were cleared using centrifugation (40,000 g, 1 hr) and the supernatant was incubated with 1 mL Ni2+-NTA resin for 1 hr. Resin was washed with lysis buffer and the protein was eluted with elution buffer (50 mM Tris pH 8.0, 500 mM NaCl, 10% glycerol, 500 mM imidazole, 10 mM BME). The elute was then diluted 5x with Buffer A (20 mM Tris pH 8.0, 1 mM DTT) and subjected to ion exchange using a MonoQ column (Buffer B = Buffer A + 1 M NaCl). Fractions were visualized by SDS page and pooled fractions were concentrated to 500 µL total volume then treated with 50 µL of 1 mg/mL TEV protease overnight at 4°C. The sample was further purified by size exclusion chromatography using

``

a Superdex 200 Increase column equilibrated in SEC buffer (20 mM Tris pH 8.0, 150 mM NaCl, 1 mM DTT). The Y1001D mutant was purified using the same procedure.

S. cerevisiae ΔN17-Arf1 and myristoylated-Arf1 were purified as previously described (Richardson and Fromme, 2015; Richardson et al., 2012).

The Gea2-Arf1 complex was prepared by incubating 1 mg of Gea2, 5 mg ΔN17Arf1, and 250 units alkaline phosphatase in 1.5 ml reaction volume at 4°C overnight. The complex was then purified by size exclusion chromatography using a Superdex 200 Increase column equilibrated in SEC buffer (20 mM Tris pH 8.0, 300 mM NaCl, 1 mM DTT).

CryoEM Sample preparation and data collection.

3.5 µL of Gea2 or the Gea2-Arf1 complex, at ~5 mg/mL in SEC Buffer containing 2 mM fluorinated fos-choline-8 (Anatrace, cat# F300F), was applied to glow discharged Quantifoil R1.2/1.3 grids, blotted for 5 seconds, then plunge-frozen into liquid ethane using a Vitrobot Mark IV. Imaging was done at 63kX nominal magnification on a Talos Arctica operating at 200kV equipped with a K3 detector and BioQuantum energy filter. For Gea2 alone, ~8000 movies were collected over multiple sessions, and for the Gea2-Arf1 complex ~2500 movies were collected. Movie exposures were collected using SerialEM (Mastronarde, 2005) using the multi-shot feature with coma correction. All data

``

was collected using 100 frames per movie exposure with a total dose of ~50 e- / Å2.

CryoEM data processing

K.m. Gea: Movie exposures were motion-corrected and dose-corrected using MotionCor2 (Zheng et al., 2017). Corrected micrographs were imported into cryoSPARC (Punjani et al., 2017) and then subjected to patch-CTF estimation. Blob picking was preformed on a subset of particles to make templates for template picking on the entire dataset. Picked particles were 2D and 3D classified in cryoSPARC before import into RELION. The particles underwent particle polishing and CTF refinements before reaching a consensus refinement. Masks were created around the DCB-HUS, GEF, and HDS1,2,3 domains for particle subtraction and focused refinements.

Gea2-Arf1 tilt data: particles were processed the same as K.m. Gea. For the dimer, separate template picking was performed to isolate those particles.

Gea2 alone:

Movie exposures were motion-corrected and dose-corrected using MotionCor2 (Zheng et al., 2017). Corrected micrographs were imported into cryoSPARC (Punjani et al., 2017) and then subjected to patch-CTF estimation. Particle picking was performed via TOPAZ (Bepler et al., 2019, 2020) using a ‘general’ model. Picked particles were parsed with 2D classification and rounds of 3D classification (see Fig.S1). A clean particle stack was generated and imported

``

into RELION 3.1 (Zivanov et al., 2018, 2020) and particles were 3D classified revealing three distinct conformations. Particles in each of the these three major classes were kept separate for the rest of the processing steps. Particles were subjected to multiple rounds of CTF refinement and Bayesian polishing (Zivanov et al., 2019). C2 symmetry was enforced during refinements of the open and closed states. After the iterative refinement process converged, particles from the closed/closed and open/open states were symmetry expanded and signal subtracted using a monomer mask (Nakane et al., 2018). For the closed/open state, an additional refinement was performed with C2 symmetry enforced in order to perform symmetry expansion and monomer particle subtraction. 3D classification was then used to generate separated particle stacks for the open and closed monomers. Following monomer refinements, subsequent signal subtraction and local refinements were performed separately on the N and C terminal regions. An additional signal subtraction and focused refinement was performed for the dimer interface of each of the three states (open, closed, and hemi). Density modification (Terwilliger et al., 2020) was then used to further improve all of the focused maps. Composite maps used for model building and refinement of each of the three dimeric conformations were generated with ‘Combine Focused Maps’ in Phenix (Liebschner et al., 2019). See Figs. S2 and S3, and Table 1.)

Gea2-Arf1 complex:

``

The cryoEM data collected for the Gea2-Arf1 complex was processed using the same procedure described above for Gea2 alone. 3D classification indicated that the sample was conformationally homogeneous, adopting a single conformation. After symmetry expansion and signal subtraction, focused refinements were performed on the DCB-HUS, GEF, and HDS1-3 regions. Density modification (Terwilliger et al., 2020) was used to further improve all of the focused maps, and composite maps used for model building and refinement were generated with 'Combine Focused Maps' in Phenix (Liebschner et al., 2019). See Fig. S6 and Table 1.

Atomic model building and refinement

The composite maps described above were used for atomic model building and refinement. Model building in Coot (Emsley et al., 2010) was guided by the AlphaFold prediction of Gea2 (Jumper et al., 2021) and by the Gea2 GEF domain - Arf1 crystal structure (Goldberg, 1998). Real space refinement and model validation was carried out using Phenix (Afonine et al., 2018; Emsley et al., 2010). See Figs. S3 and S6 and Table 1.

Yeast complementation assay

Gea2-expressing yeast plasmids (Table S1) were transformed into a Gea1/2 yeast shuffling strain (*gea1*Δ *gea2*Δ strain CFY2872, Table S2) and grown overnight at 30°C. Cultures were normalized by OD600 and serial diluted on

``

selection media. Plates were then incubated for three days at 30°C before imaging.

Fluorescence microscopy

Gea2-expressing yeast plasmids (Table S1) were transformed into *gea2*Δ yeast strain (CFY1470, Table S2) and grown at 30°C in selection media to an OD600 of 0.6. Cells were added to an imaging dish (MatTek), allowed to settle for 10 mins, then washed with fresh media. Cells were imaged using a CSU-X spinning-disk confocal system (Intelligent Imaging Innovations) with a DMI6000 B microscope (Leica), 100X 1.46 NA oil immersion objective, and a QuantME EMCCD camera (Photmetrics), using with a 200 μs exposure time.

Liposome Preparation

Liposomes were prepared in HK buffer (20mM HEPES pH 7.5, 150 mM KOAc) as described previously (Richardson and Fromme, 2015). Hydrated lipid mixes were extruded with 100 nm filters for GEF assays and 400 nm filters for the membrane-binding liposome pelleting assay.

In vitro membrane-binding assay

Liposome pelleting assays were performed as previously described (Gustafson and Fromme, 2017; Paczkowski and Fromme, 2016), using liposomes composed of 94% DOPC, 5% Nickel-DOGS, and 1% DiR lipids. 500 μg liposomes were incubated with 8 ug of protein in 50 μL total reaction

``

volume in HK buffer for 10 mins at room temperature. Reactions were then subjected to ultracentrifugation (128,000g for 10 mins). The supernatant was separated and the liposome pellet was resuspended in HK buffer. Supernatant and pellet samples were analyzed by SDS-PAGE.

In vitro GEF activity assay

GEF activity assays were performed as previously described, monitoring native tryptophan fluorescence (Gustafson and Fromme, 2017; Richardson and Fromme, 2015) using 99% DOPC and 1% DiR lipids. All reactions were performed in HKM buffer (20mM HEPES pH 7.5, 150 mM KOAc, 1 mM MgCl2) at 30°C. Myristoylated-Arf1 activation reactions were performed by incubating 333 μM liposomes, 200 nM Gea2, 200 μM GTP for 2 minutes before adding 1 μM myr-Arf1. ΔN-Arf1 activation was assessed in similar reactions, except liposomes were omitted, Gea2 concentration was 25 nM, and ΔN-Arf1 concentration was 500 nM.

``

APPENDIX II

PLASMIDS GENERATED IN THIS STUDY

Name	Description	Host Vector	Source
pAM001	6xHis-TEV-KmGea2	pET28	This study
pAM002	MBP-TEV-Sft1(1-75)-6xHis	pBCR353	This study
pAM003	MBP-TEV-Gos1(1-201)-6xHis	pBCR353	This study
pAM004	MBP-TEV-Ykt6(1-194)-6xHis	pBCR353	This study
pAM005	MBP-TEV-Sed5(1-319)-6xHis	pBCR353	This study
pAM006	MBP-TEV-Gos1(136-201)-6xHis	pBCR353	This study
pAM007	MBP-TEV-Ykt6(138-194)-6xHis	pBCR353	This study
pAM008	MBP-TEV-Sed5(252-319)-6xHis	pET28 pBCR353	This study
pAM009			This study
pAM010	pST50Trc1-Ykt6(1-194)-6xHis	pST50	This study
pAM011	pST50Trc2-Sft1(1-75)-6xHis	pST50	This study
pAM012	pST50Trc3-Sed5(1-319)-6xHis	pST50	This study
pAM013	pST50Trc4-MBP-TEV-Gos1(1-201)-6xHis	pST50	This study
pAM014	Gos1 Snare Bundle	pST44	This study
pAM015	pET28a-6xHis-TEV-Sly1	pET28a	This study
pAM016	Bos1 pop-in/out	pRS306	This study
pAM017	Gos1 pop-in/out	pRS306	This study
pAM018	mNeonGreen-Bos1	pRS306	This study
pAM019	MARS-Bos1	pRS306	This study
pAM020	mNeonGreen-Gos1	pRS306	This study

``

pAM021	**pGEX-6p-GEA1**	**pGEX**	**This study**
pAM022	**pGEX-6p-GEA2**	**pGEX**	**This study**
pAM023	**Bos1 Snare Bundle (SNARE domains only)**	**pST44**	**This study**
pAM024	**3xHA-Bos1**	**pRS306**	**This study**
pAM025	**3xHA-Gos1**	**pRS306**	**This study**
pAM026	**pGea1-Gea1(1-464)-Gea2(483-1459)-mNeonGreen**	**pRS415**	**This study**
pAM027	**pGea2-Gea2(1-462)-Gea1(465-1408)-mNeonGreen**	**pRS415**	**This study**
pAM028	**pGea1-Gea1(1-260)-Gea2(258-1459)-mNeonGreen**	**pRS415**	**This study**
pAM029	**pGea2-Gea2(1-257)-Gea1(261-1408)-mNeonGreen**	**pRS415**	**This study**
pAM030	**pRS425-Sec7, Sec7 promoter, CYC1 terminator**	**pRS425**	**This study**
pAM031	**pRS415-Gea1(L862S)**	**pRS415**	**This study**
pAM032	**pRS416-Bos1**	**pRS416**	**This study**
pAM033	**pRS40N**		**This study**
pAM034	**6xHis-TEV-Gea2 *P. pastoris* integration plasmid**	**pPICZ**	**This study**
pAM035	**pRRS416-Vps74 (own promoter and terminator**	**pRS416**	**This study**
pAM036	**pPICZ-Gea2(K.lactis)**	**pPICZ**	**This study**
pAM037	**pPICZ-Gea2(K.marxianus)**	**pPICZ**	**This study**
pAM039	**pPICZ-Gea2(K.thermo)**	**pPICZ**	**This study**
pAM040	**pET28a-6xHis-TEV-Arf1(K.m.)**	**pPICZ**	**This study**
pAM041	**Gea1-D257K-mNeonGreen**	**pRS415**	**This study**
pAM042	**Gea2-N-mNeonGreen**	**pRS415**	**This study**
pAM043	**Gea2 (Δ996-1004)-GFP yeast expression plasmid**	**pRS415**	**This study**

``

pAM045	Gea2 (Δ996-1004)-GFP yeast expression plasmid	pRS415	This study
pAM046	Gea2-pETH-Y1001D	pET28	This study
pAM047	Gea2-K124D-GFP	pRS415	This study
pAM048	pPICZ-Gea2-K124D	pPICZ	This study
pAM049	pPICZ-Gea2-F998D	pPICZ	This study
pAM050	pPICZ-Gea2-Y1001D	pPICZ	This study
pAM051	pPICZ-Gea2-E654K	pPICZ	This study
pAM052	Gea2-759-780GSlinker		This study
pAM053	Gea2- Δ759-761	pRS415	This study
pAM054	Gea2- Δ759-768	pRS415	This study
pAM055	Gea2- Δ759-776	pRS415	This study
pAM056	Gea2- Δ759-780	pRS415	This study
pAM057	pPICZ-Gea2- Δ759-761	pPICZ	This study
pAM058	pPICZ-Gea2- Δ759-768	pPICZ	This study
pAM059	pPICZ-Gea2- Δ759-776	pPICZ	This study
pAM060	pPICZ-Gea2- Δ759-780	pPICZ	This study
pMG001	Gea2-GFP yeast expression plasmid	pRS415	(Gustafson and Fromme, 2017)
pCF1053	ΔN17-Arf1 expression plasmid	pET28	(Richardson and Fromme, 2015; Richardson et al., 2012)
pArf1	Full-length Arf1 expression plasmid	pET3c	(Weiss et al., 1989)
pNmt1	Nmt1 expression	pCYC	(Duronio et al., 1990)

``

APPENDIX III

STRAINS GENERATED IN THIS STRAIN

SEY6210	*S.c.*	*MATα suc2-Δ9 ura3-52 his3-Δ200 leu2-3,112 lys2-801 trp1-Δ901*	(Robinson et al., 1988)
SEY6210	*S.c.*	*MATa suc2-Δ9 ura3-52 his3-Δ200 leu2-3,112 lys2-801 trp1-Δ901*	(Robinson et al., 1988)
CFY2872	*S.c.*	*BY4741α gea1Δ::KanMX gea2Δ::HIS3* +pCF1248	(Gustafson and Fromme, 2017; Liu et al., 2010)
CFY3148	*S.c.*	SEY6210.5 Sec7-Mars::*TRP1* Neon-Bos1::*URA3*	This study
CFY3328	*S.c.*	SEY6210.5 Sec7-Mars::*TRP1* Neon-Gos1::*URA3*	This study
CFY3329	*S.c.*	SEY6210 Gea1-3xMars::*TRP1* mNeonGreen-Gos1::*URA3*	This study
CFY3350	*S.c.*	SEY6211 Gea1-3xMars::*TRP1* mNeonGreen-Gos1::*URA3*	This study
CFY3351	*S.c.*	SEY6211 Gea2-3xMars::*TRP1* mNeonGreen-Gos1::*URA3*	This study
CFY3352	*S.c.*	SEY6211 Gea2-3xMars::*TRP1* mNeonGreen-Gos1::*URA3*	This study
CFY3353	*S.c.*	SEY6211 Gea1-3xMars::TRP1 mNeonGreen-Gos1::*URA3*	This study
CFY3374	*S.c.*	SEY6211 Gea1-3xMars::TRP1 mNeonGreen-Gos1	This study
CFY3375	*S.c.*	SEY6211 Gea2-3xMars::*TRP1* mNeonGreen-Gos1	This study
CFY3389	*S.c.*	SEY6211 Gea1-3xMars::*TRP1* mNeonGreen-Bos1::*URA3*	This study
CFY3390	*S.c.*	SEY6211 Gea2-3xMars::*TRP1* mNeonGreen-Bos1::*URA3*	This study
CFY3420	*S.c.*	SEY6211 Gea2-GFP::*HIS3* 3xHA-Bos1::*URA3*	This study
CFY3421	*S.c.*	SEY6211 Gea2-GFP::*HIS3* 3xHA-Gos1::*URA3*	This study
CFY3422	*S.c.*	SEY6211 Gea2-GFP::*HIS3* 3xHA-Bos1::*URA3*	This study
CFY3423	*S.c.*	SEY6211 Gea2-GFP::H*IS3* 3xHA-Gos1::*URA3*	This study
CFY3434	*S.c.*	SEY6211 Gea2-3xMars::*TRP1* GFP-Vrg4	This study
CFY3435	*S.c.*	SEY6211 SEY6211 Gea2-3xMars::*TRP1* GFP-Vrg4	This study
CFY3438	*S.c.*	SEY6211 Gea2-HA::HIS3GEA2-3xFLAG-6xHis::*TRP1*	This study
CFY3439	*S.c.*	SEY6211 Gea2-HA::HIS3GEA2-3xFLAG-6xHis::T*RP1*	This study
CFY3578	*S.c.*	SEY6211 Anp1-mNeonGreen::*HIS3*	This study
CFY3579	*S.c.*	SEY6211 Och1-mNeonGreen::*HIS3*	This study
CFY3580	*S.c.*	SEY6211 Alg5-mNeonGreen::*HIS3*	This study
CFY3698	*S.c.*		This study
CFY3767	*S.c.*	SEY6211 COP1-mCherry::K*anMX* GFP-P4C::*URA3*	This study
CFY3768	*S.c.*	SEY6211 Gea1-3xMars::*TRP1* GFP-P4C::*URA3*	This study
CFY3826	*S.c.*	SEY6210 Anp1-mNeonGreen	This study
CFY3853	*S.c.*	Anp1-mNeonGreen::*HIS3*	This study
CFY3863	*S.c.*	Anp1-mNeonGreen::HIS3Sec7-6xDsRed::*URA3*	This study
CFY3876	*S.c.*	Sec7-6xDsRed::*URA3*	This study
CFY3882	p.p.	KMH71h 6xHis-TEV-Gea2::BleoR	This study
CFY3890	*S.c.*	SEY6210 Sec7-6xDsRed::*URA3* Och1-mNeonGreen::*HIS3*	This study
CFY3891	*S.c.*	SEY6210 Sec7-6xDsRed::*URA*3 Alg5-mNeonGreen::*HIS3*	This study

``

CFY3897	*S.c.*	SEY6210 Sec7-6xDsRed::*URA3* Erd2-mNeonGreen::*HIS3*	This study
CFY3935	p.p.	KMH71h 6xHis-TEV-Gea(K. Marxianus)	This study
CFY3942	*S.c.*	SEY6211 Gea1-3xMars::TRP1Anp1-mNeonGreen::*HIS3*	This study
CFY3943	*S.c.*	SEY6211 Gea2-3xMars::TRP1Anp1-mNeonGreen::H*IS*	This study
CFY3962	p.p.	KMH71h 6xHis-TEV-Gea1	This study
CFY3977	*S.c.*	Sec7-6xDsRed*::URA3* Erd2-mNeonGreen*::HIS3*	This study
CFY3978	*S.c.*	Sec7-6xDsRed*::URA3* Erd2-mNeonGreen*::HIS3*	This study
CFY3979	*S.c.*	s*ec23-1* Sec7-6xDsRed*::URA3* Erd2-mNeonGreen*::HIS3*	This study
CFY3980	*S.c.*	*sec 23-1* Sec7-6xDsRed*::URA3* Erd2-mNeonGreen*::HIS3*	This study

``

REFERENCES

Ackema, K.B., Hench, J., Böckler, S., Wang, S.C., Sauder, U., Mergentaler, H., Westermann, B., Bard, F., Frank, S., and Spang, A. (2014). The small GTPase Arf1 modulates mitochondrial morphology and function. EMBO J. 33, 2659–2675.

Adarska, P., Wong-Dilworth, L., and Bottanelli, F. (2021). ARF GTPases and Their Ubiquitous Role in Intracellular Trafficking Beyond the Golgi. Front Cell Dev Biol 9, 679046.

Afonine, P.V., Klaholz, B.P., Moriarty, N.W., Poon, B.K., Sobolev, O.V., Terwilliger, T.C., Adams, P.D., and Urzhumtsev, A. (2018). New tools for the analysis and validation of cryo-EM maps and atomic models. Acta Crystallogr D Struct Biol 74, 814–840.

Aiyer, S., Zhang, C., Baldwin, P.R., and Lyumkis, D. (2021). Evaluating Local and Directional Resolution of Density Maps. In CryoEM, T. Gonen, and B.L. Nannenga, eds. (New York, NY: Springer US), pp. 161–187.

Aizel, K., Biou, V., Navaza, J., Duarte, L.V., Campanacci, V., Cherfils, J., and Zeghouf, M. (2013). Integrated conformational and lipid-sensing regulation of endosomal ArfGEF BRAG2. PLoS Biol. 11, e1001652.

Akopian, D., Shen, K., Zhang, X., and Shan, S. (2013). Signal Recognition Particle: An Essential Protein-Targeting Machine. Annu. Rev. Biochem. 82, 693–721. https://doi.org/10.1146/annurev-biochem-072711-164732.

Alberts, B., Johnson, A., Lewis, J., Raff, M., Roberts, K., and Walter, P. (2002). Molecular Biology of the Cell (Garland Science).

Alexandrov, K., Horiuchi, H., Steele-Mortimer, O., Seabra, M.C., and Zerial, M. (1994). Rab escort protein-1 is a multifunctional protein that accompanies newly prenylated rab proteins to their target membranes. EMBO J. 13, 5262–5273. https://doi.org/10.1002/j.1460-2075.1994.tb06860.x.

Amor, J.C., Harrison, D.H., Kahn, R.A., and Ringe, D. (1994). Structure of the human ADP-ribosylation factor 1 complexed with GDP. Nature 372, 704–708.

Antonny, B., Beraud-Dufour, S., Chardin, P., and Chabre, M. (1997). N-terminal hydrophobic residues of the G-protein ADP-ribosylation factor-1 insert into membrane phospholipids upon GDP to GTP exchange. Biochemistry 36, 4675–4684.

Arakel, E.C., Schwappach, B., Arakel, E.C., and Schwappach, B. (2018). Correction : Formation of COPI-coated vesicles at a glance (doi : 10 . 1242 /

``

jcs . 209890) Formation of COPI-coated vesicles at a glance. https://doi.org/10.1242/209890.

Arst, H.N., Jr, Hernandez-Gonzalez, M., Peñalva, M.A., and Pantazopoulou, A. (2014). GBF/Gea mutant with a single substitution sustains fungal growth in the absence of BIG/Sec7. FEBS Lett. 588, 4799–4806.

Barlowe, C., Orci, L., Yeung, T., Hosobuchi, M., Hamamoto, S., Salama, N., Rexach, M.F., Ravazzola, M., Amherdt, M., and Schekman, R. (1994). COPII: a membrane coat formed by Sec proteins that drive vesicle budding from the endoplasmic reticulum. Cell 77, 895–907. https://doi.org/10.1016/0092-8674(94)90138-4.

Barr, F.A. (2009). Rab GTPase function in Golgi trafficking. Semin. Cell Dev. Biol. 20, 780–783. https://doi.org/10.1016/j.semcdb.2009.03.007.

Barreto-Vieira, D.F., and Barth, O.M. (2015). Negative and Positive Staining in Transmission Electron Microscopy for Virus Diagnosis. In Microbiology in Agriculture and Human Health, M.M. Shah, ed. (InTech), p.

Beck, M., and Hurt, E. (2017). The nuclear pore complex: understanding its function through structural insight. Nat. Rev. Mol. Cell Biol. 18, 73–89. https://doi.org/10.1038/nrm.2016.147.

Bepler, T., Kelley, K., Noble, A.J., and Berger, B. (2020). Topaz-Denoise: general deep denoising models for cryoEM and cryoET. Nat. Commun. 11, 5208.

Bepler, T., Morin, A., Rapp, M., Brasch, J., Shapiro, L., Noble, A.J., and Berger, B. (2019). Positive-unlabeled convolutional neural networks for particle picking in cryo-electron micrographs. Nat. Methods 16, 1153–1160.

Bhatt, J.M., Viktorova, E.G., Busby, T., Wyrozumska, P., Newman, L.E., Lin, H., Lee, E., Wright, J., Belov, G.A., Kahn, R.A., et al. (2016). Oligomerization of the Sec7 domain Arf guanine nucleotide exchange factor GBF1 is dispensable for Golgi localization and function but regulates degradation. Am. J. Physiol. Cell Physiol. 310, C456–C469.

Bonifacino, J.S. (2014). Adaptor proteins involved in polarized sorting. J. Cell Biol. 204, 7–17. https://doi.org/10.1083/jcb.201310021.

Bonifacino, J.S., and Glick, B.S. (2004). The Mechanisms of Vesicle Budding and Fusion. Cell 116, 153–166. https://doi.org/10.1016/S0092-8674(03)01079-1.

``

Bonifacino, J.S., and Lippincott-Schwartz, J. (2003). Coat proteins: shaping membrane transport. Nat. Rev. Mol. Cell Biol. 4, 409–414. https://doi.org/10.1038/nrm1099.

Bouvet, S., Golinelli-Cohen, M.-P., Contremoulins, V., and Jackson, C.L. (2013). Targeting of the Arf-GEF GBF1 to lipid droplets and Golgi membranes. J. Cell Sci. 126, 4794–4805.

Bui, Q.T., Golinelli-Cohen, M.-P., and Jackson, C.L. (2009). Large Arf1 guanine nucleotide exchange factors: evolution, domain structure, and roles in membrane trafficking and human disease. Mol. Genet. Genomics 282, 329–350.

Cai, H., Reinisch, K., and Ferro-Novick, S. (2007). Coats, Tethers, Rabs, and SNAREs Work Together to Mediate the Intracellular Destination of a Transport Vesicle. Dev. Cell 12, 671–682. https://doi.org/10.1016/j.devcel.2007.04.005.

Cao, X. (1998). Initial docking of ER-derived vesicles requires Uso1p and Ypt1p but is independent of SNARE proteins. EMBO J. 17, 2156–2165. https://doi.org/10.1093/emboj/17.8.2156.

Casanova, J.E. (2007). Regulation of Arf activation: The Sec7 family of guanine nucleotide exchange factors. Traffic 8, 1476–1485. https://doi.org/10.1111/j.1600-0854.2007.00634.x.

Casler, J.C., Papanikou, E., Barrero, J.J., and Glick, B.S. (2019). Maturation-driven transport and AP-1–dependent recycling of a secretory cargo in the Golgi. J. Cell Biol. 218, 1582–1601. https://doi.org/10.1083/jcb.201807195.

Chen, Y.-T., Wang, I.-H., Wang, Y.-H., Chiu, W.-Y., Hu, J.-H., Chen, W.-H., and Lee, F.-J.S. (2019). Action of Arl1 GTPase and golgin Imh1 in Ypt6-independent retrograde transport from endosomes to the trans-Golgi network. Mol. Biol. Cell 30, 1008–1019. https://doi.org/10.1091/mbc.E18-09-0579.

Cherfils, J. (2014). Arf GTPases and their effectors: assembling multivalent membrane-binding platforms. Curr. Opin. Struct. Biol. 29, 67–76.

Cherfils, J., and Zeghouf, M. (2013). Regulation of small GTPases by GEFs, GAPs, and GDIs. Physiol. Rev. 93, 269–309. https://doi.org/10.1152/physrev.00003.2012.

Christis, C., and Munro, S. (2012). The small G protein Arl1 directs the trans-Golgi-specific targeting of the Arf1 exchange factors BIG1 and BIG2. J. Cell Biol. 196, 327–335.

Claude, A., Zhao, B.P., Kuziemsky, C.E., Dahan, S., Berger, S.J., Yan, J.P., Armold, A.D., Sullivan, E.M., and Melançon, P. (1999). GBF1: A novel Golgi-

associated BFA-resistant guanine nucleotide exchange factor that displays specificity for ADP-ribosylation factor 5. J. Cell Biol. 146, 71–84.

Cronin, T.C., DiNitto, J.P., Czech, M.P., and Lambright, D.G. (2004). Structural determinants of phosphoinositide selectivity in splice variants of Grp1 family PH domains. EMBO J. 23, 3711–3720.

D'Souza-Schorey, C., and Chavrier, P. (2006). ARF proteins: roles in membrane traffic and beyond. Nat. Rev. Mol. Cell Biol. 7, 347–358. https://doi.org/10.1038/nrm1910.

Das, S., Malaby, A.W., Nawrotek, A., Zhang, W., Zeghouf, M., Maslen, S., Skehel, M., Chakravarthy, S., Irving, T.C., Bilsel, O., et al. (2019). Structural Organization and Dynamics of Homodimeric Cytohesin Family Arf GTPase Exchange Factors in Solution and on Membranes. Structure 27, 1782–1797.e7.

De Matteis, M.A., and Luini, A. (2008). Exiting the Golgi complex. Nat. Rev. Mol. Cell Biol. 9, 273–284. https://doi.org/10.1038/nrm2378.

Dechant, R., Saad, S., Ibáñez, A.J., and Peter, M. (2014). Cytosolic pH regulates cell growth through distinct GTPases, Arf1 and Gtr1, to promote Ras/PKA and TORC1 activity. Mol. Cell 55, 409–421.

Delprato, A., and Lambright, D.G. (2007). Structural basis for Rab GTPase activation by VPS9 domain exchange factors. Nat. Struct. Mol. Biol. 14, 406–412.

DiNitto, J.P., Delprato, A., Gabe Lee, M.-T., Cronin, T.C., Huang, S., Guilherme, A., Czech, M.P., and Lambright, D.G. (2007). Structural basis and mechanism of autoregulation in 3-phosphoinositide-dependent Grp1 family Arf GTPase exchange factors. Mol. Cell 28, 569–583.

Donaldson, J.G., and Jackson, C.L. (2011). ARF family G proteins and their regulators: roles in membrane transport, development and disease. Nat. Rev. Mol. Cell Biol. 12, 362–375.

Drin, G., and Antonny, B. (2010). Amphipathic helices and membrane curvature. FEBS Lett. 584, 1840–1847.

Dubochet, J., Adrian, M., Chang, J.-J., Homo, J.-C., Lepault, J., McDowall, A.W., and Schultz, P. (1988). Cryo-electron microscopy of vitrified specimens. Q. Rev. Biophys. 21, 129–228. https://doi.org/10.1017/S0033583500004297.

Duke, E.M.H., and Johnson, L.N. (2010). Macromolecular crystallography at synchrotron radiation sources: current status and future developments. Proc.

``

R. Soc. Math. Phys. Eng. Sci. 466, 3421–3452. https://doi.org/10.1098/rspa.2010.0448.

Duronio, R.J., Jackson-Machelski, E., Heuckeroth, R.O., Olins, P.O., Devine, C.S., Yonemoto, W., Slice, L.W., Taylor, S.S., and Gordon, J.I. (1990). Protein N-myristoylation in Escherichia coli: reconstitution of a eukaryotic protein modification in bacteria. Proc. Natl. Acad. Sci. U. S. A. 87, 1506–1510.

Ellgaard, L., and Helenius, A. (2003). Quality control in the endoplasmic reticulum. Nat. Rev. Mol. Cell Biol. 4, 181–191. https://doi.org/10.1038/nrm1052.

Emsley, P., Lohkamp, B., Scott, W.G., and Cowtan, K. (2010). Features and development of Coot. Acta Crystallogr. D Biol. Crystallogr. 66, 486–501.

Franco, M., Chardin, P., Chabre, M., and Paris, S. (1995). Myristoylation of ADP-ribosylation factor 1 facilitates nucleotide exchange at physiological Mg2+ levels. J. Biol. Chem. 270, 1337–1341.

Franzusoff, A., Redding, K., Crosby, J., Fuller, R.S., and Schekman, R. (1991). Localization of components involved in protein transport and processing through the yeast Golgi apparatus. J. Cell Biol. 112, 27–37.

Fromme, J.C., Orci, L., and Schekman, R. (2008). Coordination of COPII vesicle trafficking by Sec23. Trends Cell Biol. 18, 330–336. https://doi.org/10.1016/j.tcb.2008.04.006.

Galindo, A., Soler, N., McLaughlin, S.H., Yu, M., Williams, R.L., and Munro, S. (2016). Structural Insights into Arl1-Mediated Targeting of the Arf-GEF BIG1 to the trans-Golgi. Cell Rep. 16, 839–850.

Gaynor, E.C., and Emr, S.D. (1997). COPI-independent anterograde transport: Cargo-selective ER to Golgi protein transport in yeast COPI mutants. J. Cell Biol. 136, 789–802. https://doi.org/10.1083/jcb.136.4.789.

Gillingham, A.K., and Munro, S. (2007). The small G proteins of the Arf family and their regulators. Annu. Rev. Cell Dev. Biol. 23, 579–611. https://doi.org/10.1146/annurev.cellbio.23.090506.123209.

Glick, B.S. (2000). Organization of the Golgi apparatus. Curr. Opin. Cell Biol. 12, 450–456. https://doi.org/10.1016/S0955-0674(00)00116-2.

Glick, B.S., and Luini, A. (2011). Models for Golgi traffic: A critical assessment. Cold Spring Harb. Perspect. Biol. 3, 1–16. https://doi.org/10.1101/cshperspect.a005215.

``

Goldberg, J. (1998). Structural basis for activation of ARF GTPase: mechanisms of guanine nucleotide exchange and GTP-myristoyl switching. Cell 95, 237–248.

Gomez-Navarro, N., and Miller, E. (2016). Protein sorting at the ER-Golgi interface. J. Cell Biol. 215, 769–778. https://doi.org/10.1083/jcb.201610031.

Grebe, M., Gadea, J., Steinmann, T., Kientz, M., Rahfeld, J.U., Salchert, K., Koncz, C., and Jürgens, G. (2000). A conserved domain of the arabidopsis GNOM protein mediates subunit interaction and cyclophilin 5 binding. Plant Cell 12, 343–356.

Gureasko, J., Galush, W.J., Boykevisch, S., Sondermann, H., Bar-Sagi, D., Groves, J.T., and Kuriyan, J. (2008). Membrane-dependent signal integration by the Ras activator Son of sevenless. Nat. Struct. Mol. Biol. 15, 452–461.

Gustafson, M.A. (2017). THE ARF-GEFS GEA1 AND GEA2 INTEGRATE SIGNALS TO COORDINATE VESICLE TRAFFICKING AT THE GOLGI COMPLEX.

Gustafson, M.A., and Fromme, J.C. (2017). Regulation of Arf activation occurs via distinct mechanisms at early and late Golgi compartments. Mol. Biol. Cell mbc.E17-06-0370. https://doi.org/10.1091/mbc.E17-06-0370.

Halaby, S.L., and Fromme, J.C. (2018). The HUS box is required for allosteric regulation of the Sec7 Arf-GEF. J. Biol. Chem. 293, 6682–6691.

Haun, R.S., Tsai, S.C., Adamik, R., Moss, J., and Vaughan, M. (1993). Effect of myristoylation on GTP-dependent binding of ADP-ribosylation factor to Golgi. J. Biol. Chem. 268, 7064–7068.

Isomura, M., Kikuchi, A., Ohga, N., and Takai, Y. (1991). Regulation of binding of rhoB p20 to membranes by its specific regulatory protein, GDP dissociation inhibitor. Oncogene 6, 119–124.

Jackson, L.P. (2014). Structure and mechanism of COPI vesicle biogenesis. Curr. Opin. Cell Biol. 29, 67–73. https://doi.org/10.1016/j.ceb.2014.04.009.

Jackson, L.P., Lewis, M., Kent, H.M., Edeling, M.A., Evans, P.R., Duden, R., and Owen, D.J. (2012). Molecular basis for recognition of dilysine trafficking motifs by COPI. Dev. Cell 23, 1255–1262. https://doi.org/10.1016/j.devcel.2012.10.017.

Jensen, D., and Schekman, R. (2011). COPII-mediated vesicle formation at a glance. J. Cell Sci. 124, 1–4. https://doi.org/10.1242/jcs.069773.

``

Jumper, J., Evans, R., Pritzel, A., Green, T., Figurnov, M., Ronneberger, O., Tunyasuvunakool, K., Bates, R., Žídek, A., Potapenko, A., et al. (2021). Highly accurate protein structure prediction with AlphaFold. Nature 596, 583–589.

Kahn, R.A., and Gilman, A.G. (1986). The protein cofactor necessary for ADP-ribosylation of Gs by cholera toxin is itself a GTP binding protein. J. Biol. Chem. 261, 7906–7911.

Kahn, R.A., Goddard, C., and Newkirk, M. (1988). Chemical and immunological characterization of the 21-kDa ADP-ribosylation factor of adenylate cyclase. J. Biol. Chem. 263, 8282–8287.

Kahn, R.A., Randazzo, P., Serafini, T., Weiss, O., Rulka, C., Clark, J., Amherdt, M., Roller, P., Orci, L., and Rothman, J.E. (1992). The amino terminus of ADP-ribosylation factor (ARF) is a critical determinant of ARF activities and is a potent and specific inhibitor of protein transport. J. Biol. Chem. 267, 13039–13046.

Kelly, E., Horgan, C., Goud, B., and Mccaffrey, M. (2012). The Rab family of proteins: 25 Years on. Biochem. Soc. Trans. 40, 1337–1347. https://doi.org/10.1042/BST20120203.

Kirchhausen, T. (2000). Clathrin. Annu. Rev. Biochem. 69, 699–727. https://doi.org/10.1146/annurev.biochem.69.1.699.

Kühlbrandt, W. (2014). The Resolution Revolution. Science 343, 1443–1444. https://doi.org/10.1126/science.1251652.

Kühlbrandt, W. (2015). Structure and function of mitochondrial membrane protein complexes. BMC Biol. 13, 89. https://doi.org/10.1186/s12915-015-0201-x.

Kumari, S., and Mayor, S. (2008). ARF1 is directly involved in dynamin-independent endocytosis. Nat. Cell Biol. 10, 30–41.

Lauer, J., Segeletz, S., Cezanne, A., Guaitoli, G., Raimondi, F., Gentzel, M., Alva, V., Habeck, M., Kalaidzidis, Y., Ueffing, M., et al. (2019). Auto-regulation of Rab5 GEF activity in Rabex5 by allosteric structural changes, catalytic core dynamics and ubiquitin binding. Elife 8.

Lee, J.Y., Chen, H., Liu, A., Alba, B.M., and Lim, A.C. (2017). Auto-induction of Pichia pastoris AOX1 promoter for membrane protein expression. Protein Expr. Purif. 137, 7–12.

Liebschner, D., Afonine, P.V., Baker, M.L., Bunkóczi, G., Chen, V.B., Croll, T.I., Hintze, B., Hung, L.W., Jain, S., McCoy, A.J., et al. (2019).

``

Macromolecular structure determination using X-rays, neutrons and electrons: recent developments in Phenix. Acta Crystallogr D Struct Biol 75, 861–877.

Lipatova, Z., Tokarev, A.A., Jin, Y., Mulholland, J., Weisman, L.S., and Segev, N. (2008). Direct Interaction between a Myosin V Motor and the Rab GTPases Ypt31/32 Is Required for Polarized Secretion. Mol. Biol. Cell 19, 4177–4187. https://doi.org/10.1091/mbc.E08-02-0220.

Liu, Y., Kahn, R.A., and Prestegard, J.H. (2010). Dynamic structure of membrane-anchored Arf*GTP. Nat. Struct. Mol. Biol. 17, 876–881.

Losev, E., Reinke, C.A., Jellen, J., Strongin, D.E., Bevis, B.J., and Glick, B.S. (2006). Golgi maturation visualized in living yeast. Nature 441, 1002–1006. https://doi.org/10.1038/nature04717.

Lowery, J., Szul, T., Styers, M., Holloway, Z., Oorschot, V., Klumperman, J., and Sztul, E. (2013). The Sec7 guanine nucleotide exchange factor GBF1 regulates membrane recruitment of BIG1 and BIG2 guanine nucleotide exchange factors to the trans-Golgi network (TGN). J. Biol. Chem. 288, 11532–11545.

Malaby, A.W., Das, S., Chakravarthy, S., Irving, T.C., Bilsel, O., and Lambright, D.G. (2018). Structural Dynamics Control Allosteric Activation of Cytohesin Family Arf GTPase Exchange Factors. Structure 26, 106–117.e6.

Martin, W.F., Garg, S., and Zimorski, V. (2015). Endosymbiotic theories for eukaryote origin. Philos. Trans. R. Soc. B Biol. Sci. 370, 20140330. https://doi.org/10.1098/rstb.2014.0330.

Mastronarde, D.N. (2005). Automated electron microscope tomography using robust prediction of specimen movements. J. Struct. Biol. 152, 36–51.

Matsuura-Tokita, K., Takeuchi, M., Ichihara, A., Mikuriya, K., and Nakano, A. (2006). Live imaging of yeast Golgi cisternal maturation. Nature 441, 1007–1010. https://doi.org/10.1038/nature04737.

McDonold, C.M., and Fromme, J.C. (2014). Four GTPases Differentially Regulate the Sec7 Arf-GEF to Direct Traffic at the trans-Golgi Network. Dev. Cell 30, 759–767. https://doi.org/10.1016/j.devcel.2014.07.016.

Meissner, J.M., Bhatt, J.M., Lee, E., Styers, M.L., Ivanova, A.A., Kahn, R.A., and Sztul, E. (2018). The ARF guanine nucleotide exchange factor GBF1 is targeted to Golgi membranes through a PIP-binding domain. J. Cell Sci. 131.

Mironov, A.A., Beznoussenko, G.V., Nicoziani, P., Martella, O., Trucco, A., Kweon, H.-S., Di Giandomenico, D., Polishchuk, R.S., Fusella, A., Lupetti, P., et al. (2001). Small cargo proteins and large aggregates can traverse the Golgi

by a common mechanism without leaving the lumen of cisternae. J. Cell Biol. 155, 1225–1238. https://doi.org/10.1083/jcb.200108073.

Monetta, P., Slavin, I., Romero, N., and Alvarez, C. (2007). Rab1b interacts with GBF1 and modulates both ARF1 dynamics and COPI association. Mol. Biol. Cell 18, 2400–2410.

Mouratou, B., Biou, V., Joubert, A., Cohen, J., Shields, D.J., Geldner, N., Jürgens, G., Melançon, P., and Cherfils, J. (2005). The domain architecture of large guanine nucleotide exchange factors for the small GTP-binding protein Arf. BMC Genomics 6, 20. https://doi.org/10.1186/1471-2164-6-20.

Nakane, T., Kimanius, D., Lindahl, E., and Scheres, S.H. (2018). Characterisation of molecular motions in cryo-EM single-particle data by multi-body refinement in RELION. Elife 7.

Nakańo, A., and Muramatsu, M. (1989). A novel GTP-binding protein, Sar1p, is involved in transport from the endoplasmic reticulum to the Golgi apparatus. J. Cell Biol. 109, 2677–2691. https://doi.org/10.1083/jcb.109.6.2677.

Novick, P., Ferro, S., and Schekman, R. (1981). Order of events in the yeast secretory pathway. Cell 25, 461–469.

Novick, P., Field, C., and Schekman, R. (1980). Identification of 23 complementation groups required for post-translational events in the yeast secretory pathway. Cell 21, 205–215. https://doi.org/10.1016/0092-8674(80)90128-2.

Paczkowski, J.E., and Fromme, J.C. (2016). Analysis of Arf1 GTPase-Dependent Membrane Binding and Remodeling Using the Exomer Secretory Vesicle Cargo Adaptor. Methods Mol. Biol. 1496, 41–53.

Palade, G. (1975). Intracellular aspects of the process of protein synthesis. Science 189, 347–358. https://doi.org/10.1126/science.1096303.

Paris, S., Béraud-Dufour, S., Robineau, S., Bigay, J., Antonny, B., Chabre, M., and Chardin, P. (1997). Role of protein-phospholipid interactions in the activation of ARF1 by the guanine nucleotide exchange factor Arno. J. Biol. Chem. 272, 22221–22226.

Park, S.-K., Hartnell, L.M., and Jackson, C.L. (2005). Mutations in a highly conserved region of the Arf1p activator GEA2 block anterograde Golgi transport but not COPI recruitment to membranes. Mol. Biol. Cell 16, 3786–3799.

Park, S.Y., and Guo, X. (2014). Adaptor protein complexes and intracellular transport. Biosci. Rep. 34, e00123. https://doi.org/10.1042/BSR20140069.

``

Pearse, B.M.F. (1975). Coated vesicles from pig brain: Purification and biochemical characterization. J. Mol. Biol. 97, 93–98. https://doi.org/10.1016/S0022-2836(75)80024-6.

Peyroche, A., Paris, S., and Jackson, C.L. (1996). Nucleotide exchange on ARF mediated by yeast Gea1 protein. Nature 384, 479–481.

Pfeffer, S.R. (1999). Transport-vesicle targeting: tethers before SNAREs. Nat. Cell Biol. 1, E17–E22. https://doi.org/10.1038/8967.

Pocognoni, C.A., Viktorova, E.G., Wright, J., Meissner, J.M., Sager, G., Lee, E., Belov, G.A., and Sztul, E. (2018). Highly conserved motifs within the large Sec7 ARF guanine nucleotide exchange factor GBF1 target it to the Golgi and are critical for GBF1 activity. Am. J. Physiol. Cell Physiol. 314, C675–C689.

Punjani, A., Rubinstein, J.L., Fleet, D.J., and Brubaker, M.A. (2017). cryoSPARC: algorithms for rapid unsupervised cryo-EM structure determination. Nat. Methods 14, 290–296. https://doi.org/10.1038/nmeth.4169.

Ramaen, O., Joubert, A., Simister, P., Belgareh-Touzé, N., Olivares-Sanchez, M.C., Zeeh, J.C., Chantalat, S., Golinelli-Cohen, M.P., Jackson, C.L., Biou, V., et al. (2007). Interactions between conserved domains within homodimers in the BIG1, BIG2, and GBF1 Arf guanine nucleotide exchange factors. J. Biol. Chem. 282, 28834–28842. https://doi.org/10.1074/jbc.M705525200.

Renault, L., Guibert, B., and Cherfils, J. (2003). Structural snapshots of the mechanism and inhibition of a guanine nucleotide exchange factor. Nature 426, 525–530. https://doi.org/10.1038/nature02197.

Richardson, B.C., and Fromme, J.C. (2012). Autoregulation of Sec7 Arf-GEF activity and localization by positive feedback. Small GTPases 3, 240–243.

Richardson, B.C., and Fromme, J.C. (2015). Biochemical methods for studying kinetic regulation of Arf1 activation by Sec7. Methods Cell Biol. 130, 101–126.

Richardson, B.C., Halaby, S.L., Gustafson, M.A., and Fromme, J.C. (2016). The Sec7 N-terminal regulatory domains facilitate membrane-proximal activation of the Arf1 GTPase. ELife 5, 1–20. https://doi.org/10.7554/eLife.12411.001.

Richardson, B.C., Halaby, S.L., Gustafson, M.A., and Fromme, J.C. (2016). The Sec7 N-terminal regulatory domains facilitate membrane-proximal activation of the Arf1 GTPase. Elife 5.

Richardson, B.C., McDonold, C.M., and Fromme, J.C. (2012). The Sec7 Arf-GEF Is Recruited to the trans-Golgi Network by Positive Feedback. Dev. Cell 22, 799–810. https://doi.org/10.1016/j.devcel.2012.02.006.

Robinson, J.S., Klionsky, D.J., Banta, L.M., and Emr, S.D. (1988). Protein sorting in Saccharomyces cerevisiae: isolation of mutants defective in the delivery and processing of multiple vacuolar hydrolases. Mol. Cell. Biol. 8, 4936–4948.

Römisch, K. (1999). Surfing the Sec61 channel: bidirectional protein translocation across the ER membrane. J. Cell Sci. 112 (Pt 23), 4185–4191. https://doi.org/10.1242/jcs.112.23.4185.

Rosenthal, P.B., and Henderson, R. (2003). Optimal Determination of Particle Orientation, Absolute Hand, and Contrast Loss in Single-particle Electron Cryomicroscopy. J. Mol. Biol. 333, 721–745. https://doi.org/10.1016/j.jmb.2003.07.013.

Rupp, B. (2010). Biomolecular crystallography: principles, practice, and application to structural biology (New York: Garland Science).

Santiago-Tirado, F.H., and Bretscher, A. (2011). Membrane-trafficking sorting hubs: cooperation between PI4P and small GTPases at the trans-Golgi network. Trends Cell Biol. 21, 515–525. https://doi.org/10.1016/j.tcb.2011.05.005.

Semenza, J.C., Hardwick, K.G., Dean, N., and Pelham, H.R.B. (1990). ERD2, a yeast gene required for the receptor-mediated retrieval of luminal ER proteins from the secretory pathway. Cell 61, 1349–1357. https://doi.org/10.1016/0092-8674(90)90698-E.

Siniossoglou, S., Peak-Chew, S.Y., and Pelham, H.R. (2000). Ric1p and Rgp1p form a complex that catalyses nucleotide exchange on Ypt6p. EMBO J. 19, 4885–4894. https://doi.org/10.1093/emboj/19.18.4885.

Soldati, T., Shapiro, A.D., Svejstrup, A.B., and Pfeffer, S.R. (1994). Membrane targeting of the small GTPase Rab9 is accompanied by nucleotide exchange. Nature 369, 76–78.

Sondermann, H., Soisson, S.M., Boykevisch, S., Yang, S.-S., Bar-Sagi, D., and Kuriyan, J. (2004). Structural analysis of autoinhibition in the Ras activator Son of sevenless. Cell 119, 393–405.

Spang, A., Herrmann, J.M., Hamamoto, S., and Schekman, R. (2001). The ADP ribosylation factor-nucleotide exchange factors Gea1p and Gea2p have overlapping, but not redundant functions in retrograde transport from the Golgi to the endoplasmic reticulum. Mol. Biol. Cell 12, 1035–1045.

Su, M.-Y., Fromm, S.A., Zoncu, R., and Hurley, J.H. (2020). Structure of the C9orf72 ARF GAP complex that is haploinsufficient in ALS and FTD. Nature 585, 251–255.

``

Terwilliger, T.C., Ludtke, S.J., Read, R.J., Adams, P.D., and Afonine, P.V. (2020). Improvement of cryo-EM maps by density modification. Nat. Methods 17, 923–927.

Thomas, L.L., and Fromme, J.C. (2016). GTPase cross talk regulates TRAPPII activation of Rab11 homologues during vesicle biogenesis. J. Cell Biol. 215, 499–513. https://doi.org/10.1083/jcb.201608123.

Thomas, L.L., Joiner, A.M.N., and Fromme, J.C. (2018). The TRA PPI II complex activates the GTPase Ypt1 (Rab1) in the secretory pathway. J. Cell Biol. 217, 283–298. https://doi.org/10.1083/jcb.201705214.

Togawa, A., Morinaga, N., Ogasawara, M., Moss, J., and Vaughan, M. (1999). Purification and cloning of a brefeldin A-inhibited guanine nucleotide-exchange protein for ADP-ribosylation factors. J. Biol. Chem. 274, 12308–12315.

Trahey, M., and Hay, J.C. (2010). Transport vesicle uncoating: it's later than you think. F1000 Biol. Rep. 2, 47. https://doi.org/10.3410/b2-47.

Trueman, S.F., Mandon, E.C., and Gilmore, R. (2012). A gating motif in the translocation channel sets the hydrophobicity threshold for signal sequence function. J. Cell Biol. 199, 907–918. https://doi.org/10.1083/jcb.201207163.

Vincent, M.J., Martin, A.S., and Compans, R.W. (1998). Function of the KKXX motif in endoplasmic reticulum retrieval of a transmembrane protein depends on the length and structure of the cytoplasmic domain. J. Biol. Chem. 273, 950–956. https://doi.org/10.1074/jbc.273.2.950.

Walch-Solimena, C., Collins, R.N., and Novick, P.J. (1997). Sec2p Mediates Nucleotide Exchange on Sec4p and Is Involved in Polarized Delivery of Post-Golgi Vesicles. J. Cell Biol. 137, 1495–1509. https://doi.org/10.1083/jcb.137.7.1495.

Walter, P., and Blobel, G. (1980). Purification of a membrane-associated protein complex required for protein translocation across the endoplasmic reticulum. Proc. Natl. Acad. Sci. 77, 7112–7116. https://doi.org/10.1073/pnas.77.12.7112.

Wang, R., Wang, Z., Wang, K., Zhang, T., and Ding, J. (2016). Structural basis for targeting BIG1 to Golgi apparatus through interaction of its DCB domain with Arl1. J. Mol. Cell Biol. 8, 459–461.

Weiss, O., Holden, J., Rulka, C., and Kahn, R.A. (1989). Nucleotide binding and cofactor activities of purified bovine brain and bacterially expressed ADP-ribosylation factor. J. Biol. Chem. 264, 21066–21072.

``

Wilfling, F., Thiam, A.R., Olarte, M.-J., Wang, J., Beck, R., Gould, T.J., Allgeyer, E.S., Pincet, F., Bewersdorf, J., Farese, R.V., Jr, et al. (2014). Arf1/COPI machinery acts directly on lipid droplets and enables their connection to the ER for protein targeting. Elife 3, e01607.

Yu, B., Martins, I.R.S., Li, P., Amarasinghe, G.K., Umetani, J., Fernandez-Zapico, M.E., Billadeau, D.D., Machius, M., Tomchick, D.R., and Rosen, M.K. (2010). Structural and energetic mechanisms of cooperative autoinhibition and activation of Vav1. Cell 140, 246–256.

Zhang, Z., Zhang, T., Wang, S., Gong, Z., Tang, C., Chen, J., and Ding, J. (2014). Molecular mechanism for Rabex-5 GEF activation by Rabaptin-5. Elife 3.

Zheng, S.Q., Palovcak, E., Armache, J.-P., Verba, K.A., Cheng, Y., and Agard, D.A. (2017). MotionCor2: anisotropic correction of beam-induced motion for improved cryo-electron microscopy. Nat. Methods 14, 331–332.

Zivanov, J., Nakane, T., and Scheres, S.H.W. (2019). A Bayesian approach to beam-induced motion correction in cryo-EM single-particle analysis. IUCrJ 6, 5–17.

Zivanov, J., Nakane, T., Forsberg, B.O., Kimanius, D., Hagen, W.J., Lindahl, E., and Scheres, S.H. (2018). New tools for automated high-resolution cryo-EM structure determination in RELION-3. ELife 7, e42166. https://doi.org/10.7554/eLife.42166.